Study of Physical Properties of Binary Mixtures of Liquid Crystals

THESIS SUBMITTED FOR THE DEGREE OF DOCTOR OF PHILOSOPHY (SCIENCE) OF THE UNIVERSITY OF NORTH BENGAL

MARCH, 2006

by

Prithwi Dev Roy

Liquid Crystal Research Laboratory

Department of Physics

University of North Bengal

Raja Rammohanpur

Darjeeling

West Bengal – 734 013

India

STOCK TAKING - 2011

"Dedicated to my late grandfather"

DEPARTMENT OF PHYSICS
UNIVERSITY OF NORTH BENGAL
P.O. NORTH BENGAL UNIVERSITY
SILIGURI. DIST. DARJEELING (WB)
PIN: 734 013 INDIA

Railway Station: New Jalpaiguri(NFR)
Airport: Bagdogra
Phone: +91 (0) 353 2699 107
Fax: +91 (0) 353 2699 001

(TO WHOM IT MAY CONCERN)

This is to certify that the work reported in this thesis entitled "***Study of Physical Properties of Binary Mixtures of Liquid Crystals***" by Mr. Prithwi Dev Roy has been carried out by the candidate himself under our joint supervision and guidance. Mr. Dev Roy has fulfilled all the requirements for the submission of the thesis for Ph.D. degree of the University of North Bengal. Some part of the research work presented in this dissertation has been performed in collaboration with others. However, even in those works his contribution is very substantial. In character and disposition Mr. Dev Roy is fit to submit the thesis for the Ph. D. degree.

Date: 03.04.2006

M.K. Das

(Malay Kumar Das)
Reader
Reader in Physics
Department of Physics
North Bengal University

Sukla Paul

(Sukla Paul)
Reader in Physics (retired)

Contents

I like to express my indebt gratitude and profound regards to my Supervisor, Dr. Malay Kumar Das, Reader in Physics, North Bengal University, whose efficacious, tireless attention, vivacious supervision and constant inspiration has made this thesis possible. He has invested his valuable academic time during the process of my research work and I am moved by his understanding and knowledge in every aspect of this subject.

I pay my special tribute and thanks to my co-supervisor Dr. (Mrs) Sukla Paul, Reader in Physics (Retired), North Bengal University, for her meticulous attention to my research work. She had played a very important role at each step of my work by spontaneously extending to me her thoughtful suggestions from time to time throughout the course of this work.

Words are not enough to express my heartiest gratitude to a man of profound knowledge and celebrity of science - Professor Ranjit Paul, (Retired) Department of Physics, North Bengal University. I am indeed grateful to him for his enormous support, enthusiastic encouragement and valuable suggestions in fulfilling the undertaken task.

I am highly grateful to E. Merck U.K for generously donating the samples (ME50.5, 5CB, 11OCB, ME6.05, ME60.5 and CPPCC) and M/S Hoffmann-La Roche & Co., Basel, Switzerland for donating the samples (1d(3)CCO$_2$ and 0d(4)CCO$_2$).

I would like to express my appreciation to Prof. P. K. Mandal, Department of Physics, North Bengal University, for his kind co-operation and help. I am also highly obliged to Prof. D. Das Gupta, Prof. S. K. Ghosal and Sri Debdas Chakravorty, Prof. B. Bhattacharjee, Prof. S. Mukherjee, Dr. N. Kar, Dr. A. Mukhopadhyay and Dr. B. C. Paul, Department of Physics, North Bengal University, all of whose encouragement had helped me enormously in the completion of my work.

I like to express my special thanks to Dr. (Mrs.) B. Adhikari (Das), Lecturer in Physics, Siliguri Institute of Technology for providing me all sorts of support by sharing her research experience and knowledge. I express my sincere thanks to Dr. A. Bhadra Assistant Register, North Bengal University for his warm support.

I would like to thank my co-workers Dr. N. K. Pradhan, Dr. S. K. Giri, Dr. P. K. Sarkar, Dr. P. Sarkar, Dr. B. R. Jaishi, Mrs. S. Biswas, Miss. M. Ghosh and Mr. M. Ghosh for their cordial cooperation during my experimental work.

A special word of thanks must be made to Mr. Sajal Kumar Sarkar, Senior Technical Assistant (Retired), Department of Physics, North Bengal University for his cheerfully

and skillfully undertaking the numerous repair and designing works of the instruments used by me. I am also thankful to Mr. S. Ray, Mr. A. Roy, Mr. S. Hazra Technical Assistant, and Mr. L. Hansda and the members of University Science Instrumentation Centre, North Bengal University for extending their practical knowledge and experience in instrumentation available to me.

I express my sincere thanks to my friends and colleagues, especially Mr. Himadri Dev, Mr. Sanjoy Bhattacharjee, Mr. Milan Naskar, Mr. Abhijit Sarkar, and Mr. Dipanjan Dutta for their co-operation, kind understanding and constant support.

I express my gratitude to my parents and in-laws for their moral support in every step. I am especially grateful for the care and affirmation given to me by my wife Smt. Jaya Biswas (Dev Roy), and special thanks to my little daughter Dyuti, who unknowingly helped me and cooperated me to complete the task.

During my research period many special people have helped me in variety of ways and have given me mental support. My heartfelt thanks are due to all of them.

Dated: - 03:04:2006.
Liquid Crystal Laboratory
Department of Physics
University of North Bengal

Prithwi Dev Roy
(Prithwi Dev Roy)

Chapter 1

Introduction

1.1 Introduction:

Liquid crystal materials are generally organic compounds, which exhibit various degrees of translational and orientational order intermediate between the crystalline solids and those of isotropic liquids. This state of matter was discovered more than hundred years ago in 1888 by F. Reinitzer [1] while investigating the optical properties of some esters of cholesterol. O. Lehmann [2], a German Physicist, reaffirmed the observations made by Reinitzer and termed such materials as 'flowing crystals' in 1889, crystalline 'liquids' in 1890 and 'liquid crystals' in 1900. Georges Friedel [3,4] suggested the term "mesomorphic phase" or "mesophase", the state of matter observed between the isotropic liquid and crystalline solid. These materials provide new thermodynamically stable phases and are excellent systems for studying phase transitions and critical phenomena. Liquid crystals combine many of the physical properties of liquids such as fluidity with the anisotropic physical properties of crystalline solids. The combination of order, mobility and easy response of these materials to electric, magnetic and surface forces have generated many applications ranging from the familiar numeric displays, temperature sensors to high resolution TV displays, projection systems and optical computing.

The molecules of the compounds showing mesophases are either anisometric molecules with a specific rod-like or disc – like shape or amphiphilic molecules or oligomers, polymers and dendrimers derived from these fundamental structures. Anisotropic dispersive forces between the molecules play a major role in the stabilization of these phases. There are several organic chemicals, which exhibit mesophases [5,6]; few organo-metallic [7,8] and inorganic chemicals [9] also show liquid crystalline properties as well. For general information on liquid crystals some books

and reviews are listed in references [10-21]. Recent development in the field of liquid crystals and applications are also available in the literature [22-33].

1.2 Classification of liquid Crystals:

Liquid crystals are broadly classified into two types, viz. thermotropic and lyotropic.

1.2.1 Lyotropic liquid crystals:

Lyotropic liquid crystals belong to a class of substances called amphiphilic compounds (surfactant). One end of the molecule is polar and attracted to water (hydrophilic), while the other end is nonpolar and attracted to hydrocarbons, or lipophilic (figure 1.1(a)). The schematic diagram of sodium laurate, a common amphiphilic molecule is shown in figure 1.1(b).

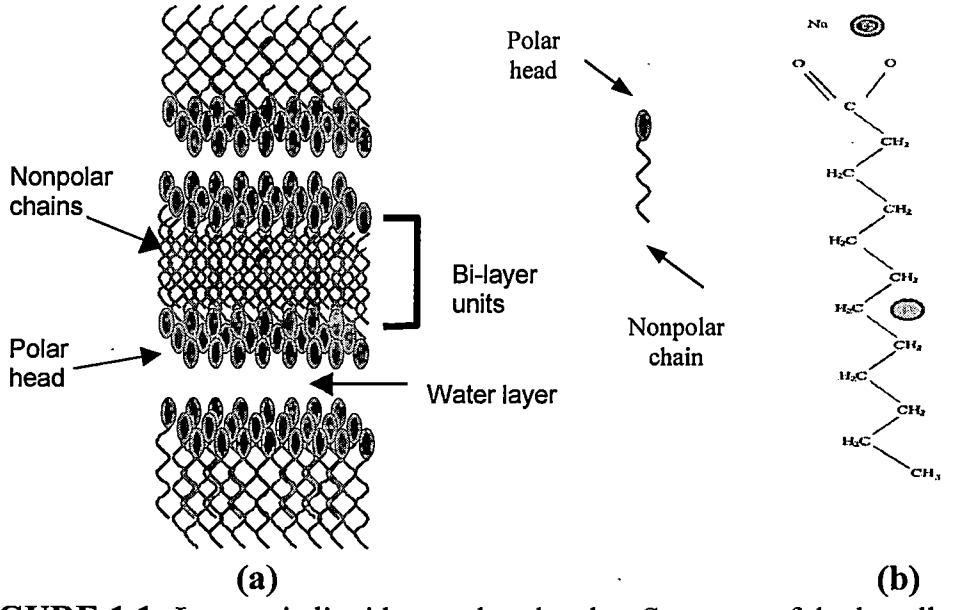

FIGURE 1.1: Lyotropic liquid crystal molecules: Structure of the lamellar lyotropic liquid crystal phase **(a)** and Sodium laurate **(b)**

In solution, the molecules arrange themselves such that either the polar ends are dissolved in a polar solvent or the nonpolar ends are dissolved in a nonpolar solvent. The opposite end is kept isolated from the unlike solvent.

As the concentration of the molecules in solution increases, they take on different arrangements, such as – lamellar, cubic and columnar (figure 1.2).

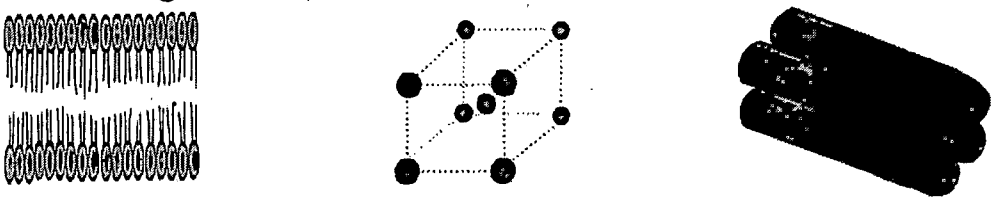

Lamellar **Cubic** **Hexagonal**

FIGURE 1.2: Schematic representations of lamellar, cubical and hexagonal phases.

The amount of solvent is the controlling parameter for forming such mesophases. Solution of soap and water are typical examples of lyotropics and their mesomorphic properties appear both as function of concentration and temperature. Lyotropic liquid crystals have relevance to biological systems [27] as bio-membranes consist of lipids and water and usually also proteins, which have liquid crystalline properties.

Recently new types of mesophases been obtained with calamitic (rod –like) amphiphilic molecules carrying long lateral chain. Elongation of the lateral chains has led to different columnar phases in the sequence with space groups Colr/*c2mm* – Colsq/*p4mm* – Colr/*p2gg* – Colh/*p6mm* – Colr2/*c2mm* – Colr4/*c2mm* –Colr/*p2mg* and further increase of the lateral chain length leads to a novel types of layer structures –Lam (lamellar) – SmAb (biaxial Smectic A) –SmA (uniaxial Smectic A). The formation of such phases has been explained by the micro-segregation of the polar amphiphilic cores from the lipophilic lateral chains, leading to mesophases built up by two or three distinct sets of subspaces [29-33]. Since this dissertation is not concerned with lyotropic liquid crystals it will not be discussed here.

1.2.2 Thermotropic liquid crystals:

In thermotropic liquid crystals, mesomorphic behaviour is induced due to change in temperature. The vast majority of thermotropic liquid crystals are composed of rod-like molecules (one molecular axis is longer than the other two) [34]. A typical calamitic liquid crystal is shown in figure 1.3.

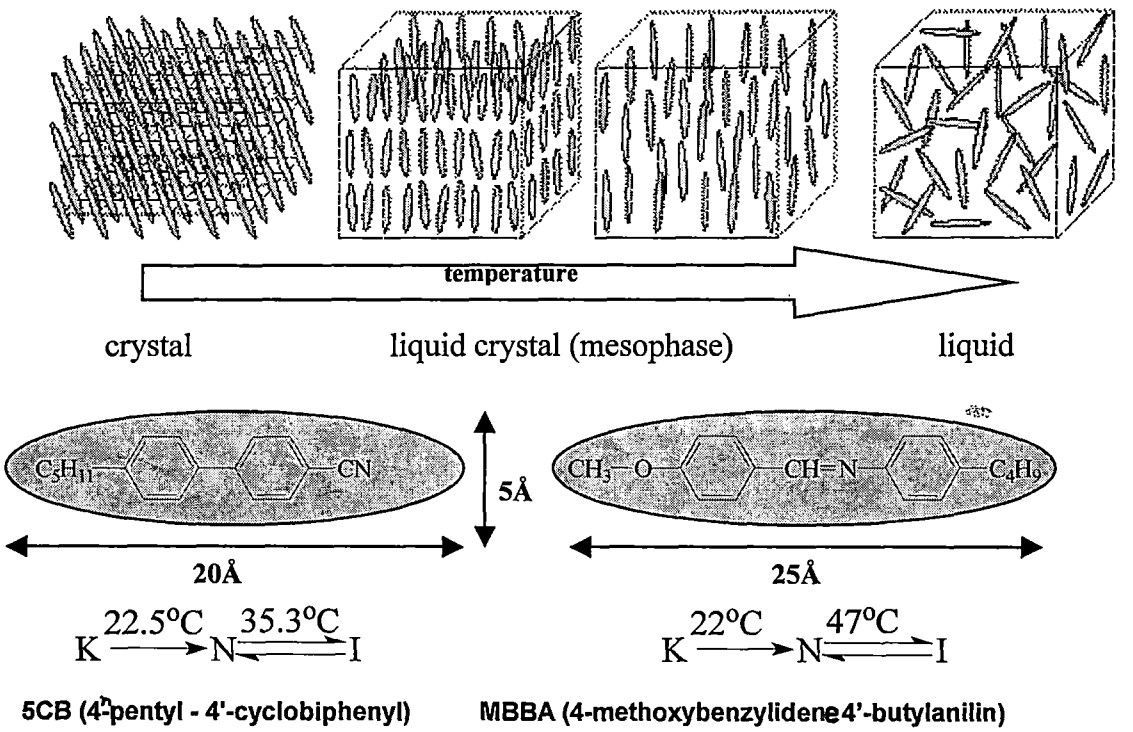

FIGURE 1.3: A typical calamitic liquid crystal with transition temperatures.

Thermotropic liquid crystals that exhibit reversibility of phase transition are called 'enantiotropic'; and in certain cases mesomorphism is observed only during cooling of the compound and these transitions are called 'monotropic' transitions. Friedel [35] from his detailed optical and x-ray studies have classified thermotropics into three main types: nematic, cholesteric and smectic. Classifications of smectic liquid crystals are based mainly on the optical and miscibility studies of Demus and Richter [36]. A brief description of different thermotropic mesophases is given below.

1.2.3 Nematic liquid crystals:

In nematics, there is no correlation between the molecular centre of gravity, but the direction of molecular long axis do statistically have a preferred direction called director denoted by **n** (figure 1.4). Since there is no restriction regarding the positions of the centre of mass, the molecules in the phase have a high degree of mobility.

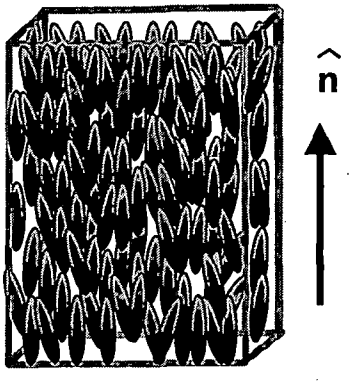

FIGURE 1.4: Schematic illustration of ordinary nematic liquid crystal.

Deformation in alignment of the nematic molecules can be induced by small external influences and this property is extremely useful in various display devices. The ordinary nematics shows an optically positive uniaxial behaviour, but a biaxial modification has also been discovered. Another characteristic property of this phase is that the mirror images are indistinguishable, i.e., achiral, indicating the system to be a racemic mixture of right- and left-handed molecules. X-ray studies indicate that fluctuation of smectic like order parameter manifest itself in certain nematic phases, called "cybotactic nematics", first observed and classified by Adrian de Vries [37].

1.2.4 Cholesteric or chiral nematic (N^*) phases:

The cholesteric (or chiral nematic) [38-40] liquid crystal phase is typically composed of nematic mesogenic molecules containing a chiral center, which produces intermolecular forces that favour alignment between molecules at a slight angle to one another. This leads to the formation of a structure that can be visualized as a stack of very thin two-dimensional nematic-like layers with the director in each layer twisted with respect to those above and below it. So the directors actually form a continuous helical [41] pattern about the layer normal as shown in figure 1.5.

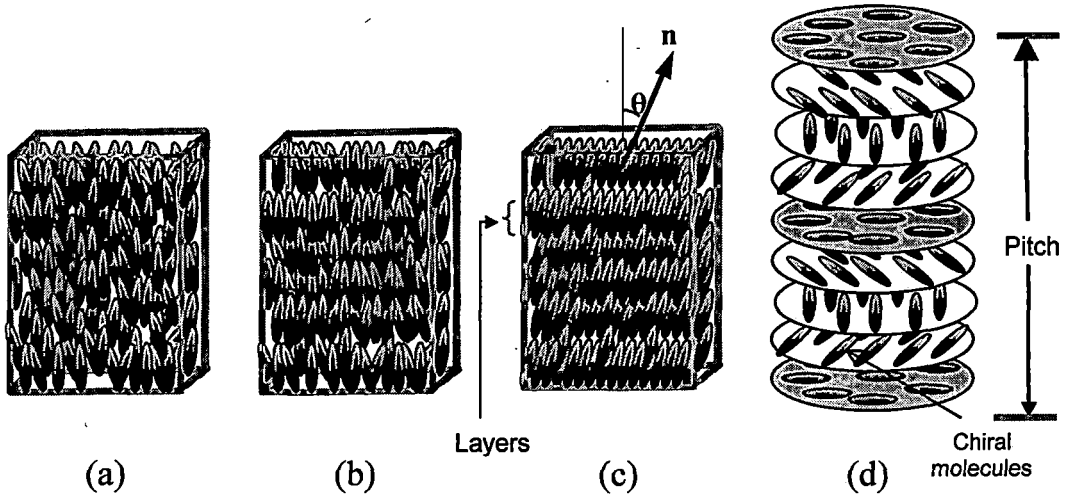

FIGURE 1.5: Schematic representation of **(a)** nematic phase **(b)** orthogonal smectic A phase and **(c)** tilted smectic C phase **(d)** helical structure of the cholesteric liquid crystals. The arrow indicates the director **n**.

The helix may be right handed or left handed depending on the molecular conformation. An important characteristic of the cholesteric mesophase is the temperature dependent pitch (p) which is defined as the distance it takes for the director to rotate one full turn in the helix. The helical structure of the chiral nematic phase enables it to selectively reflect light of wavelengths equal to the pitch length. This property is utilized in liquid crystal thermometers.

1.2.5 Smectic liquid crystals:

Smectic liquid crystals have layered structure. The centres of gravity of the elongated molecules lie in equidistant planes. The molecules are parallel to the preferred direction, which may be normal to the plane or may be tilted at a certain angle. The arrangement of the molecules within the plane may be random or regular. The smectic liquid crystals are generally more viscous than nematics. The interlayer attractions are smaller in comparison to the lateral forces between the molecules and the layers can slide over one another [42-52], thus showing fluid behaviour. A large number of smectic phases identified [8,52-55] by observed variants are as follows

SmA, SmC, SmB, SmD, SmE, SmF, SmG, SmH, ...

Since my work is concerned with nematic, smectic A and smectic B phases only, I will not go into details of other smectic phases here.

1.2.6 Smectic A phase (SmA):

In smectic A liquid crystals, the molecular orientation is perpendicular to the plane in which the centers of mass of the molecules are situated. There is a long-range positional order normal to the smectic layers, but within each layer the distribution of the molecular centers is random [42-44] or with only a short-range order typical of liquids. The smectic A molecules can rotate about the long axis sweeping out a volume which is cylindrical in shape. Due to this infinite fold rotational symmetry about an axis parallel to the direction normal to the layer, smectic A liquid crystals at thermal equilibrium are uniaxial systems [11,56]. In this phase usually the layer spacing (d) is approximately equal to the molecular length (l). However, other modifications are also possible. Smectic A phase can be subdivided into several distinct phases [45-52,53-60] such as monolayer smectic A

(SmA_1), bilayer smectic A (SmA_2), partially bilayer smectic A_d (SmA_d) and smectic antiphase/Smectic Ã, as shown in figure 1.6 (a-d) respectively.

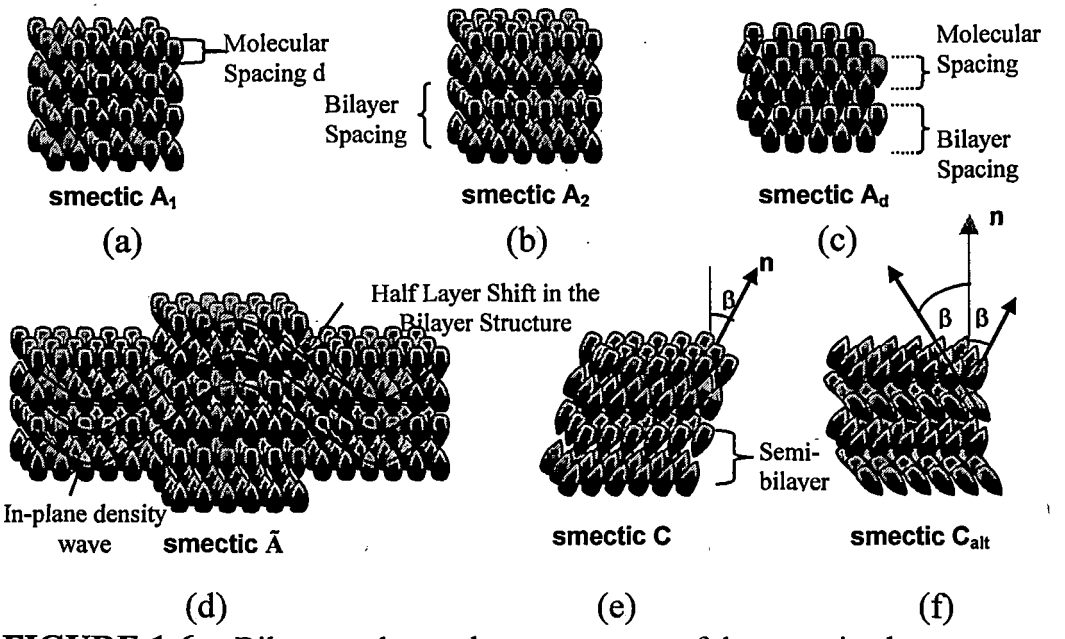

FIGURE 1.6: Bilayer and monolayer structures of the smectic phases.

1.2.7 Smectic C phase (SmC):

In the smectic-C mesophase, molecules are arranged in layers as in the smectic-A mesophase, but the molecules are inclined with respect to the layer normal as shown in figure 1.6(e). The layer thickness $d = l\cos\beta$, (where l is the length of the molecule and β is the tilt angle) in the smectic C phase is less than that of the corresponding smectic A phase due to this tilt. The tilt angle β varies from compound to compound, and for a given compound it may or may not be temperature dependent. The smectic C phase is optically biaxial and more viscous than that of nematics. Levelut et al [53-55,60-63] has reclassified the SmC phase as alternating smectic C phase (SmC_{alt}), wherein the tilt angle of the molecules are rotated by 180° while passing from one layer to the other, in contrast to that of traditional SmC phase (figure 1.6(f)).

1.2.8 Smectic B phase (SmB):

The smectic-B liquid crystals also have layered structure with the molecular long axis perpendicular to the layer normal. However, within the layers the molecules are arranged into a network of hexagons. According to Birgeneau and Lister [64], the smectic B phase is a realization of the stacked hexagonal phases possessing bond orientational order (BOO) found in two dimensions. On the basis of x-ray [65] and electron diffraction [66] experiments done on bulk aligned samples as well as on thin films the traditional smectic B phase has been further reclassified into the Hexatic B (SmB_{hex}) [67] and Crystal B (Cry B) phase.

The SmB_{hex} phase has short range in-plane positional order and long-range bond orientational order as shown in figure 1.7(a). The crystal B phase however has long-range inter- and intra- layer translational order and long-range bond orientational order as well. The Crystal B phase is still considered liquid crystal because of weak coupling between the smectic layers. Hence they exhibit shear and flow properties under stress and the Mossbauer spectra of this phase is also inconsistent with that of solid.

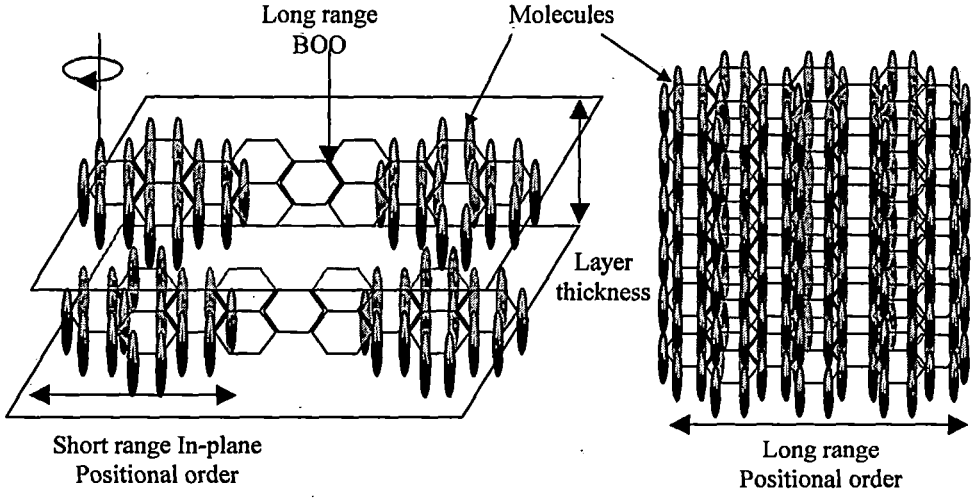

FIGURE 1.7: Structure of the **(a)** hexatic smectic B phase and **(b)** crystal B phase

1.3 Other liquid crystalline phases:

1.3.1 Blue phase:

Cholesterics liquid crystals of pitch less than about 0.5mm exhibit what are known as blue phases. These phases exist over a small temperature range (~1°C) between the liquid crystal phase and the isotropic liquid. These liquid crystalline materials display bluish-violet colour below its cholesteric-isotropic phase transition temperature [68-72], which may be due to the defects in a cubical array. Blue phases exhibit optical activity and selective reflection of circularly polarized light without possessing optical birefringence [73].

1.3.2 Twist grain boundary smectic A (TGBA) phase:

Goodby et al [74,75] have discovered a new liquid crystal phase in 1989, called Twist Grain Boundary Smectic A (TGBA) phase, wherein the molecules are arranged in layers with their long axis perpendicular to the layer plane. Due to the rotation of different blocks of the layers around the normal to the long axis of the molecules a helical structure is formed with the axis of the helix parallel to the layer plane. Renn and Lubensky [76,77] in their model specified that TGBA are responsible for rotating each blocks of the chiral A^* layers with respect to each other. Since then many new TGBA and TGBC phases have been identified.

1.3.3 Ferroelectric liquid crystals (FLC):

Ferroelectricity in liquid crystals has been known from the pioneering work of R. B. Meyer et al [78]. Chirality in a tilted Smectic C phase is introduced by chiral dopants or by chirality of the constituting molecules themselves results in a breaking of mirror symmetry and this chiral smectic phase is

denoted by SmC^*. In such chiral tilted phases the symmetry group is reduced to C_2. Hence it permits the appearance of the spontaneous electric polarization P_s in each layer of the smectic C^* phase. However, in bulk the equilibrium structure will be twisted into a helix so that the polarization of the layers precesses around the layer normal and in macroscopic sample the spontaneous polarization averages to zero and a surface stabilization is required to obtain bi-stable ferroelectric switching. Anti-ferroelectric [79] and ferrielectric smectic phases were also discovered in liquid crystal materials [80-82]. A very successful concept for ferro and anti-ferroelectric smectic phases is based on achiral bent shape molecules – the so-called "banana" [83] phases. Because of the close packing of bent molecules and high rotational hindrance about the long molecular axis an in-layer polar order emerges despite the achiral nature of the molecules. To have material with high information content colour displays and of fast switching speed, study of both ferroelectric and antiferroelectric liquid crystals has become important today.

1.3.4 Discotic liquid crystals:

In 1977, Chandrasekhar, Sadashiv and Suresh discovered that [84] disc like molecules also form liquid crystalline phases in which the axis perpendicular to the plane of the molecule (the director) tends to be along a specific direction. In the nematic (N_D) state, the disc-like molecules appear to stack one on top of the other, rather like a pile of disordered plates. Apart from the N_D phase disc like molecules give rise to columnar phases [85] in which the molecules are in stacks that lie side by side to form a two dimensional lattice. The different columnar phases are classified into orthogonal or tilted phases (figure 1.8). The tilt refers to the angle between the director and columnar axis. Different type of lattice structures have been

identified by Levelute [85] viz., hexagonal, rectangular and oblique. Significant research works have been performed during last ten years [86,87].

FIGURE 1.8: Schematic representation of columnar structures of discotic mesogens: (a) upright columns and (b) tilted columns.

1.3.5 Polymer liquid crystals:

Liquid crystal polymers (PLC's) exhibit both the characteristic properties of ordinary liquid crystals, as well as retain the versatile properties of polymers. For a polymer to display liquid crystal characteristics they must incorporate either rod-like (calamitic), discotic, amphiphilic or chiral molecules of low molecular weight, which are attached to the polymer backbone either in the main chain, or as side groups into their chains. Placement of these monomers plays an important role into the determination of the type of PLC's. Main chain polymer liquid crystals are formed when the mesogens are themselves becomes a part of the main chain of a polymer, whereas in the side chain polymer liquid crystals mesogens are connected as side chains to the polymer by a flexible 'bridge'. Factors that may affect the mesomorphic behavior of the polymer include the presence of long flexible spacers, a low molecular weight, and regular alternation of rigid and flexible units along the main chain. Polymer dispersed liquid crystals (PDLC's) are widely used in displays, switchable windows and other light shutter devices [88-90]

1.4 Liquid crystal mixtures:

In the past 20-30 years liquid crystalline materials have received significant attention due to their increased applicability in display devices. Although more than 100,000 liquid crystalline compounds have been synthesized so far [33], to meet the specific demands of the electro-optic display devices, mixtures of pure compounds are often used where the compositions of the individual components are adjusted so that better materials may be produced for display applications. Mixtures enable us not only to lower the melting point but also to adjust the mixture properties such as viscosity, birefringence, electric permittivity and elastic constants. In this way mixtures with optimal electro-optical characteristics for the best display performance can be obtained. The physical properties of such mixtures however, cannot always be interpolated from the properties of the pure components, notable examples being formation of an induced smectic phase in a mixture of pure nematogens [91-103], and exhibition of re-entrant phenomena in mixtures of liquid crystal chemicals [104-105], which do not show such phase in their pure form. Intermolecular attractive forces such as Vander Waals forces, hydrogen bonds, electron-donor interactions and intermolecular repulsion (steric forces) influence the situation of molecules in the mesophase. Each of those forces, separately or together, may be responsible for increasing or decreasing the stability of liquid crystalline phases or for creating new phases.

The presence of induced smectic phase in the operational temperature range of the display device must be avoided. However, its presence at a lower temperature is advantageous since it decreases the bend to splay elastic constant ratio [106] thus increasing the sharpness of the electro-optical display devices. Hence, measurement of physical properties of mixtures is very important from the point of view of selection of proper

liquid crystal materials for display devices. A considerable volume of work has been reported in the literature on systems involving polar non-polar mixtures exhibiting the induced smectic phase behaviour [91-103,107-115]. The creation of new phases in binary mixtures of mesogenic compounds will be discussed here.

1.4.1 Formation of induced and enhanced smectic phases:

(1) Liquid crystalline phases (nematic or smectic) existing in pure compounds in bi-component or multi-component systems enhance their own thermal stability or new phases of higher order are injected. These enhanced or injected phases are commonly termed as induced phases or chemically induced phases [92,116-117]. Such behavior is usually observed in binary mixtures of a compound having a strongly polar terminal group and a compound having a non-polar terminal group [104, 118-119]. The induction of smectic phases is also possible in systems containing two polar nematics [111-112]. This phase can be induced in mixtures of non-polar nematics [89-90,92] as well.

(2) Smectic phases existing in pure compounds in the bi-component or multi-component systems decrease their smectic stability and new phases of lower order are created. These phases are termed as phases created by depressing smectic stability [116-117].

A quantitative theory of induced smectic phase is difficult since it would require the inclusion of position dependent attractive and repulsive interactions for both the components. Wagner [120] has tried with limited success to explain the phase diagram of mixtures showing induced smectic phase using McMillan's theory for smectics. He however, could not reproduce the nematic – isotropic phase boundary. Longa and de Jeu [121]

using mean field approximation gave a theoretical model in which the influence of complex formation on the nematic–smecticA transition temperature was estimated. Their model confirms that the complication involved at S_A-N phase transition is a consequence of the interactions between complexes. Dispersion forces are mainly responsible for these interactions. Using an extension of Maier-Saupe theory [122], Palffy-Muhoray et al [123] have determined the nematic-isotropic co-existence region for the entire range of concentrations of induced smectic system and they have proposed a relation between the refractive index of the binary mixture and order parameters of its components in the nematic phase. Sharma and Schneider [95,96], Matsunaga and Araya [112-113], Iida [114] observed charge-transfer bands in the investigated mixtures and on that basis they attributed a great deal of importance to donor-acceptor interactions.

1.4.2 The Re-entrant phenomena:

One of the most interesting phenomena exhibited by liquid crystals is the formation of re-entrant phase. When a compound exhibits both smectic and nematic phases, then as a rule, the nematic phase occur at the higher temperature. An exception to this rule, Cladis [105] discovered the re-entrant phase, in certain strongly polar materials in 1975. This phase has been observed in mixtures [124-125] as well as in single component at high [126] and atmospheric [127-128] pressures. Evidence shows that the re-entrant phenomenon is not only possible in strong polar systems, but also in low polar systems containing calamitic [103] or discotic [129] molecules and in mixed systems containing compounds of high and low polarity [130-133]. Systems including chiral compounds [134-135] and low and high molecular weight [136] compounds are also described to exhibit this phase. Re-entrant smectic phases have also been reported in

terminal polar compounds [137]. In binary mixtures of terminal non-polar compounds the phase sequence SmA-SmC-SmA has been detected [138-139]. A multiple re-entrant polymorphism has also been found in pure substances as well [8, 137].

Cladis [140-141] has explained the mechanism of formation of nematic phase at lower temperature. A more complete theoretical discussion by considering attractive forces and hard-core repulsions, Longa and de Jeu [142] showed that there could exist a low temperature nematic phase. From the molecular point of view, S. Chandrasekhar [143] has discussed the re-entrant phenomena qualitatively. By extending McMillan's treatment of SmA phase, Luckhurst and Timmi [144] have developed a molecular theory for re-entrant nematic and SmA mesophases.

Reference:

1. F. Reinitzer, "Zur Kenntnis des Cholesterins", *Monasch, Chem.*, **9,** 421 (1888).
2. O. Lehmann, "Fließende Kristalle", *Z. physik. Chem.*, **4,** 462 (1889).
3. G. Friedel and E. Friedel, *Z. Krist*, **79**, 1 (1931).
4. G. Friedel: "*In Colloid Chemistry*", ed. J. Alexander, **1**, 102ff. The Chemical Catalogue Company, Inc., N. Y. (1926).
5. W. Kast, Landelt-Borstein Tables, **2**, 266, 6th edition, Springer-Verlag (1969).
6. D. Demus, H. Demus, and H. Zaschke, *Flüssige Kristalle in Tabellen,* Deutscher Verlag fur Grundstoffindustrie, Leipzig (1974).
7. G. H. Brown, *J. Electrical Materials*, **2**, 402 (1973).
8. H. Kelker and R. Hatz, *"Handbook of liquid crystals"*, Verlag Chemie, Weinheim. Deerfiel Beach, Florida. Basel, Chapter 1, 6 (1980).
9. H. Zocher, *Liquid crystals (2)*, part 1, ed. G. H. Brown, G & B Science Publisher, Inc. N.Y., 115 (1969).
10. I. G. Chistyakov, "*Zhidkie Kristally (Liquid Crystals)*", Nauka, Moscow (1966).
11. P. G. de Gennes, *"The Physics of Liquid Crystal"*, Clarendon Press, Oxford (1974).
12. L. M. Blinov, Usp. Fiz. Nauk, **114**, 67 (1974) (Sov. Phys. Usp., **17**, 658 (1975)).
13. S. Chandrasekhar, *"Liquid Crystals"*, Cambridge University Press, Cambridge (1977).
14. E. B. Priestley, P. J. Wojtowicz and P. Sheng, eds., *"Introduction to Liquid Crystals"*, Plenum, N.K. (1974).
15. G. W. Gray, *"Molecular structure and the properties of Liquid Crystals"*, Academic Press (1962).

16. G. Vertogen and W. H. de Jeu, *"Thermotropic Liquid Crystals, Fundamentals"*, Springer-Verlag (1988).
17. G. W. Gray and P. A. Winsor (Ed.), *"Liquid Crystals"*, **1** & **2**, Ellis Horwood Ltd. (1974).
18. G. W. Brown (Ed.), *"Advances in Liquid Crystals"*, **1-6**, Academic Press (1975-1983)
19. A. Buka, (Ed.), *"Modern Topics in Liquid Crystals"*, World Scientific (1993).
20. S. J. Elston and J. R. Sambles (Edn.), *"The Optics Of Thermotropic Liquid Crystals"*, Taylor & Francis (1998).
21. D. Demus, in *Liquid Crystals Applications and Uses*, Ed. by B. Bahadur (Utopia Press, Singapore, New Jersey, London, Hong Kong, 1990), Vol.I.
22. Xin - Jin Wang, Kun Tao, Jing – An Zhao and Liang – Yu Wang, *Liq. Crystal,* **5(2)**, 563 (1996).
23. T. Niori, T. Sekine, J. Watanabe, T. Furukawa and H. Takezoe, *J. Mater. Chem.*, **6**, 1213 (1998).
24. W. Weissflog, Ch. Lischka, I. Benne, T. Scharf. G. Pelzl, S. Diele and H. Kruth, *SPIE*, **3319**, 14 (1998).
25. J. Watanabe, T. Niori, S. W. Choi, Y. Takanishi and H. Takezoe. *Jpn. J. Appl. Phys.*, **37,** L401 (1998).
26. W. Haase, S. Wróbel (Eds.), *"Relaxation Phenomena": Liquid Crystals,Magnetic Systems, Polymers, High-T_c Superconductors, Metallic Glasses*, Springer-Verlag Berlin Heidelberg (2003).
27. B. Bahadur, *"Liquid Crystals, Applications and Uses"*, Ed., World Scientific, vol. **1, 2, 3** (1991).
28. A. J. Leadbetter, *Thermotropic Liquid Crystals,* Critical Reports on Applied Chemistry, ed. G. W. Gray, Wiley, Chichester, U. K., **22**, 1-27 (1987).

29. X. H. Cheng, M. K. Das, S. Diele and C. Tschierske, *Langmuir*, **18**, 6521 (2002).
30. X. Cheng, M. K. Das, S Diele and C. Tschierske, *Angew. Chem.*, Vol **114**, No. 21, 4203(2002).
31. M. Prehm, X. H. Cheng, S. Diele, M. K. Das and C. Tschierske, *J. Am Chem. Soc.*, **124**, 12072 (2002).
32. Marco Prehm, Siegmar Diele, Malay Kr. Das, and Carsten Tschierske, *J. Am. Chem. Soc.*, **125**, no.3 615 (2003).
33. X. H. Cheng, M. Prehm, M. K. Das, J. Kain, S. Diele, D. Leine, A. Blume and C. Tschierske. *J. Am. Chem. Soc.*, **125**, 10977 (2003).
34. A. L. Tsykalo, *"Thermophysical properties of liquid crystals"*, Gordon and Breach Science Publishers (1991).
35. G. Friedel, *Ann. Physique*, **18**, 273 (1922).
36. D. Demus and L. Richter, *"Textures of Liquid Crystals"*, Verlag Chemie, New York (1978).
37. A. de Vries, *Mol. Cryst. Liq. Cryst.* **10**,31 (1970); ibid **10**,219 (1970); ibid **11**,36 (1970).
38. G. H. Brown, *Amer. Scientist*, **60**, 64 (1972).
39. T. Nakagiri, H. Kodama and K. K. Kobayashi, *Phys. Rev. Lett.*, **27**, 564 (1971).
40. I. G. Chistyakov, *Sov. Phys.* Upsekki, **9**, 551 (1967).
41. F. D. Saeva, *Mol. Cryst. Liq. Cryst.*, **23**, 171 (1973).
42. S. Diele, P. Brand and H. Sackmann, *Mol. Cryst. Liq. Cryst.*, **16**, 105 (1972).
43. G. C. Fryberg, E. Gelerinter and D. L. Fisher, *Mol. Cryst. Liq. Cryst.*, **16**, 39 (1972).
44. G. R. Luckhurst and A. Sanson, *Mol. Cryst. Liq. Cryst.*, **16**, 179 (1972).
45. H. Sackmann and D. Demus, *Mol. Cryst. Liq. Cryst.*,**21**, 239 (1973).

46. D. Demus, S. Diele, M. Klapperstuck, V. Link and H. Zaschke, *Mol. Cryst. Liq. Cryst.*, **15**, 161 (1971).
47. P. J. Collings and M. Hird, *"Introduction to liquid crystals chemistry and physics"*, Taylor and Francis, UK (1997).
48. A. de Vries, *Proc. of the International Liquid Crystal Conference*, Bangalore, December, Pramana Supplement I, 93 (1973).
49. F. D Saeva (Ed.), *"Liquid Cryastals: The Fourth State of Matter"*, Marcel Dekker, New York (1979).
50. G. R. Luckhurst and G. W. Gray (Eds.), *"The molecular physics of liquid crystals"*, Academic Press, London (1979).
51. S. Chandrasekhar (Ed.), *"Liquid Crystals"*, Heyden, London (1980).
52. P. S. Pershan, *"Structure of Liquid Crystal Phases"*, World Scientific Lecture Notes in Physics, Singapore, **23** (1988).
53. A. M. Levelut, R. J. Tarento, F. Hardouin, M. F. Achard and G. Sigaud, *Phys. Rev.*, **A24**, 2180 (1981).
54. G. Sigaud, F. Hardouin, M. F. Achard and A. M. Levelut, *J. Physique*, **42**, 107 (1981).
55. F. Hardouin, N. H. Tinh, M. F. Achard and A. M. Levelut, *J. Physique*, **43**, L.327 (1982).
56. P. G. de Gennes and J. Prost, *"The Physics of Liquid Crystals"*, Clarendon Press, Oxford, 2nd Edn. (1993).
57. C. Druon and J. M. Wacrenier, *Mol. Cryst. Liq. Cryst.*, **98**, 201 (1983).
58. I. Hatta, Y. Nagai, T. Nakayama and S. Imaizumi, *J. Phys.* Soc. Jpn., **52**, Suppl. 47 (1983).
59. C. Chiang and C. W. Garland, *Proc. of 10th ILCC*, York, July, 1994 abstract E20.
60. F. Hardouin, A. M. Levelut, M. F. Achard and G. Sigaud, *J. de Chemie Physique*, **80**, 53 (1983).

61. D. Demus, J. Goodby, G. W. Gray, H. –W. Spiess, V. Vill, (Eds.), *"Handbook of Liquid Crystals": Low Molecular Weight Liquid Crystals I*, **2A**, Wiley-VCH (1998).
62. M. Watanabe, M. Eguchi, K. Kakimoto and T. Hibiya, *J. Crystal Growth,* **133**, 23 (1993).
63. S. Dumrograttana, G. Nounesis, C. C. Huang, *Phys. Rev.* **A33**, 2181 (1986).
64. R. J. Birgeneau, and J. D. Lister, *J. Phys. Lett.,* **39**, L-399 (1978).
65. R. Pindak, D. E. Moncton, S. C. Davey and J. W. Goodby, *Phys. Rev. Lett.*, **46**, 1135 (1981).
66. M. Cheng, J. H. Ho, S. W. Hui and R. Pindak, *Phys. Rev. Letts.*, **59**, 1112 (1987).
67. C. C. Huang, *"Bond Orientational Order in Condensed Matter Systems"*, (Ed. K. J. Strandburg), Springer – Verlag, Berlin – New York, p.78-136 (1992).
68. C. Destrade, P. Foucher, H. Gasparoux, H. T. Nguyen, *Mol. Cryst. Liq. Cryst.,* **106**, 121 (1984).
69. C. Destrade, H. T. Nguyen, H. Gasparoux, J. Malthete and A. M. Levelut, *Mol. Cryst. Liq. Cryst.,* **71**, 111 (1981).
70. S. Meiboom, M. Sammon, *Phys. Rev. Lett.,* **44**, 882 (1980).
71. M. Brodzik and R. Dabrowski, *Liq. Cryst.*, **18**, 61 (1995).
72. H. Stegemeyer, Th Blumel, K. Hiltop, H. Onusseit and F. Porsch, *Liq. Cryst.*, **1**, 1 (1996).
73. G. Pelzl, H. Sacknann, *Z. Phys. Chem.*, **254**, 354 (1973).
74. J. W. Goodby, M. A. Waugh, S. M. Stein, E. Chin, R. Pindak and J. S. Patel, *Nature*, London, **337**, 449 (1989).
75. J. W. Goodby, M. A. Waugh, S. M. Stein, E. Chin, R. Pindak and J.

S. Patel, *J. Am. Chem. Soc.*, **111**, 8119 (1989).

76. S. R. Renn and T. C. Lubensky, *Phys. Rev.*, **A38**, 2132 (1988).
77. S. R. Renn and T. C. Lubensky, *Mol. Cryst. Liq. Cryst.*, **209**, 349 (1991).
78. R. B. Meyer, L. Liebert, L. Strzekecki and P. Keller, *J. de Phys. Lett.* **36**, 69, (1995).
79. A. M. Lavelut, C. Germain, P. Keller, L. Liebert, J. Billard, *J. Phys.* (Paris), **44**, 623 (1983).
80. A. P. L. Chandani, Y. Ouchi, H. Takezoe, A. Fukuda, H. Tereshima, K. Furukawa and A. Kishi, *Jpn. J. Appl. Phys.*, **28**, L1261 (1989).
81. A. Fukuda, Y. Takanishi, T. Isozaki, K. Ishikawa and H. Takezoe, *J. Mater. Chem.*, **4**, 997 (1994).
82. J. W. Goodby, R. Blinc, A. N. Clark, T. S. Lagerwall, M. A. Osipov, S. A. Pikin, T. Sakurai, K. Yoshino, B. Žekš, *"Ferroelectric Liquid Crystals: Principles, Properties and Applications*, vol-7, Gordon and Breach Science Publisher (1991).
83. H. Nadasi, W. Weissflog, A. Eremin, G. Pelzl, S. Diele, B. Das and S. Grande, *J. Mater. Chem.*, **12**, 1316-1324 (2002).
84. S. Chandrasekhar, B. K. Sadashiv and A. K. Suresh, *Pramana*, **9**, 471 (1977).
85. A. M. Lavelut, *J. Chim. Phys*, **80**, 149 (1983).
86. S. Chandrasekhar, *Phil. Trans. R. Soc. A*, **309**, 93 (1983).
87. S. Chandrasekhar, *Liq. Cryst.*, **14**, 3 (1993).
88. J. W. Doane, a. Golemme, J. L. West, J. B. Whitehead and B. G. Wu, *Mol. Cryst. Liq. Cryst.*, **165**, 511 (1988).
89. G. P. Montgomery, *"Large-Area Chromogenics: Materials and Devices for Transmittance Control"*, C. M. Lampert and G. G. Granqvist (Ed. SPIE).
90. P. S. Drzaic, *J. Appl. Phys.*, **60**, 2142 (1986).

91. J. W. Park, C. S. Bak and M. M. labes, *J. Am. Chem. Soc.*, **97**, 4398 (1975).
92. C. S. Oh, *Mol. Cryst. Liq. Cryst.*, **42**, 1(1977).
93. B. Engelen and F. Schneider, *Z. Naturforsch*, **33A**, 1077 (1978).
94. M. Domon and J. Billard, *J. Phys, (Paris)*, **40**, C3-413 (1979).
95. F. Schneider and N.K. Sharma, *Z. Naturforsch.*, **36a**, 62, (1981).
96. F. Schneider and N.K. Sharma, *Z. Naturforsch.*, **36a**, 1086, (1981).
97. M. K. Das and R. Paul, *Phase Transitions*, **46**, 185(1994).
98. M. K. Das and R. Paul, *Phase Transitions*, **48**, 255(1994).
99. M. K. Das, R. Paul , *Mol. Cryst. Liq. Cryst.*, **260**, 477(1995).
100. M. K. Das, R. Paul and D.A. Dunmur, *Mol. Cryst. Liq. Cryst.*, **285**, 239 (1995).
101. D. A. Dunmur, R.G. Walker and P. Palffy-Muhoray, *Mol. Cryst. Liq. Cryst.*, **122,** 321(1985).
102. M. Brodzik and R. Dabrowski, *Mol. Cryst. Liq. Cryst.*, 260, 361(1995).
103. M. Tykarska, B. Wazynska, I. Ulbin, *Proceeding of SPIE*, Vol. **4147**, 55 (2000).
104. S. Diele, G. Pelzl, I. Latif and D. Demus, *Mol. Cryst. Liq. Cryst.*, **92,** 27 (1983).
105. P. E. Cladis, *Phys. Rev. Lett.*, **35**, 48 (1975).
106. M. Bradshaw and E. P. Raynes, *Mol. Cryst. Liq. Cryst.*,**91**, 145 (1983).
107. K. W. Sadowska, A. Zywocinski, J. Steckiand and R. Dabrowski, *J. Phys. (Fr.)*, **43,** 1673 (1982).
108. T. G. Churjusova and T. P. Sokolova, *Mol. Cryst. Liq. Cryst.*, **213**, 207 (1992).
109. J. Szabon and F. Janossy, *Advances in Liquid Crystal Research and Applications*, ed. by L. Bata (Pergamon Press, Oxford-Akademia Kiado, Budapest, 1980) p-229.

110. V. V. Belyaev, T. P. Antonyan, L. V. Lisetske, M. F. Grebyonkin, G. G. Slashchova and V. Petrov, *Mol. Cryst. Liq. Cryst.*, **129**, 221 (1985).

111. N. K. Sharma, G. Pelzl, D. Demus and W. Weissflog, *Z. Phys. Chem.*, **261** 579(1980).

112. K. Araya and Y. Matsunaga, Bull. *Chem. Soc. Jap.*, **53**, 3079 (1980).

113. K. Araya and Y. Matsunaga, *Mol. Cryst. Liq. Cryst.*, **67**, 153 (1981).

114. Y. Iida, *Bull. Chem.. Soc. Jap.*, **55**, 2661 (1980).

115. J. Andersch, S. Diele, P. Goering, J. –A. Schroeter and X. Tschierske, *J. Chem. Soc.*, Chem. Commun. 107-108 (1995).

116. J. S. Dave, P. R. Patel and K. L. Vasant, *"Mol. Cryst. Liq. Cryst.*, **8**, 93 (1969).

117. R. Dabrowski and B. Wazyanska, B. Sosnowska, *Liq. Cryst.*, **1**, 415(1986).

118. L. K. M. Chen, G. W. Gray, D. Lacey, S. Srilhauratana and k. L. Toyne, *Mol. Cryst. Liq. Cryst.*, **150B**, 335 (1985).

119. G. Pelzl, I. Latif, S. Diele, M. Novak, D. Demus, H. Sackmann, *Mol. Cryst. Liq. Cryst.*, **139**, 333 (1986).

120. W. Wagner, *Cryst. Res. Tech.*, **17**, K67 (1982).

121. W. H. de Jeu, L. Longa , *J. Chem. Phys.*, **84**, 6410(1986).

122. A. Saupe and W. Mayer, *Z. Natureforsch.*, **14a**, 882 (1959) and **15a**, 287 (1960).

123. P. Palffy-Muhoray, D. A. Dunmur, W. H. Miller and D. A. Balzarini, *Liquid Crystaland Ordered Fluid*, **Vol 4**, Ed. A. C. Griggin and J. F. Johonson Plenum, N.Y., p. 615(1984).

124. R. Dabrowski and K. Czuprynski, *Mol. Cryst. Liq. Cryst.*, **146**, 341 (1987).

125. K. Czuprynski and R. Dabrowski, *Mol. Cryst. Liq. Cryst. Lett.*, **4**, 153 (1987).

126. R. Dabrowski and K. Czuprynski, J. Przedmojski, B. Wazynska, *Liq.*

Cryst., **14**, 1359 (1993).

127. B. Wazynska, *Liq. Cryst.*, **4**, 399(1989).

128. H. T. Nguyen, *J. Chem Phys.*, 80, 83 (1983).

129. S. Wrobel, M. Brodzik, Roman Dabrowski, B. Gestblom, W. Hasse and S. Hiller, *Mol. Cryst. Liq. Cryst.*, **302**, 223 (1997).

130. S. Takenaka, H. Nakai and S. Kusabayashi, *Mol. Cryst. Liq. Cryst.*,**100**, 299 (1986).

131. W. Weissflog, N. K. Sharma, G. Pelzl and D. Demus, *Krist. And Techn.*, **15**, K35 (1980).

132. G. Pelzl, U. Bottger and D. Demus, *Cryst. Res. Technol.*, 16, K67 (1981).

133. B. Engelen, G. Heppke, R. Hopf and F. Schneider, *Mol. Cryst. Liq. Cryst.*, **49**, 193 (1979).

134. G. Pelzl, B. Oertel and D. Demus, *Cryst. Res. Technol.*, **18**, K18 (1983).

135. P. Pollmann and W. Wiege, *Mol. Cryst. Liq. Cryst. Lett.*,**102**, 119 (1984).

136. F. Harddouin, G. Sigaud, P. Keller, H. Richard, H. T. Nguyen, M. Mauzak and F.A. Chard, *Liq. Cryst.*, **5**, 463 (1989).

137. H. T. Nguyen, F. Hardouin and C. Destrade, *J. Phys (Paris)*, **43**, 1127 (1982).

138. D. Guillon, P.E. Cladis and J. Stamatoff, *Phys. Rev. Lett.*, **41**, 1598 (1978).

139. G. Pelzl, S. Diele, I. Latif, D. Demus, W. Schafer and H. Zaschke, *Mol. Cryst. Liq. Cryst.*, **1**, 39 (1985).

140. P. E. Cladis, R. K. Bodardus, W. B. Daniels and G. N. Taylor, *Phys. Rev. Lett*, **39**, 720 (1977).

141. P. E. Cladis, R. K. Bodardus, and D. Aadsen, *Phys. Rev.*, A**18**, 2292 (1978).

142. L. Longa and W. H. de Jeu, Phy. Rev., **A26**, 1632 (1982).

143. S. Chandrasekhar, *"Mol. Cryst. Liq. Cryst.,* **124**, 1 (1985).

144. G. R. Luckhurst, B. A. Timmi, *"Mol. Cryst. Liq. Cryst.Lettes.,* **64**, 253 (1981).

Chapter 2

Theoretical Background And Experimental Methods

2.1 Introduction:

To explain the behaviour of liquid crystalline phases many theories were proposed and described in many books, some of which are listed in the references [1-6]. One of the theories is molecular field approximation. Most acceptable and widely used theories based on molecular field approximation are given by Maier-Saupe [7] for nematics and McMillan [8] for smectic A. I am describing these two theories in brief, as I have compared the experimental values with the theoretical ones obtained from these theories.

2.2 Theories of Liquid Crystalline Phases:

2.2.1 Maier-Saupe mean field theory of nematic phase of rod like molecules:

Maier and Saupe have given a molecular statistical theory of the nematic phase (N) and nematic to isotropic (N-I) phase transition. The stability of the nematic liquid crystal phase arises from the existence of the anisotropic part of the dispersion interaction energy between the molecules. This energy originates from the intermolecular electrostatic interaction. Maier and Saupe approximated the electrostatic interaction by the first term of its multipole expansion and assumed that:

i) the influence of the permanent dipoles can be neglected as far as long range nematic order is concerned.
ii) only the effect of the induced dipole-dipole interaction need to be considered.
iii) the molecules may be considered to be cylindrically symmetric about its long axis.

iv) with respect to a given molecule the distribution of the centre of mass of the remaining molecules may be taken to be spherically symmetric.

The distribution of the molecular long axis about the director is given by an orientational distribution function f(cosθ), where θ is the angle between the director and the molecular long axis. As the molecules have no head to tail asymmetry, f(cosθ) is an even function of cosθ. Thus the orientational distribution function can be written as,

$$f(\cos\theta) = \sum_{L-even} \frac{(2L+1)}{2} < P_L(\cos\theta) > P_L(\cos\theta) \qquad \textbf{2.1}$$

where $P_L(\cos\theta)$ are the L^{th} even order Legendre polynomials, and $<P_L(\cos\theta)>$ are the statistical average given by

$$< P_L(\cos\theta) >= \int_0^1 P_L(\cos\theta) f(\cos\theta) d(\cos\theta) \qquad \textbf{2.2}$$

$<P_L>$ are defined as the orientational order parameters. Humphries et al [9] has given a more comprehensive concept by including higher order terms in the mean field potential for cylindrically symmetric molecules as,

$$V(\cos\theta) = \sum_{L-even} U_L < P_L > P_L(\cos\theta) \qquad (L\neq 0) \quad \textbf{2.3}$$

where U_L are the functions of distance between the central molecule and its neighbours only. Putting Legendre polynomials, L = 2 in equation 2.2 we get,

$$< P_2(\cos\theta) >= \int_0^1 P_2(\cos\theta) f(\cos\theta) d(\cos\theta) \qquad \textbf{2.4}$$

$<P_2>$ is called the order parameter of second order. For isotropic liquid $<P_2>$ = 0 and for perfectly ordered sample $<P_2>$ =1.

Retaining the first term of the right hand side of equation 2.3, the expression for the potential energy of a single molecule can be written as

$$V(\cos\theta) = -vP_2(\cos\theta) < P_2 > \qquad \textbf{2.5}$$

where $v = -U_2$

The orientational distribution function for a single molecule is given by

$$f(\cos\theta) = Z^{-1} \exp[\, -V(\cos\theta) / kT\,] \qquad \textbf{2.6}$$

where Z is the single molecule partition function given by

$$Z = \int_0^1 \exp[\, -V(\cos\theta) / kT\,] d(\cos\theta) \qquad \textbf{2.7}$$

and k is the Boltzmann's constant.

Substituting the value of V(cosθ) and f(cosθ) from equation 2.5 and equation 2.6 into equation 2.4 we can write

$$< P_2(\cos\theta) >= \frac{\int_0^1 P_2(\cos\theta) \exp[\, P_2(\cos\theta) < P_2 > / T^*] d(\cos\theta)}{\int_0^1 \exp[\, P_2(\cos\theta) < P_2 > / T^*] d(\cos\theta)} \qquad \textbf{2.8}$$

where $T^* = kT / v$ and equation 2.8 is a self-consistent equation. For every temperature T^* we can obtain the value of $<P_2>$ that satisfies the self-consistent equation. For normal liquids corresponding to the isotropic state, the value of $<P_2> = 0$ is a solution at all temperatures. In addition, for temperatures $T^* < 0.22284$, two more solutions of $<P_2>$ appear. It has been found that the nematic phase with $<P_2> > 0$ is stable when the T^* satisfies the condition $0 \leq T^* \leq 0.22019$. When $T^* > 0.22019$, we have a stable isotropic phase with $<P_2> = 0$.

The order parameter $<P_2>$ decreases from unity to a minimum value of 0.4289 at $T^*=0.22019$. The nematic - isotropic phase transition takes place at $T^*=0.22019$ and it is of first order, as a discontinuous change of order parameter $<P_2>$ from 0.4289 to 0 occurs.

2.2.2 McMillan's theory for smectic phase:

In smectic A phase, there is a periodic density variation along the layer normal (say, z-direction) in addition to the orientational distribution of the molecular axes. McMillan proposed a simple and elegant description of smectic A liquid crystal by extending the Maier-Saupe theory to include an additional order parameter for characterizing the one-dimensional translational periodicity of a layered structure. Therefore, the single molecule distribution function can be written as:

$$\mathbf{f}(\cos\theta, z) = \sum_{\mathbf{L-even}} \sum_{\mathbf{n}} \mathbf{A}_{\mathbf{L,n}} \mathbf{P}_{\mathbf{L}}(\cos\theta)\cos\left(\frac{2\pi \mathbf{nz}}{\mathbf{d}}\right) \qquad \mathbf{2.9}$$

where d is the layer thickness. McMillan [8,10] following Kobayashi [11,12] expressed the pair potential as

$$V_M(\cos\theta, z) = -v[\delta\alpha\tau \cos\left(\frac{2\pi z}{d}\right) + \{\eta + \alpha\delta \cos\left(\frac{2\pi z}{d}\right)\} P_2(\cos\theta) \qquad \mathbf{2.10}$$

where v and δ are constants characterizing the strengths of the anisotropic and isotropic parts of interaction respectively. Here

orientational order parameter $\eta =< \mathbf{P}_2(\cos\theta) >$,

translational order parameter $\tau =< \cos\left(\frac{2\pi \mathbf{z}}{\mathbf{d}}\right) >$ and

mixed order parameter $\sigma =< \mathbf{P}_2(\cos\theta)\cos\left(\frac{2\pi \mathbf{z}}{\mathbf{d}}\right) >$

The distribution function can thus be written as

$$f_M(\cos\theta, z) = Z^{-1} \exp[\, -V_M(\cos\theta, z) / kT\,] \qquad \mathbf{2.11}$$

where Z is the single molecule partition function given by

$$Z = \int_0^1 \int_0^d \exp[\, -V_1(\cos\theta, z) / kT\,] d(\cos\theta) dz \qquad \mathbf{2.12}$$

$$\left.\begin{aligned}
\eta &= \int_0^1 \int_0^d P_2(\cos\theta) f_1(\cos\theta, z) d(\cos\theta) dz \\
\tau &= \int_0^1 \int_0^d \cos\left(\frac{2\pi z}{d}\right) f_1(\cos\theta, z) d(\cos\theta) dz \\
\sigma &= \int_0^1 \int_0^d P_2(\cos\theta) \cos\left(\frac{2\pi z}{d}\right) f_1(\cos\theta, z) d(\cos\theta) dz
\end{aligned}\right\} \quad \textbf{2.13}$$

Once again, three self-consistent equations containing η, τ and σ can be written and solved iteratively. Depending on the values of the coupling parameters, the following three possible solutions are

i) $\eta = \tau = \sigma = 0$, this describes the isotropic liquid or disordered phase;

ii) $\eta \neq 0$, $\tau = \sigma = 0$, orientational order characteristic of the nematic phase in accordance with the Maier Saupe theory;

iii) $\eta \neq 0$, $\tau \neq 0$, $\sigma \neq 0$, orientational and translational order characteristic of the smectic A phase.

For $\alpha > 0.98$, the smectic A phase transforms directly into the isotropic phase, while for $\alpha < 0.98$ there is a smectic A-nematic transition followed by a nematic-isotropic transition at higher temperature. Although nematic-isotropic transition temperature is always first order according to McMillan theory, the smectic A-nematic transition can be either first order or second order. For $T_{SN} / T_{NI} < 0.87$, the smectic A - nematic transition is second order while for $T_{SN} / T_{NI} > 0.87$, the smectic A - nematic transition is first order. T_{SN} and T_{NI} are the smectic A - nematic and nematic - isotropic transition temperature respectively.

2.3 Texture studies:

Wide variety of visual patterns are displayed by liquid crystalline substances when viewed under polarized light. These patterns are called textures, which are entirely due to the defects in structure that occurs in the long-range molecular ordering of the liquid crystalline materials. Observation of textures is one of the most important techniques for the identification and determination of transition temperatures of liquid crystalline phases. They are observed in thin layers about 10-20μm placed in between a glass slide and a cover slip. Change in textures at particular temperature indicate occurrence of phase transition. Classification of different liquid crystalline phases by the observation of textures alone is often ambiguous, and other methods are needed to support it. Detailed description of various textures, with photographs, is given by Demus and Richter [13]

2.4 X - ray diffraction from mesophases:

The structure and hence the properties of the liquid crystalline compound can best be understood from the x-ray diffraction studies of the liquid crystal compounds. Although a number of review articles are available in this field, Vainshtein [14-15] and Leadbetter [16] have given the theoretical interpretation. From x-ray experiment, the Fourier image of the correlation density function can be determined, the reconstruction of which from the scattered data yields information both on the mutual arrangement of molecules in a liquid crystal and the specific features of the orientational and translational order.

The general formula for the intensity of scattering from a system of molecules is

$$\mathbf{I(S)} = \sum_k \sum_l \sum_m \sum_n \left\langle f_{km}(\mathbf{S})\, f_{ln}^{*}(\mathbf{S}) \exp\left[i\mathbf{S}.(r_k - r_l)\right] \exp\left[\, i\mathbf{S}.(R_{ln} - R_{km})\right]\right\rangle \quad \mathbf{2.14}$$

where the brackets indicate an average over all the molecules involved. $\mathbf{r}_k$ is the centre of mass of the k^{th} molecule , f_{km} is the atomic scattering factor of the m^{th} atom in the k^{th} molecule and R_{km} is the position of the m^{th} atom in the k^{th} molecule. The scattering vector is given by $\mathbf{S} = \mathbf{K}_s - \mathbf{K}_i$, where $\mathbf{K}_s$ and $\mathbf{K}_i$ are the scattered and incident wave vectors.

For elastic scattering $|\mathbf{K}_s| = |\mathbf{K}_s| = 2\pi/\lambda$, the intensity can be written as,

$$I(S) = I_m(S) + D(S)$$

$I_m(S)$ is the molecular structure factor and D(S) is called the interference function.

$$\mathbf{I}_m(\mathbf{S}) = \sum_k \left\langle \sum_{m,n} f_{km}(\mathbf{S})\, f_{ln}^{*}(\mathbf{S}) \exp\left[\, i\mathbf{S}.(R_{ln} - R_{km})\right]\right\rangle$$

$$= \mathbf{N}\left\langle \left| \sum_m f_{kn} \exp\left(-i\mathbf{S}.R_{km}\right)\right|^2 \right\rangle$$

$$\mathbf{D(S)} = \left\langle \sum_k^m \exp\left(\, iS.r_{kl}\right) \sum_{m,n} \left\langle f_{km}(\mathbf{S})\, f_{ln}^{*}(\mathbf{S}) \exp\left[\, i\mathbf{S}.(R_{ln} - R_{km})\right]\right\rangle \right\rangle \qquad \mathbf{2.15}$$

$$\mathbf{r}_{kl} = \mathbf{r}_k - \mathbf{r}_l$$

The term $I_m(S)$ gives the scattered intensity which would be observed from a random distribution of identical molecules. D(S) contains information regarding : **(i)** molecular packing, **(ii)** orientational distribution function, **(iii)** order parameters P_L, **(iv)** apparent molecular length, **(v)** average lateral distance between the molecules, **(vi)** layer thickness in smectics, **(vii)** layer order parameters τ and $\langle z^2 \rangle$ in SmA, **(viii)** correlation lengths, **(ix)** tilt angle, **(x)** bond orientational order parameter and **(xii)** critical exponents.

X-ray diffraction of the unoriented nematic phase consists of a uniform halo just like that of an isotropic liquid. This is due to the fact that a nematic liquid crystal generally consists of a large number of domains, the molecules being ordered within each domain along the director **n**, but there is no preferred direction for the sample as a whole so that the diffraction pattern has symmetry of revolution around the direction of the x-ray beam. However, application of suitable magnetic or electric field can produce a 'monodomain' or 'aligned' or 'oriented' sample of liquid crystal.

The small angle x-ray diffraction pattern from a nematic liquid crystal oriented perpendicular to the direction of the incident x-ray beam is shown in the Figure 2.1(a).

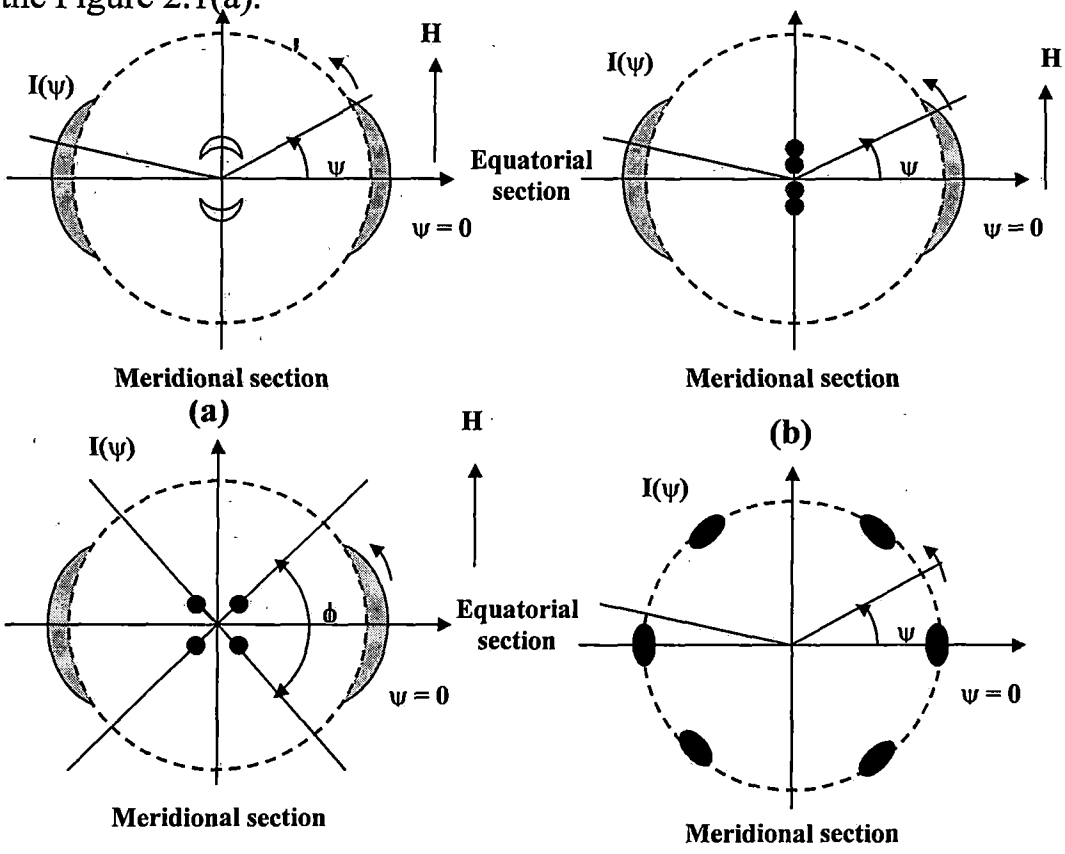

FIGURE 2.1: Schematic representation of x-ray diffraction pattern of an oriented **(a)** nematic, **(b)** smectic A, **(c)** skewed cybotactic nematic and **(d)** smectic B phase with x-ray beam parallel to the layer normal.

The outer halo splits into two crescents for each of which intensity is maxima in the equatorial direction. These crescents are formed mainly due to the intermolecular scattering and the corresponding Bragg angle is a measure of lateral intermolecular distance. The angular distribution of the x-ray intensity $I(\psi)$ vs. ψ curve, also gives the orientational distribution function $f(\cos\theta)$ and order parameter $\langle P_L \rangle$, (L= 2, 4).

At much lower scattering angle intensity peaks usually in the shape of short bar are in the meridional direction. Measuring the corresponding angle we get the value of apparent molecular length. Sometimes, the inner diffuse crescents are replaced by sharp spots (figure 2.1(c)) and the corresponding phase is called "cybotactic phase". The presence of the sharp spots indicates smectic like clusters in the nematic phase, which are called "cybotactic" groups [17].

The x-ray diffraction pattern of smectic A phase is shown in Figure 2.1(b). The meridional spots are formed due to Bragg reflection from the layers and provide the value of layer thickness. Since smectic A can have only quasi-long range order along its layer normal [3], the second order Bragg reflections in the meridional direction are generally very weak and are often absent in the x-ray photographs.

Figure 2.1(d) is the schematic representation of a three-dimensional ordered system with hexagonal symmetry, as in the smectic B phase, with the incident x-ray beam parallel to the layer normal. The outer diffraction ring is split up into six spots of strong intensity. The bond orientational order can be determined from the angular distribution of x-ray intensity $I(\psi)$ versus ψ.

2.5 Experimental technique and data analysis of X-ray diffraction studies:

The x-ray diffraction set up has been designed and fabricated in our laboratory by Jha and Paul [18]. The schematic representation of the whole set up is shown in Figure 2.2.

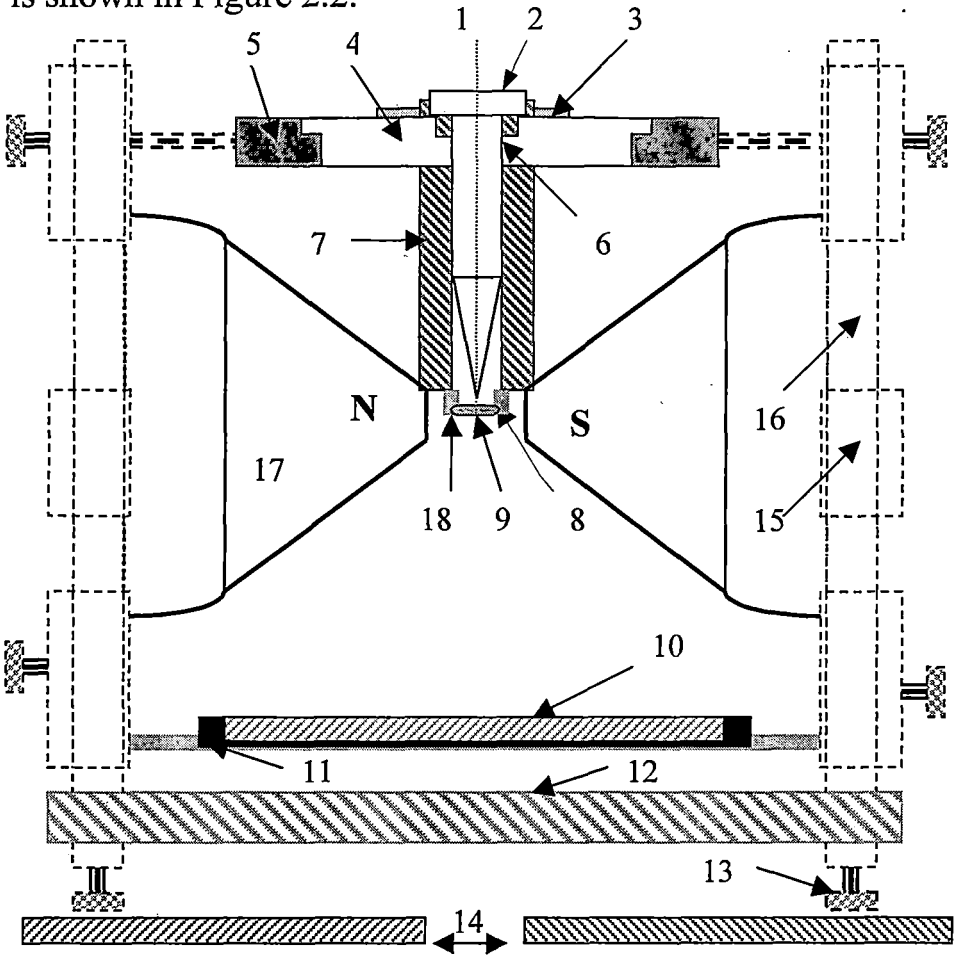

FIGURE 2.2: Sectional diagram of the X-ray diffraction camera.

1. X-ray beam, **2.** Collimator, **3.** Brass ring, **4.** Ring of syndanyo board, **5.** Brass ring, **6.** Cylindrical brass chamber, **7.** Asbestos insulation and heater winding, **8.** Specimen holder and thermocouple, **9.** Sample position, **10.** Film Cassette, **11.** Film cassette holder, **12.** Base plate, **13.** Levelling screw, **14.** Brass plates over the coils of the electromagnet, **15.** Removable spacer, **16.** Supporting brass stand, **17.** Pole pieces and **18.** Asbestos insulation.

The set up has flat-plate camera provided with the sample holder with heating arrangement. The temperature is controlled by a temperature controller of accuracy ± 0.5°C (Indotherm model IT401D2). The sample holder is fitted with a changeable collimator of aperture 0.8 mm and is well insulated. The sample was taken in a lindemann glass capillary of diameter 0.1mm and is introduced into the sample holder. The camera is then placed between the pole pieces of a strong electromagnet of field strength ~0.5 T in such a way that the sample remains at the centre of the pole pieces and the magnetic field acts along the axis of the capillary. At first the sample was heated to the isotropic phase and was slowly cooled to the desired temperature in presence of the magnetic field. X-ray photographs were taken with nickel filtered (of thickness 0.009 mm) CuK_{α} radiation of wavelength 1.5418 Å.

a) Conversion of optical density to x-ray intensity:

The optical density values obtained from the scan were then converted to relative intensity values by a method explained by Klug and Alexander [19]. The optical densities of these spots were measured with the help of photographs scanned by a Mustek 1200 UB scanner. The gray mode scan was used and the resolution was set at 600 dpi. A graph is then plotted with optical density vs. time in seconds. Since x-ray intensity is proportional to the time of exposure, the optical density vs. time curve actually corresponds to x-ray intensity and hence it is used as calibration curve to convert x-ray intensity to optical density.

b) Circular scanning of x-ray photographs:

Photographs were scanned to measure angular intensity distribution $I(\psi)$ which was used to calculate the orientational distribution function $f(\beta)$ and order parameters $< P_2>$ and $<P_4>$. Reading of the circular scan of the outer diffraction arc were taken from $\psi = 0$ to $\psi = 360^\circ$ at 1° interval near the peak and at larger intervals elsewhere. The optical density values, thus obtained, were converted into corresponding x-ray intensity with the help of the calibration curve. The experimental intensities values were then corrected for the background intensity values arising due to the air scattering. The peak intensity position which corresponds to $\psi = 0$ was determined from intensity $I(\psi)$ vs. angle (ψ) curve. $I(\psi)$ vs. ψ curve were smoothed, and nineteen values of $I(\psi)$ were taken from $\psi = 0$ to $\psi = 90^\circ$ at 5° intervals. From the values of $I(\psi)$, we have calculated the distribution function $f(\beta)$, and order parameters ($<P_2>$ and $<P_4>$) by Leadbetter's expression. A computer program was written in our laboratory for these calculations.

2.6 Orientational distribution functions and order parameters:

The x-ray diffraction pattern of an oriented sample consists of equatorial arcs. The orientational distribution function is related to the distribution of x-ray intensity along the diffused equatorial arc according to the relation given by Leadbetter and Norris [20]

$$I(\psi) = c \int_{\beta=\Psi}^{\pi/2} f_d(\beta) \sec^2 \Psi [\tan^2\beta - \tan^2\Psi]^{-1/2} \sin\beta \, d\beta \qquad \textbf{2.16}$$

where, $f_d(\beta)$ describes the distribution function of the directors of clusters in which the molecules are perfectly aligned and β is the angle between the

director **n** and molecular long axis. As molecular distribution in the nematic phase is centrosymmetric, the distribution function and the intensity can be expanded as even cosine power series.

$$I(\psi) = \sum_{n=0}^{r} a_{2n} \cos^{2n} \psi \qquad \textbf{2.17}$$

$$f_d(\beta) = \sum_{n=0}^{r} b_{2n} \cos^{2n} \beta \qquad \textbf{2.18}$$

The series converge rapidly. Retaining eight terms in the truncated series, a least square fitting was made with observed $I(\psi)$ values to get the coefficients of eqn. 2.17. These values of a_{2n} were then used to calculate the coefficients of b_{2n}.

To calculate $f_d(\beta)$ and order parameter we need $I(\psi)$ values from $\psi = 0$ to $\psi = 90^\circ$ i.e. one quadrant. I have measured $I(\psi)$ values of four quadrants separately and the average values of $I(\psi)$ is considered to calculate $f(\beta)$ as well as $\langle P_2 \rangle$ and $\langle P_4 \rangle$ for all the samples. The errors in the calculation of $\langle P_2 \rangle$ and $\langle P_4 \rangle$ in our experiment are estimated to be within $\pm$ 0.015.

$$< P_L >= \frac{\int_0^1 P_L(\cos\beta) f_d(\beta) d(\cos\beta)}{\int_0^1 f_d(\beta) d(\cos\beta)} \qquad \textbf{2.19}$$

where, L = 2,4.

2.7 Determination of Bond Orientational Order:

The order parameter associated with a system having six-fold symmetry (shown in figure 2.1(d)), as in the case of smectic B liquid crystals is the

Bond Orientational Order [21], defined to be the thermal average of the quantity

$$\psi(r) = \langle \exp(i6\theta(r)) \rangle \qquad \textbf{2.20}$$

where, the bond angle $\theta(\mathbf{r})$ is the orientation, relative to any fixed laboratory axis, of a bond between two nearest neighbour molecules. The x-ray diffraction patterns have been analysed to determine the temperature dependence of the Bond Orientational Order (BOO) in the smectic B phase. The BOO has been calculated by evaluating the expression,

$$\langle \cos(6\theta) \rangle = \int_0^{\pi/6} \cos(6\theta) f(\theta) d\theta \,/\, \int_0^{\pi/6} \cos f(\theta) d\theta \qquad \textbf{2.21}$$

where, $f(\theta)$ is the angular distribution function of centre of mass of the neighbouring molecules with respect to a central molecule and the angular distribution function has a maximum at $\theta = 0$. The above equation can be approximated by the following expression,

$$\langle \cos(6\theta) \rangle \approx \int_0^{\pi/6} \cos(6\theta) I(\theta) d\theta \,/\, \int_0^{\pi/6} I(\theta) d\theta \qquad \textbf{2.22}$$

where $I(\theta)$ is the azimuthal distribution of the x-ray diffraction intensity. According to Vainshtein [14] it has been assumed that $I(\theta)$, the intensity distribution, is proportional to $f(\theta)$ the distribution function and has its maximum at $\theta = 0$. BOO is calculated for each peak and finally the average over six peaks are taken. The intensity values plotted against azimuthal angular positions have been corrected for the background (scattered) intensity values.

a) Intermolecular distance:

The average lateral distance between the neighbouring molecules (D) is related to the corresponding Bragg angle (2θ) according to the formula [17];

$$2D \sin \theta = k\lambda \qquad \textbf{2.23}$$

where, θ is the Bragg angle for the equatorial diffraction, λ is the wavelength of CuK_α line and k is a constant varying with order parameter [23]. For perfectly ordered state k = 1.117 as given by de Vries [17].

b) Apparent molecular length or layer thickness:

Linear scanning of inner hallo or spot of x-ray diffraction photograph gives the apparent molecular length for nematic phase or layer thickness (d) for smectic phase, by using Bragg equation (2d sinθ =λ).

c) Transverse Correlation Length:

The transverse correlation length is determined from a linear scan of the x-ray diffraction peaks. X-ray intensities are at first corrected for the use of a flat plate camera following inverse square law. This corrected intensity data are then deconvoluted for finite width of the collimator. The deconvoluted intensity profile I(q) is fitted to a Lorentzian form with a quadratic background viz.,

$$I(q) = \frac{a_1}{a_2 + (q - q_o)^2} + a_3 q^2 + a_4 q + a_5 \qquad \textbf{2.24}$$

q being the magnitude of the scattering vector. The transverse correlation length is defined as $\xi = 2\pi(a_2)^{-1/2}$. For this instrument, the in-plane transverse resolution $\Delta q = 6 \times 10^{-3}$ Å^{-1}.

2.8 Refractive index of mesophases:

Most of the nematic liquid crystals are optically uniaxial and strongly birefringent. A uniaxial liquid crystal has two principal refractive indices viz. ordinary refractive index (n_o) and extraordinary refractive index (n_e). The birefringence is defined by the following equation:

$$\Delta n = n_e - n_o \qquad \textbf{2.25}$$

Birefringence of liquid crystals was first determined experimentally by E. Dorn [24] for nematogen. Subsequently Δn was measured in smectic phases [25-32]. Birefringence is positive for conventional nematics with its value lying between 0 to 0.4, while it is negative for chiral nematics. The Δn is related to the molecular polarizability (α), which originates due to π-electrons and delocalised electrons not participating in chemical bonds of the organic sample. As internal field is anisotropic in nature for mesogens, Lorentz-Lorentz force, valid for liquid state, is not applicable here; and the molecular polarizability can be determined by knowing the value of internal field. Saupe and Maier [33] applied a more elaborate internal field suggested by Neugebauer. I have followed the Neugebauer [34] and Vuks [35] modified formula for calculation of α.

i) Neugebauer's Method:

Neugebauer [34] extended Lorentz-Lorentz equations for an isotropic system to an anisotropic system. In this model the effective polarizabilities α_o and α_e of the liquid crystals are related to the refractive indices n_e and n_o according to the following equations:

$$n_e^2 - 1 = \frac{1}{4\pi N\alpha_e(1 - N\alpha_e\gamma_e)} \qquad \textbf{2.26}$$

and

$$n_o^2 - 1 = \frac{1}{4\pi N\alpha_o(1 - N\alpha_o\gamma_o)} \qquad \textbf{2.27}$$

where, γ_o and γ_e are the respective internal field constants for ordinary and extraordinary rays, N is the number of molecules per cm^3 and n_e and n_o are the extraordinary and ordinary refractive indices respectively. The relevant equations for calculating polarizabilities (α_o,α_e) as obtained from the equations 2.26 and 2.27 are as follows

$$\frac{1}{\alpha_e} + \frac{2}{\alpha_o} = \frac{4\pi N}{3}\left[\frac{n_e^2 + 2}{n_o^2 - 1} + \frac{2(n_o^2 + 2)}{n_o^2 - 1}\right] \qquad \textbf{2.28}$$

and

$$\alpha_e + 2\alpha_o = \frac{9}{4\pi N}\left[\frac{n^2 - 1}{n^2 + 2}\right] \qquad \textbf{2.29}$$

where, n is the mean refractive index

$$n^2 = \frac{1}{3}\left(2n_o^2 + n_e^2\right)$$

α_o and α_e values are obtained by directly solving equations 2.28 and 2.29.

ii) Vuks method:

Vuks [35] considered that the internal field is independent of molecular interaction and the corresponding relations are:

$$\frac{n_o^2 - 1}{n_e^2 + 2} = \frac{4\pi N}{3}\alpha_o \qquad \textbf{2.30}$$

and $$\frac{n_o^2 - 1}{n_e^2 + 2} = \frac{4\pi N}{3}\alpha_e \qquad \textbf{2.31}$$

where, $n^2 = \frac{1}{3}\left(2n_o^2 + n_e^2\right)$, n is the mean refractive index.

α_o and α_e can be calculated directly from the refractive index values.

2.9 Calculation of orientational order parameter from the refractive index measurement:

The relation between orientational order parameter $<P_2>$ and the principal polarizabilities are given by de Gennes [36] as

$$\alpha_e = \bar{\alpha} + \frac{2}{3}\alpha_a \langle P_2 \rangle \qquad \textbf{2.32}$$

$$\alpha_o = \bar{\alpha} + \frac{2}{3}\alpha_a \langle P_2 \rangle \qquad \textbf{2.33}$$

where, $\bar{\alpha} = \frac{(2\alpha_o + \alpha_e)}{3}$, is the mean polarizability

and $\bar{\alpha_a} = (\alpha_{\parallel} - \alpha_{\perp})$, molecular polarizability anisotropy

where $\alpha_{\parallel}$ and $\alpha_{\perp}$ are the principal polarizabilities, parallel and perpendicular to the long axes of the molecules in the crystalline state.

From equation 2.32 and 2.33, we obtained

$$< P_2 >= \frac{\alpha_e - \alpha_o}{\alpha_{\parallel} - \alpha_{\perp}} \qquad \textbf{2.34}$$

Due to strong absorption in the crystalline state, we used Haller's extrapolation method [37] to calculate α_a. The graph was plotted with $\log(\alpha_e-\alpha_o)$ vs. $\log(T_c - T)$ giving a straight line which is extrapolated to $\log(T_c)$, where T_c corresponds to nematic isotropic transition temperature. At T = 0 K, i.e., in the crystalline state, $<P_2>$ is considered to be equal to 1and then $(\alpha_\parallel-\alpha_\perp)$ is equal to $(\alpha_e-\alpha_o)$. For a given sample, α_e and α_o are calculated at various constant temperatures from which $(\alpha_\parallel-\alpha_\perp)$ is obtained. The order parameter $<P_2>$ is then calculated by using equation 2.34.

2.10 Measurement of refractive indices:

The principal refractive indices (n_o, n_e) of a liquid crystal were measured using thin hallow prisms with the refracting angle less than 2°. The details of the preparation of the prism and the experimental procedure have already been reported by Zemindar et al [38]. To prepare prism optically flat glass plates are taken, and they are first cleaned with conc. HNO_3.Then washed it with water several times till there is no acid reagent. The glass plates are then dried and then by dipped in acetone to remove any organic impurities. One surface of the glass plates was rubbed on bond paper in a direction parallel to one of their edges. The rubbed surface is then coated with thin layer of 1% solution of polyvinyl alcohol (PVA) and then dried. The preferred direction on the substrate can be obtained by rubbing the same surface in the same direction again by a tissue paper. The prism was then prepared by placing the rubbed surfaces inside, with the rubbing direction parallel to the refracting edge of the prism. A thin glass spacer was introduced between one of the vertical edge of the prism for getting the desired refracting angle of the prism. The glass plates of the prism were

sealed together by using high temperature adhesive and were baked in an oven. Liquid crystal sample was introduced into the prism from its top open side by melting. The system was alternately heated to isotropic phase and cooled slowly so that the liquid crystals were perfectly aligned with its optic axis parallel to the refraction edge of the prism. The prism was then placed inside a brass oven provided with transparent opening at the centre and the temperature of the oven was maintained at a desired value by a temperature controller (Indotherm model IT401D2) within an accuracy of ±0.5 °C. The refractive indices (n_o, n_e) were measured for wavelengths λ = 5890Å, corresponding to mercury source by means of a precision spectrometer and an optical monochromator.

2.11 Measurements of densities:

Measurements of density of the mesogens were performed with the help of a dilatometer of the capillary type. Dilatometer with weighed amount of the liquid crystal was kept immersed in a thermo-stated liquid bath. With the help of travelling microscope the height of the liquid crystal column was measured at different temperatures. Sufficient time was given to attain equilibrium at any desired temperature. The accuracy of density measurement lies within ± 0.1%.

2.12 Magnetic susceptibility measurements:

The orientational order parameter of liquid crystal is related to the magnetic susceptibility [37-39] in a more or less straightforward way. It is widely accepted to be one of the best methods for studying the variation of order parameter with temperature. The determination of diamagnetic properties is

of great importance in the study of liquid crystals. The theoretical treatment regarding the effect of external magnetic field on liquid crystal was given by J. P. Dias [40] and J. O. Kessler [41]. The magnetisation **M** induced by the applied magnetic field **H** is given by,

$$\mathbf{M}_o = \chi_{\alpha\beta}\mathbf{H}_\beta \qquad \alpha,\beta = x,y,z \qquad \textbf{2.35}$$

where $\chi_{\alpha\beta}$ is an element of the magnetic susceptibility tensor $\bar{\chi}$ and the summation convention over repeated index is followed. For uniaxial phase like nematic or smectic A phase and choosing the director **n** along the z-axis we have

$$\bar{\chi} = \begin{bmatrix} \chi_\perp & 0 & 0 \\ 0 & \chi_\perp & 0 \\ 0 & 0 & \chi_\parallel \end{bmatrix}$$

The subscript $\chi_\parallel$ and $\chi_\perp$ are the components parallel and perpendicular to the director respectively. The average susceptibility is given by

$$\bar{\chi} = \frac{1}{3}\sum_r \chi_{rr} = \frac{1}{3}(\chi_\parallel - 2\chi_\perp) \qquad \textbf{2.36}$$

The magnetic susceptibility anisotropy is defined as

$$\Delta\chi = (\chi_\parallel - \chi_\perp) = \frac{3}{2}(\chi_\parallel - \bar{\chi}) \qquad \textbf{2.37}$$

Hence the susceptibility tensor has only two different non zero elements,

$\mathbf{M} = \chi_\parallel \mathbf{H}$, if **H** is parallel to **n**

$\mathbf{M} = \chi_\perp \mathbf{H}$, if **H** is perpendicular to **n**

For an arbitrary angle (θ) between **H** and **n** we derive for total magnetisation

$$\mathbf{M} = \chi_\perp \mathbf{H} + \Delta\chi(\mathbf{H}.\mathbf{n})\mathbf{n} \qquad \textbf{2.38}$$

Therefore the free energy in a magnetic field is given by:

$$\mathbf{F}_m = -\int_0^H \mathbf{M}\cdot d\mathbf{H}$$

$$= \frac{1}{2}\chi_\perp \mathbf{H}^2 - \frac{1}{2}\Delta\chi(\mathbf{H}\cdot\mathbf{n})^2 \qquad \textbf{2.39}$$

Since the first term of the above equation is free from **n**, it may be omitted as far as orientation related problems are concerned. For positive anisotropy i.e. $\Delta\chi > 0$, the last term is minimised when **H** is collinear with **n**. Therefore the liquid crystal with positive $\Delta\chi$ tend to align with their molecular long axes along the direction of the applied magnetic field. However, for liquid crystal with negative$\Delta\chi$, the molecules tend to align perpendicular to the applied magnetic field.

2.13 Relation between order parameter and magnetic anisotropy:

The order parameter Q is defined by considering the anisotropic part of the susceptibility χ as follows,

$$Q_{\alpha\beta} = \chi_{\alpha\beta} - \delta_{\alpha\beta}\overline{\chi} \qquad \textbf{2.40}$$

where, $\alpha,\beta = x,y,z$ and $\delta_{\alpha\beta}$ is the kronecker delta function, S is a second rank tensor, which is diagonal. Considering the director **n** along the z-axis, then Q has zero trace and vanishes for the isotropic phase. If we consider uniaxial symmetry around **n**, it is sufficient to consider only one element Q_{zz}. Equation 2.40 can also be written as

$$Q_{\alpha\beta} = \chi_{\alpha\beta} - \frac{1}{3}\delta_{\alpha\beta}\sum_\gamma \overline{\chi}_{\gamma\gamma} \qquad \textbf{2.41}$$

$$\text{then,}\quad Q_{ZZ} = \chi_{ZZ} - \frac{1}{3}(\chi_{XX} + \chi_{YY} + \chi_{ZZ})$$

$$\text{Therefore,}\quad Q_{ZZ} = \frac{2}{3}(\chi_\parallel - \chi_\perp) \qquad \textbf{2.42}$$

Here we have assumed, $\chi_{XX} = \chi_{YY} = \chi_\perp$ **and** $\chi_{ZZ} = \chi_\parallel$

In order to relate Q to the microscopic order parameter S, let K be the tensor of the molecular magnetic polarizability which is assumed to be diagonal in the molecule - fixed co-ordinate system ξ,η,ζ.

Therefore, $$\chi_{\alpha\beta} = N\sum_{i,j} K_{ij} < i_\alpha \; j_\beta > \qquad 2.43$$

where $i, j = \xi,\eta,\zeta$; $\alpha, \beta =$ x, y, z and i_α is the α - component of a unit vector along ξ,η,ζ axes, N is the number of molecules per unit volume and the bracket $< >$ stands for statistical average.

The order parameter represented by equation 2.41 can be expressed in terms of equation 2.43, as $$Q_{\alpha\beta} = N\sum_{i,j} K_{ij} < i_\alpha \; j_\beta - \frac{1}{3}\delta_{\alpha\beta}\delta_{ij} > \qquad 2.44$$

Therefore,
$$Q_{ZZ} = N\sum_{i,j} K_{ij} < i_Z \; j_Z - \frac{1}{3}\delta_{ij} >$$
$$= \frac{2}{3}N\sum_{i,j} K_{ij}\frac{1}{2} < 3i_Z \; j_Z - \frac{1}{3}\delta_{ij} >$$
$$= \frac{2}{3}N\sum_{i,j} K_{ij}S_{ij} \qquad 2.45$$

where, $S_{ij} = \frac{1}{2} < 3i_Z \; j_Z - \delta_{ij} >$ is the generalised order parameter. Thus from equation 2.42 and 2.45 we have,

$$Q_{ZZ} = \frac{2}{3}(\chi_{\parallel} - \chi_{\perp})$$
$$= \frac{2}{3}N\sum_{i,j} K_{ij}S_{ij} \qquad 2.46$$

As S_{ij} is diagonal in a molecular fixed coordinate system ξ, η, ζ with the ζ-axis as the long molecular axis and has zero trace, there are two independent scalar order parameter, for which we choose $S = S_{\zeta\zeta}$ and $D = S_{\eta\eta} - S_{\zeta\zeta}$.

Thus equation 2.46 can be written as

$$\frac{(\chi_{\parallel} - \chi_{\perp})}{N} = \{K_{\xi\xi} - \frac{1}{2}(K_{\eta\eta} + K_{\xi\xi})\}S + \frac{1}{2}(K_{\xi\xi} - K_{\eta\eta})D \qquad 2.47$$

where S is the order parameter which have a value between 0 and 1.

Thus, $$<S>=\frac{1}{2}<3\xi_z^2-1>$$

Therefore, $$<S>=\frac{1}{2}<3\cos^2\theta-1>$$

where 'θ' is the angle between z and ζ axes.

Furthermore, $$D=\frac{1}{2}<3\xi_z^2-1>-\frac{1}{2}<3\eta_z^2-1>$$

$$=\frac{3}{2}<\xi_z^2-\eta_z^2>$$

$$=\frac{3}{2}<\sin^2\theta\cos2\psi>$$

where ψ is the Euler angle specifying the rotation around the ζ-axis. D measures the difference in tendency of the two transverse molecular axes to project on the z-axis. By considering the molecule to be axially symmetric, we have D = 0.

Now equation 2.47 can be written as,

$$<S>=\frac{(\chi_{\parallel}-\chi_{\perp})}{(\chi_l-\chi_t)} \qquad \textbf{2.48}$$

where $\chi_l = NK_{\xi\xi}$ and $\chi_t = \frac{1}{2}N(K_{\eta\eta}+K_{\xi\xi})$

Equation 2.47 is known as Tsvetkov's expression for order parameters [42]. To determine the order parameter (S) we need the value of (χ_l - χ_t) which can be obtained from solid single crystal measurements. In the present case (χ_l - χ_t) is determined by Haller method [37]. (χ_l - χ_t) plotted against ln(T_c-T) extrapolated to a point T = 0°K where S is assumed to be unity.

2.14 Determination of χ:

The magnetic susceptibility has been measured by the classical Faraday-Curie method. The total force (F) experienced by a sample in an

inhomogeneous magnetic field with a gradient in the horizontal x-direction is given by

$$F = \frac{1}{2}(m\chi - m_0\chi_0)\left(\frac{dH^2}{dx}\right)_{avg} \qquad 2.49$$

where χ, m are the mass susceptibility and the mass of the sample and χ_0, m_0 are those of air driven out of the sample. The subscript 'avg' indicates the average value. If we assume that the sample is replaced by almost same volume of the reference sample and is placed at more or less at the same position between the pole pieces of the magnet, then (dH^2/dx) will be same for both the cases. By indicating the reference sample with the subscript 'r', the force acting on the reference sample is given by:

$$F = \frac{1}{2}(m_r\chi_r - m_0\chi_0)\left(\frac{dH^2}{dx}\right)_{avg} \qquad 2.50$$

Using equation 2.49 and 2.50 the magnetic susceptibility can be written as

$$\chi(t) = \frac{Fm_r}{F_r m}[\chi_r - \frac{\rho_0(t_0)}{\rho_r(t_0)}\chi_0(t_0)] + \frac{\rho_0(t)}{\rho(t)}\chi_0(t) \qquad 2.51$$

where ρ, ρ_r and ρ_0 are densities of the experimental sample, reference sample and air respectively; t_0 is the temperature at which the measurement of the reference sample is made.

The sample was put in a cylindrical quartz container having a volume of nearly 0.1 cm^3. It was hung by a glass capillary between the pole pieces, the value of (dH^2/dx) being 1.1 K. $gauss^2$ / cm approximately. The variation of (dH^2/dx) is 1% over a distance of 1cm along x-direction, while along y and z direction it is practically constant over sufficiently large distances. The temperature of the sample was controlled by temperature controller (Indotherm model 401 D2) having accuracy $\pm 0.5^{\circ}C$. The whole system is

evacuated to avoid disturbance to the balance due to convection in air. The accuracy of measurement using this balance is about 1%.

Trans-decaline a non-volatile liquid at room temperature having $\chi_r = 0.779 \times 10^{-6}$ cm^3 gm^{-1} [43] and density ρ_r=0.869 gm cm^{-3} [44] was used as a reference substance. The necessary correction term in equation 2.51 for $\chi_o(t)$ can be calculated by using the tabulated density of air [45], the magnetic susceptibility of air ($\chi_o = 106.3 \times 10^{-6}$ cm^3 gm^{-1} at 20°C) [46] and the use of curie law $\chi_o \sim 1/T$. I have also neglected the influence of dissolved oxygen as discussed and ignored by de Jeu et al [47].

In the experimental arrangement, the force acting on the sample is exactly balanced by the force exerted on the horizontal coil rigidly attached to the beam balance, placed inside a hollow permanent magnet with a uniform radial field and carrying a suitable current i.

$$F = 2\pi rniH \qquad \textbf{2.52}$$

where, n is number of turns in the coil, r is the radius of the coil and H is the magnetic field intensity. In general the suspended system will experience a force even in the absence of any sample due to the diamagnetism of the sample holder. To compensate this pull an initial current i_o is passed through the coil. In this case, the potential drop across a standard resistance of the order 10KΩ with the help of precision digital voltmeter has been measured. So the final expression for the susceptibility becomes,

$$\chi(t) = \frac{(V - V_o)m_r}{(V_r - V_o)m}\left[\chi_r - \frac{\rho_o(t_o)}{\rho_r(t_o)}\chi_o(t_o)\right] + \frac{\rho_o(t)}{\rho(t)}\chi_o(t) \qquad \textbf{2.53}$$

All the values of magnetic susceptibilities given by me in this thesis are mass susceptibility in c.g.s. unit (erg $gauss^{-2}$ gm^{-1}).

2.15 Description of the experimental set-up for determination of diamagnetic susceptibilities:

The electromagnetic balance for measuring susceptibilities have been designed and fabricated in our laboratory by M. Mitra and R. Paul [48]. Basically the instrument is of the Curie type, the movement of the arms being restricted to the horizontal plane. Schematic diagram of which is shown in Figure 2.3. A horizontal light glass beam (A) is kept suspended at the middle with vertically stretched phosphor-bronze strips (S). The upper portion of which is soldered to a torsion head T, used for adjusting the position of the beam, whereas, the lower end of it terminates in an elliptic spring (E) secured to a universal adjustable holder (H) which can be moved horizontally in two directions. The torsion head is fixed to a brass pillar (D), which serves the electrical connectivity with the brass plate (B) as well. The holder (H) is also fixed on a flat brass plate (B) resting on levelling screws (W). A small perspex block (R) is fixed at one end of the beam balance which is attached to a long glass capillary tube (U) carrying a small glass capsule type sample holder (L) passing through a vertical hole (h2). A damping vane (V) made of thin mica sheet dipping into diffuse pump oil fixed to the other side of the glass beam effectively damps out all spurious vibrations. On the same side of the balance beam is attached a balancing coil of 50 turns of 42 s.w.g. enamelled copper wire wound over a hollow perspex cylinder (C) and the coil is free to move inside a hollow magnet (M) having a radial field of about 200 gauss. The balance assembly is covered with a greased ground bell jar (J). Two holes h1 and h2 are drilled in the base plate. In one of this hole, is fixed an ebonite block with binding terminal, sealed vacuum tight with araldite, for leading in the coil currents. The other terminal of the coil is attached to the brass plate. The second aperture (h2) is

about 3 cm in diameter is fitted with a brass collar for fitting the glass tube extension of the experimental chamber.

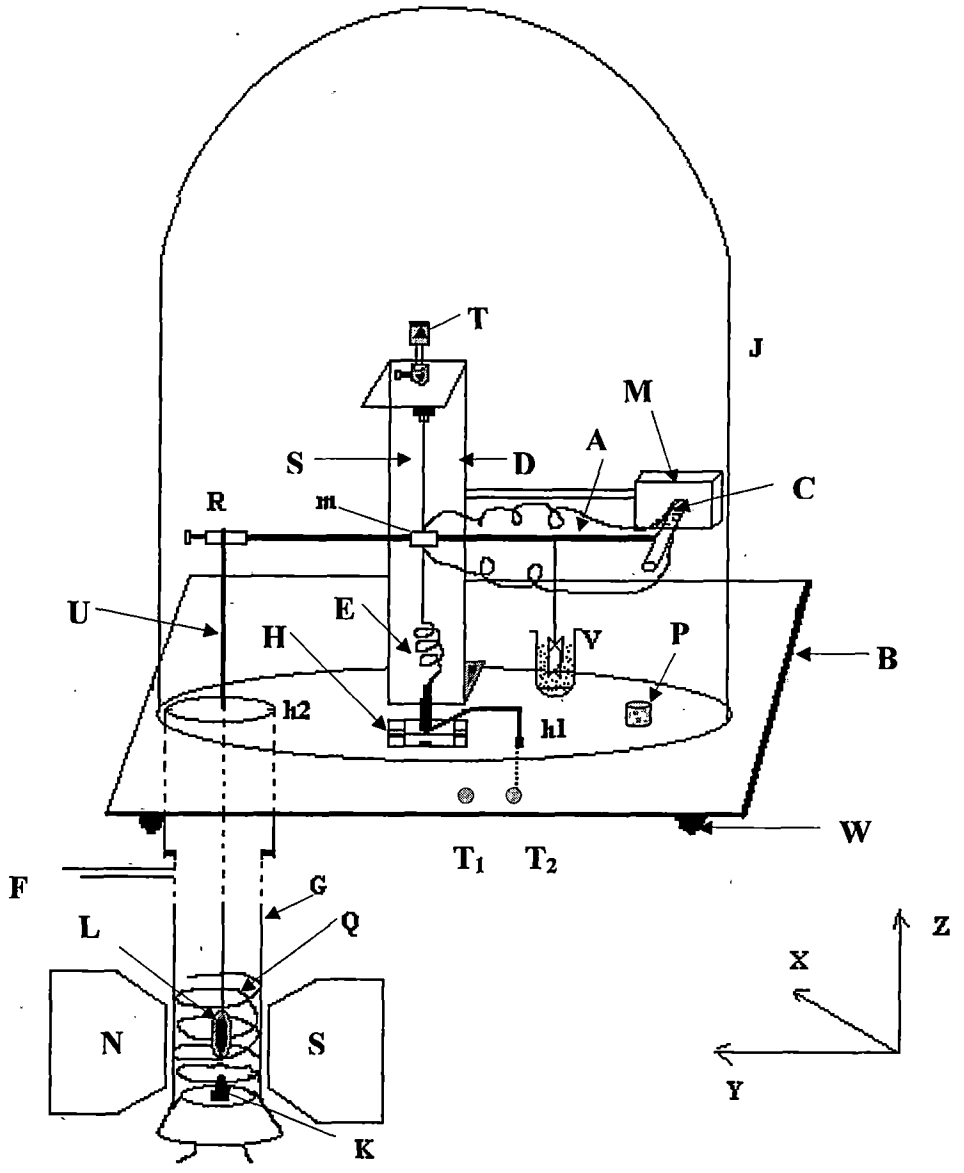

FIGURE 2.3: Schematic diagrams of magnetic susceptibility apparatus.
T- Torsion head, **D**- Brass pillar, **S**- Phosphor-bronze strip, **m**- mirror, **A**- Balance beam, **M**- Magnet, **C**- Coil, **E**- Spring, **G**- Glass tube, **Q**- Heater, **K**- Thermo-couple, **P**- Beaker Containing calcium chloride, **V**- Damping vane, **H**- Adjustable platform, **J**- Bell jar, **B**- Brass plate, **R**- Perspex block, **h1**and **h2**- holes through the brass plate, **U**- Glass capillary tube, **L**- Sample holder, **F**-Side tube connected to vacuum pump, **W**- Levelling screw, T_1-Terminal connected with brass plate & T_2 that with the spring.

The joint of the glass tube (G) and brass tube is made vacuum tight with o-ring. A heater (Q) of constantant wire and a thermocouple (K) is fixed through a rubber stopper and is introduced into the glass tube, which is made vacuum tight. The sample holder, thermocouple and the heater are placed between the pole pieces of an electromagnet. The brass tube is also provided with a side tube (F) through which the balance chamber and the experimental chamber can be evacuated. The sucksmith form of a pole piece is adopted and any change in the position of the sample was detected with the help of a photocells. A laser beam of low intensity is focused on the mirror (m) fixed at the centre of the glass balance and the reflected beam is detected by the photocells, the electrical signal is then amplified and feed to a sensitive moving coil galvanometer, for detecting any change in the position of the sample holder. It should be notated that since the director of the mesogens aligns itself in the direction of the magnetic field ($\Delta\chi > 0$) in most samples, the magnetic susceptibility determined by this method is $\chi_{\parallel}$ in mesophase and $\bar{\chi}$ in isotropic phase. Since non-metallic organic mesogens are diamagnetic, $\bar{\chi}$ should be independent of temperature. Therefore, magnetic susceptibility anisptropy $\Delta\chi$ is calculated by using equation 2.37. Thus the order parameter $\langle S \rangle$ is then calculated using equation 2.48.

2.16 Dielectric permittivity measurement:

One can study the response of the mesogenic substances to the application of electric field by its dielectric behaviour. The liquid crystal molecules may possess permanent dipole moments; in addition induced dipoles are created when external field is applied. Due to the geometrical anisotropy in the molecular structures liquid crystals exhibits anisotropic behaviour. One can

determine $\varepsilon_{\parallel}$ and $\varepsilon_{\perp}$, parallel and perpendicular components of dielectric permittivity by applying electric field parallel and perpendicular to the director. A brief description of experimental set-up is shown in figure 2.4. The dielectric permittivity was measured by a digital LCR-bridge at 10 KHz. The liquid crystal samples were filled in a glass cell. The construction of the cell was done by means of two plane parallel indium tin oxide (ITO) coated (thickness 7000Å and conductivity 10.5-11.5 Ω/square) glass plates separated by glass-spacer of thickness 120μm. The cell was equipped with a guard ring to avoid errors due to stray fields. The guard ring was produced by etching the conducting surfaces on the glass plates. The effective electrode area was 2.3cm x 1.5cm.

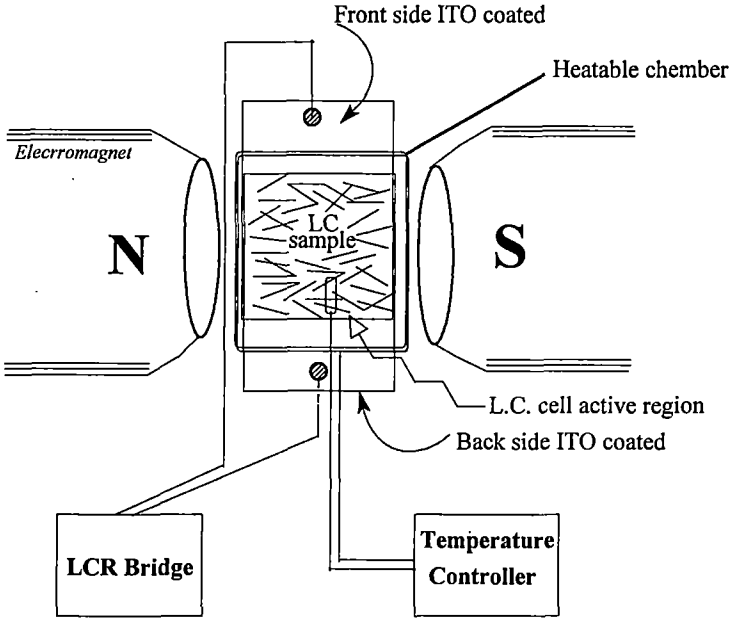

FIGURE 2.4: Schematic diagram of experimental setup for dielectric constant measurement.

The cell was kept inside an electrically heated thermostated brass block having dimension 2.6cm x 2.8cm x 0.5cm, whose temperature was accurately controlled within ±0.5°C using a temperature controller

(Indotherm-457). The whole system was placed between the pole pieces (area 40cm^2, pole gap 3.5cm) of an electromagnet whose field strength could be varied up to 0.32T. The cell was calibrated by measuring the capacitances of standard dielectric liquids within an accuracy of 1%. To determine $\varepsilon_{\parallel}$ and $\varepsilon_{\perp}$, the parallel and perpendicular components of dielectric permittivity capacitances C_a, C_b and C_x of the cell filled with air, benzene (as standard materials) and the liquid crystal sample respectively were measured by applying electric field parallel and perpendicular to the director of the liquid crystal using the following expression

$$\varepsilon_x = 1 + \frac{(C_x - C_a)}{(C_b - C_a)}(\varepsilon_b - 1) \qquad \textbf{2.54}$$

where ε_b and ε_x are the relative permittivities of benzene and the liquid crystalline substance; and that of air is taken as unity.

The dielectric constants $\varepsilon_{\parallel}$ and $\varepsilon_{\perp}$ were determined by measuring the capacitance of the cell with and without the sample at various temperatures keeping the magnetic field parallel and perpendicular to the director respectively [49-52]. The capacitance of the empty cell was found to be 27.4pF at 20°C. Alignment of the sample was established by observing the saturation value of capacitance as magnetic field was increased to about 0.3T. It may be mentioned here that in a magnetic field of about 0.3T we have been able to take well aligned x-ray diffraction photographs in both nematic as well as smectic phases. Since the liquid crystal samples studied are highly insulating the contributions to the capacitance from space charges could be neglected.

2.17 Elastic constant and deformation free energy of nematic liquid crystal:

The elastic properties of a liquid crystal are generated due to restoring torques, which become apparent when the system is perturbed from its equilibrium configuration by some external electric or magnetic field. The director pattern is no longer uniform in space, but curved. If n(r) changes noticeably only over a large distances compared to the molecular dimensions, this curvature can be described in terms of a continuum theory which disregards the details of the structure on a molecular scale. Based on this viewpoint, Zocher [53], Oseen [54], and Frank [55] developed a phenomenological continuum theory of liquid crystals that can successfully explain the various magnetic or electric field induced effect of liquid crystals. According to the continuum theory of liquid crystals, the elastic part of the internal energy density of a perturbed liquid crystal is given by the equation,

$$\mathbf{F}_{def} = \frac{1}{2}[\mathbf{K}_{11}(\nabla \cdot \mathbf{n})^2 + \mathbf{K}_{22}(\mathbf{n} \cdot \nabla \times \mathbf{n})^2 + \mathbf{K}_{33}(\mathbf{n} \times \nabla \times \mathbf{n})^2] \qquad \mathbf{2.55}$$

where **n** is the director; and the coefficients K_{11}, K_{22}, K_{33} are so-called elastic constants associated with three basic types of distortions viz., splay, twist, and bend respectively and are collectively known as the Frank elastic constants. The above equation is the fundamental formula for the continuum theory of nematics. It is possible to generate deformations that are pure splay, pure twist or pure bend. Thus each constant should be positive, if not, the undistorted nematic conformation would not corresponds to a minimum of the free energy F_{def}.

2.18 Fréedericksz transition:

The elastic constants of the liquid crystals can be determined by various methods, of which Fréedericksz transition is one of the simplest and convenient methods. The term Freedericksz transition refers to the deformation of a thin layer of nematic liquid crystal sample with a uniform director pattern in an external electric [56-59] or magnetic field [60-67]. Fréedericksz observed that when a planar surface aligned nematic liquid crystal cell is subjected to magnetic field normal to the director then the cell undergoes an abrupt change in its optical properties if the strength of the external field exceeds the threshold value, known as the critical field. If the nematic liquid crystals have positive diamagnetic anisotropy or dielectric anisotropy, then as the field exceeds the critical value, the director starts to align along the external field. Fréedericksz transitions can be use to measure directly the elastic constants, provided the geometry i.e., the boundary conditions and the direction of the applied field are chosen in a appropriate way as shown schematically in figures 2.4.

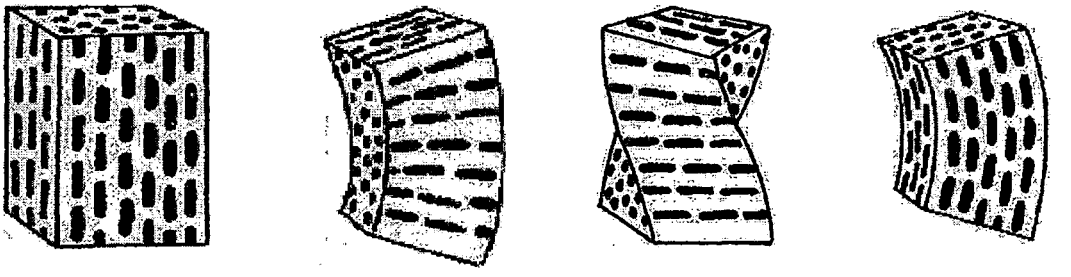

Equilibrium Configuration **Splay** **Twist** **Bend**
(a) (b) (c) (d)

FIGURE 2.4: (a) An ordered liquid crystal in equilibrium configuration. The deformation states – (b) splay, (c) twist, and (d) bend.

From the geometry of arrangement as shown in figure 2.5(a-c), one can determine the splay, twist or bend elastic constants in the magnetic field H.

The threshold magnetic field for the splay, bend or twist deformation is related to the elastic constants by the equation

$$(H_C)_i = \frac{1}{2}\left(\frac{K_{ii}}{\Delta\chi}\right)^{\frac{1}{2}}\frac{\pi}{d} \qquad 2.56$$

where d is the sample thickness, $\Delta\chi$ is the diamagnetic anisotropy and $(H_c)_i$ is the respective critical magnetic field. Also the subscript i =1, 2, 3 refers to the splay, twist and the bend deformation respectively.

To explain the Fréedericksz transition, I have considered a uniform planer layer i.e., in the splay mode, for a magnetic field $H>H_c$, applied along z-axis, the uniform planer structure (figure 2.5(d)) is unstable and the system jumps into one of the two possible states (figure 2.5(e) or 2.5(g)). If the field is increase further ($H >> H_c$) these states develop into pattern as shown in figure 2.5(f) and 2.5(h).

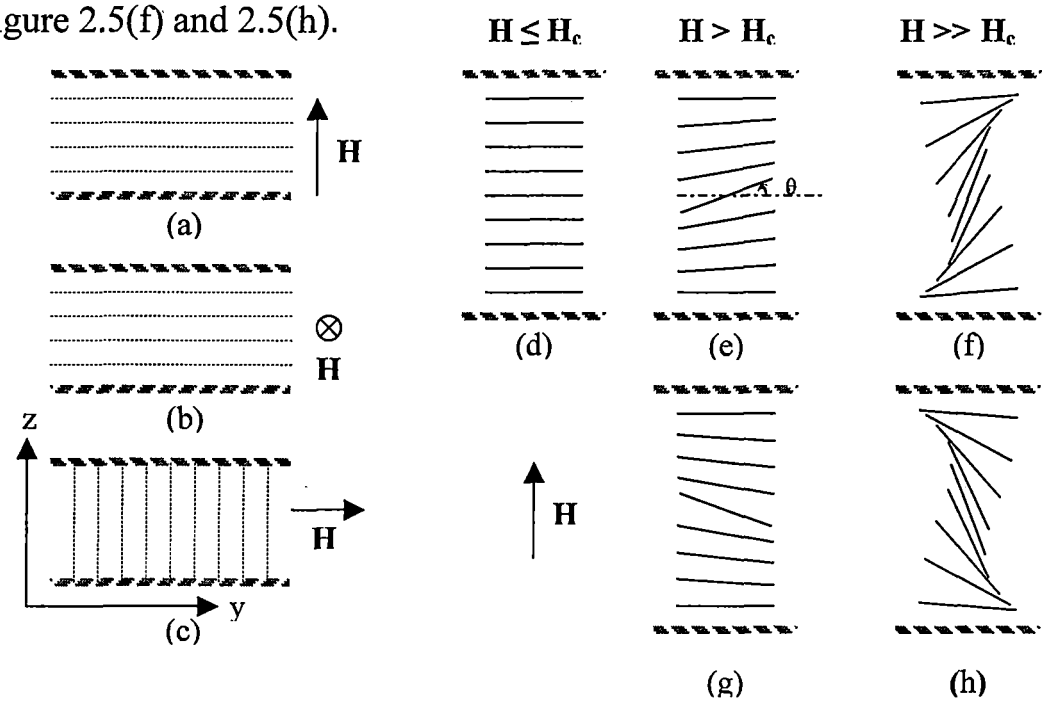

FIGURE 2.5: Schematic experimental set-up for determination of (a) splay, (b) twist, and (c) bend; Deformation of director pattern above threshold field in the splay (d-h) mode.

2.19 Description of Experimental set-up for determination of K_{11} and K_{33}:

The apparatus of the determination of the elastic constants (K_{11} and K_{33}) has been designed and fabricated in our laboratory by M. K. Das and R. Paul [68]. The block diagram of the experimental set-up has been shown in figure 2.6 for studying elastic constants by Freedericksz transition method.

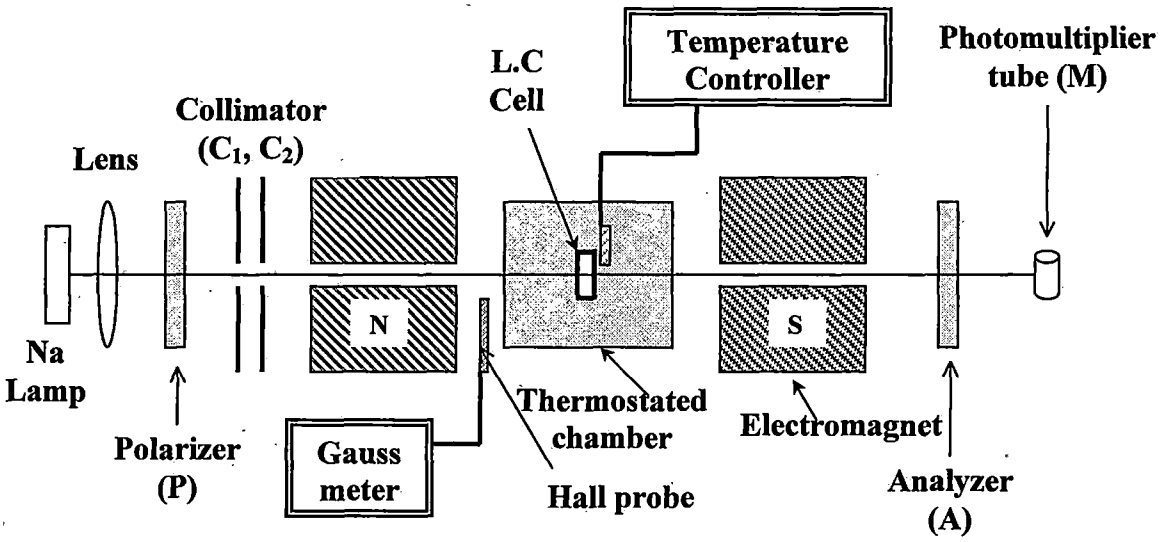

FIGURE 2.6: Schematic experimental set-up for the determination of the elastic constants from Freedericksz transition: (a) splay, (b) twist and (c) bend.

The liquid crystal sample was taken in a glass cell housed in a thermo-stated brass oven that has a groove at the proper angle, whose temperature was controlled within an accuracy of ± 0.5°C by means of a temperature controller (Indotherm model 457). A monochromatic beam of sodium-D light is incident on the sample through a lens (L), polarizer (P) and collimating circular slits (C_1, C_2). The transmitted light intensity was detected by a photomultiplier tube (M) that counts photon and corresponding current was measured by a nano-ammeter. The polarizer (P) and the analyzer

(A) were placed in crossed position (at ±45° relative to the vertical axis) in front of the photomultiplier. For the Fréedericksz transition to occur, the director must be truly oriented at right angle to the external field. In order to ensure this exact alignment, the brass oven was mounted on a specially constructed platform whose alignment with respect to the field could be adjusted to an accuracy of 1-2′ of arc. The magnetic field is varied slowly so that the nematic orientation remains in equilibrium with the applied magnetic field. For desired temperature, it was observed that when the field (H) exceeds a critical value (H_c) then there was a drastic change in the optical properties of the sample. Thus we could measure the threshold field intensity (H_c) from the field versus intensity curve within an accuracy of ±10 Gauss. The magnetic field was measured using a Hall-probe Gaussmeter (Model DGM-102). If the field was increased gradually beyond its critical value, the transmitted light exhibits oscillations due to the change of phase relation.

The liquid crystal sample is taken between two plane parallel glass plates separated by glass spacer of thickness 160μm. The splay elastic constant (K_{11}) is measured using a cells with homogeneous planer alignment, where inside surface of the glass plates were treated with 1% aqueous solution of polyvinyl alcohol dried and then rubbed the layer in one direction with tissue paper. Whereas in case of bend elastic constant (K_{33}) measured by using homeotropic cells, which were prepared by the surface treatment of the glass plates with dilute solution of cetyl tri-methyl ammonium bromide (CTAB) or lecithin.

In the present set-up it is not possible to measure K_{22}. The threshold field for twist deformation cannot be detected optically when viewed along the twist axis. Due to the large birefringence of the medium for this direction of propagation, the state of polarisation of the transmitted beam is indistinguishable from that of the emerging beam from the untwist nematics. A total internal reflection technique can be used to measure the K_{22} values of the twist deformation. In my present work however, I have measured only K_{11} and K_{33} values at different composition of a binary liquid crystalline mixture.

2.20 Structure and chemical name of the liquid crystals studied:

The chemical names of the liquid crystals studied in the present investigation and their structural formula are given below:

1. 4-n-pentyl phenyl 4 - n′- pentyloxy benzoate (ME5O.5 in short).

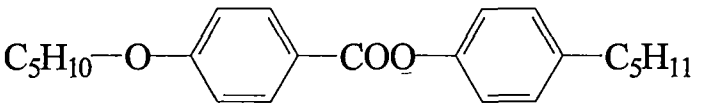

2. 4-n-pentyl 4′ cyanobiphenyl (5CB in short).

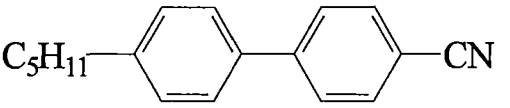

3. undecycloxy cyanobiphenyl (11OCB in short).

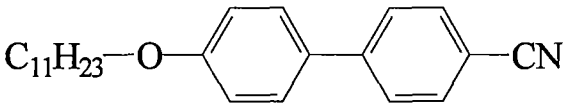

4. 4-n-hexyl phenyl 4-n′-pentyloxy benzoate (ME6.O5 in short).

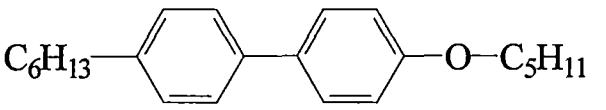

5. 4-n-pentyl phenyl 4-n′-hexyloxy benzoate (ME6O.5 in short).

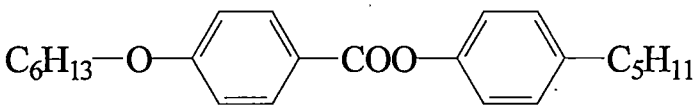

6. p-cyanophenyl trans –4-pentyl cyclohexane carboxylate (CPPCC in short)

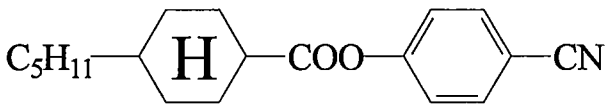

7. 4(3"-pentenyl) 4′(ethoxyl) 1,1′ bicyclohexane (1d(3)CCO_2) in short)

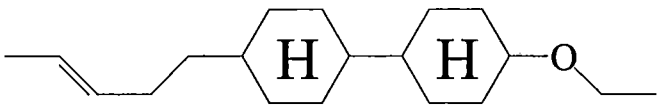

8. 4-ethoxy, 4′-Pent-4"-enyl bicyclohexane (0d(4)CCO_2) in short)

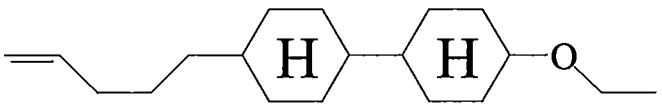

The liquid crystals 1, 2, 3, 4, 5, 6 were obtained from E. Merck, UK; and 7, 8 were obtained from M/S Hoffmann-La Roche & Co., Basel, Switzerland. All the samples were obtained in the pure state and were studied without further purification.

References:

1. E. B. Priestley, P. J. Wojtowicz and P. Sheng, (Eds.), *"Introduction to Liquid Crystals"*, Plenum, New York, (1974).
2. S. Chandrasekhar, *"Liquid Crystals"*, Cambridge University Press, Cambridge, (1977).
3. G. Vertogen and W. H. de Jue, *"Thermotropic Liquid Crystals, Fundamentals"*, Springer-Verlag (1988).
4. G. R. Luckhurst and G. W. Gray, (Eds.), *"The Molecular Physics of Liquid Crystals"*, Academic Press (1979).
5. P. G. de Gennes, *"The Physics of Liquid Crystal"*, Clarendon Press, Oxford, (1974).
6. G. H. Brown, (Ed.), *"Advances in Liquid Crystals"*, **6**, Chapter 1, Academic Press (1983).
7. W. Maier and A. Saupe, *Z. Natureforch*, **13a**, 564 (1958); ibid., **14a**, 882 (1959); ibid., **15a**, 287 (1960).
8. W. L. McMillan, *Phys. Rev.*, **A4**, 1238 (1971).
9. R. L. Humphries, P. G. James and G. R. Luckhurst, *J. Chem. Soc., Faraday Trans. II*, **68**, 1031 (1972).
10. W. L. McMillan, *Phys. Rev.*, **A6**, 936 (1972).
11. K. K. Kobayashi, *J. Phys. Soc.* (Japan), **29**, 101 (1970).
12. K. K. Kobayashi, *Mol. Cryst. Liq. Cryst.*, **13**, 137 (1971).
13. D. Demus and L. Richter, *"Textures of Liquid Crystals"*, Verlag Chemie, New York (1978).
14. B. K. Vainstein and I. G. Chistyakov, *"Problem of Modern Crystallography"*, Nauka, Moscow (1975).

15. B. K. Vainstein, *"Diffraction of x-rays by Chain Molecules"*, Elsevier Pub. Co. (1966).

16. A. J. Leadbetter, *"The Molecular Physics of Liquid Crystals"*, Eds. G. R. Luckhurst & G. W. Gray, Chap.13, Academic Press (1979).

17. A. de Vries, *Mol. Cryst. Liq. Cryst.*, **10**, 219 (1970).

18. B. Jha and R. Paul, *Proc. Nucl. Phys. Solid State Phys. Symp.*, India, **19c**, 491 (1976).

19. H. P. Klug and L. E. Alexander, *"X-ray diffraction procedures"*, John Wiley and Sons, N.Y., p.114 and 473 (1974).

20. A. J. Leadbetter and E. K. Norris, *Mol. Phys.*, **38**, 669 (1979).

21. R. J. Birgeneau and J. D. Litster, *J. Phys. Letts.*, **39**, L399, (1978).

22. A. de Vries, *Liquid Crystals*, Ed. F. D. Saeva, M. Dekker Inc., NY(1979).

23. R. Paul and G. Chaudhuri, Abstract in the 14th International Liquid Crystal Conference, Pisa, 1992, Abs.no.- H-P23.

24. E. Dorn, *Z. Physik*, **11**, 111, (1910).

25. E. Gorecka, Li Chen, O. Lavrentovich and W. Pyzuk, *Europhysics Letters*, **27(7)**, 507 (1994).

26. O. Weiner, S. Ber. Sachs. Ges. Wissensch., **61**, 113 (1909).

27. W. H. Pness, S. A. Teukolsky, W. T. Vellering and B. P. Flannery, Cambridge University Press, Chap- 15. (1986).

28. S. Ergun, *J. Appl. Cryst.*, **1**, 19 (1968).

29. H. Zocher, *Naturwiss.*, **13**, 1015 (1925).

30. H. Zocher, *Z. Krist.*, 79, 122 (1931).

31. F. Grandjean, *Compt. Rend.*, **168**, 408 (1919).

32. N. V. Madhusudana, R. Sashidhar and S. Chandrasekhar, *Mol. Cryst. Liq. Cryst.*, **13**, 61 (1971).

33. A. Saupe and W. Maier, *Z. Natureforsch*, **16a**, 816 (1961).

34. H. E. Neugebauer, *Canad. J. Phys.*, **32**, 1 (1954).

35. M. F. Vuks, *Optics and Spectroscopy*, **20**, 361 (1966).

36. P. G. de Gennes, *Mol. Cryst. Liq. Cryst.*, **12**, 193 (1971).

37. I. Haller, H. A. Huggins, H. R. Lilienthal and T. R. McGuire, *J. Phys. Chem.*, **77**, 950 (1973).

38. A. K. Zeminder, S. Paul and R. Paul, *Mol. Cryst. Liq. Cryst.* , **61**, 191 (1980).

39.P. G. de Gennes, *"The Physics of Liquid Crystal"*, Clarendon Press, Oxford, p.31 (1974). (1961).

40. J. P. Dias, *C. R. Acad. Sci.*, Se'r, **A282**, 71 (1976).

41. J. O. Kessler, *Liq. Cryst. Ord. Fluids*, p. 361 (1970).

42. V. Tsvetkov, *Acta Physicochim.* USSR, **16**, 132, (1942).

43. CRC Handbook of Chemistry and Physics, 58th edition, p. E-128. (1977-78).

44. CRC Handbook of Chemistry and Physics, 58th edition, p. C-270 (1977-78).

45. CRC Handbook of Chemistry and Physics, 58th edition, p. F-9 (1977-78).

46. A. Burris and C. D. Hause, *J. Chem. Phys.*, **11**, 442 (1943).

47. W. H. de Jue and W. A. P. Claassen, *J. Chem. Phys.*, **68**, 102 (1978).

48. M. Mitra and R. Paul, *Mol. Cryst. Liq. Cryst.*, **148**, 185 (1987).

49. A. Christine Rauch, Shila Garg and D.T. Jacobs, *Phase transitions in a nematic binary mixture, J. Chem. Phys*, **116**, 2213(2002).

50. Shila Garg and Tom Spears, Dielectric properties of nematic binary mixture. *Mol. Cryst. Liq. Cryst.*, **409**, 335(2004).

51.H. Kresse, (Ed.) G. H. Brown *Dielectric behaviour of liquid crystal, Adv. Liquid Crystal*, **6**, 109 (1983).

52. W. Haase and S. Wróbel (Eds.), *Relaxation Phenomena*, (2003).

53.H. Zocher, *Trans Faraday Soc.*, **29**, 945 (1933).

54. C. W. Oseen, *Trans Faraday Soc.*, **29**, 883 (1933).

55. F. C. Frank, *Faraday Soc. Discussion*, **25**, 19 (1958).

56. H. Gruler, T. J. Schiffer and G. Meier, *Z. Natureforsh*, **27a**, 966 (1972).

57. H. Gruler and L. Cheung, *J. Appl. Phys.*, **46**, 5097 (1975).

58. H. Deuling, (Ed.) L. Liebert, *Liquid Crystals, Solid State Physics* Suppl. no. 14, p. 77, Academic Press, NY.

59. M. J. Bradshaw and E. P. Rayens, *Mol. Cryst. Liq. Cryst.*, **72**, 35 (1980).

60. V. Freedericksz and V. Tsvetkov, *Phy. Z. Soviet Union*, **6**, 490 (1934).

61. V. Freedericksz and V. zolina, *Trans. Faraday Soc.*, **29**, 919 (1933).

62. P. P. Karat and N. V. Madhusudana, *Mol. Cryst. Liq. Cryst.*, **40**, 239 (1977).

63. H. P. Schad, M. A. Osman, *J. Chem. Phys.*, 75 (2), 880 (1981).

64. F. Leenhouts, H. J. Boeber, A. J. Dekker and J. J. Jonker, *J. Phys. (Paris) Colloque.*, **40**, C3-291 (1979).

65. H. P. Schad, G. Bauer and G. Maier, *J. Chem. Phys.*, **67**, 3705 (1977).

66. F. Leenhouts and A. J. Dekker, *J. Chem. Phys.*, **74**, 1956 (1981).

67. H. P. Schad, G. Bauer and G. Maier, *J. Chem. Phys.*, **70**, 2770 (1979).

68. M. K. Das and R. Paul, *Mol. Cryst. Liq. Cryst.*, **259**, 13 (1995).

Chapter 3

Orientational Order Parameter of a Binary Liquid Crystal Mixture Showing Induced Smectic Phase

3.1 Introduction:

Binary mixture of 4-n-pentyl 4′-cyanobiphenyl (5CB) and 4-n-pentyl phenyl 4-n′-pentyloxy benzoate (ME5O.5) shows the presence of an induced smectic A phase whereas the pure compounds show only nematic phase. Phase diagram of this system has been reported by Dunmur et al [1]. They have measured transition enthalpies, refractive indices and electric permittivities at different composition of mixtures of these compounds. Using an empirical scaling procedure they have calculated the orientational order parameter only in the nematic phase above the induced smectic phase. Using an extension of Maier-Saupe theory, Palffy-Muhoray et al [2] have determined the nematic-isotropic co-existence region for the entire range of concentrations of this system and they have proposed a relation between the refractive index of the binary mixture and order parameters of its components in the nematic phase. Das et al [3] using x-ray diffraction technique have earlier reported the orientational order parameters, layer thickness and apparent molecular length for a series of mixtures at different temperatures and different concentrations for this system. Hence, it is of interest to determine order parameters from refractive index and density measurements in both induced smectic and nematic phases and compared with those found from x-ray studies.

In this chapter, I have reported the density and refractive indices (n_o, n_e) of this system in the entire composition range. The refractive index and density data have been analyzed to measure the orientational order parameters. These values have been compared with McMillan's theory [4-5] for mixtures having smectic A phase and Maier-Saupe theory [6] for others having nematic phase only. Since both layer thickness [3] and density values as observed in this work show a definite minimum near equimolar concentration, it is of great interest to know how the molecules

are arranged in a plane perpendicular to the director. Hence I have taken the x-ray diffraction photographs of orientated sample for all the mixtures at a temperature T = 35°C, in order to measure the average lateral distance between the molecules, which has not been reported in the previous x-ray work [3].

3.2 Texture study and phase diagram:

The chemicals ME5O.5 and 5CB were donated by E. Merck, U.K. Ten mixtures with mole fractions (x) of 5CB equal to 0.15, 0.207, 0.305, 0.40, 0.465, 0.501, 0.590, 0.64, 0.702, 0.80 were prepared.

Compound 1:

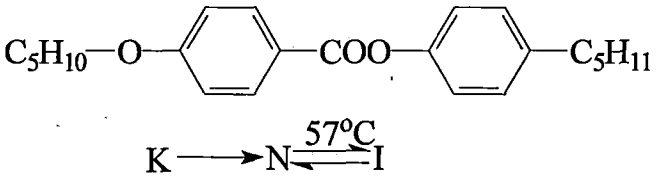

4-n-pentyl phenyl 4 - n′- pentyloxy benzoate (ME5O.5 in short)

Compound 2:

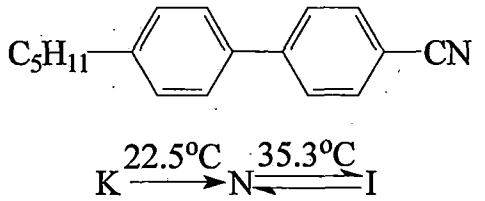

4-n-pentyl 4′ cyanobiphenyl (5CB in short)

The phase diagram of this system is obtained by studying the transition temperatures and textures of different mixtures under crossed polariser with a polarizing microscope equipped with a hot stage (Mettler FP 80/82). The measured transition temperature values agree well with the values obtained from the phase diagram of this system given by Dunmur et al [1].

Phase diagram of this system as observed by me, is similar to that obtained by Dunmur et al [1], and is shown in figure 3.1.

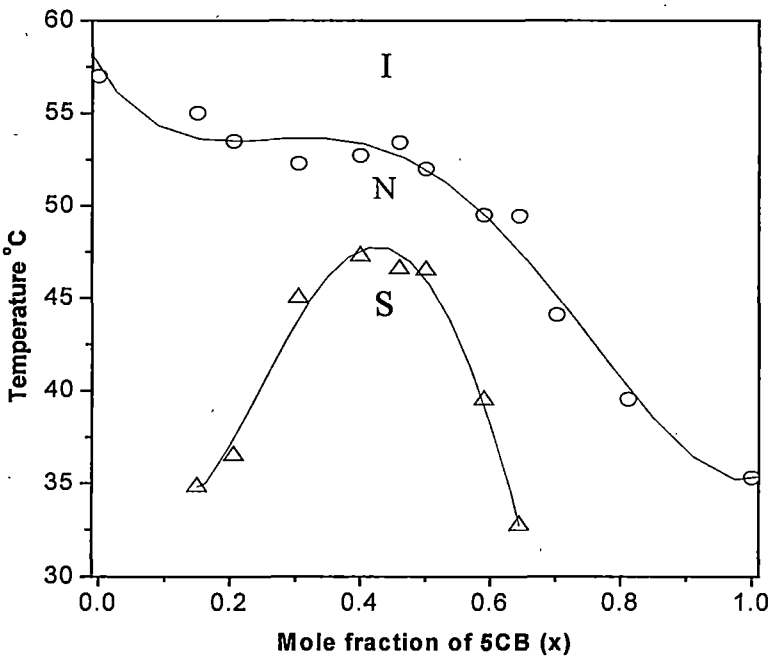

FIGURE 3.1: Phase diagram of 5CB/ME5O.5 as a function of mole fraction (x) of 5CB. ○ T_{NI}, △ T_{SN}.

3.3 Density measurement:

I have measured the variation of density for the entire mesomorphic range; the experimental technique is given in chapter 2 of this thesis. Figure 3.2 shows the variation of density values with temperature. The density as a function of temperature for x=0.4 only have been reported by Das et al [3].

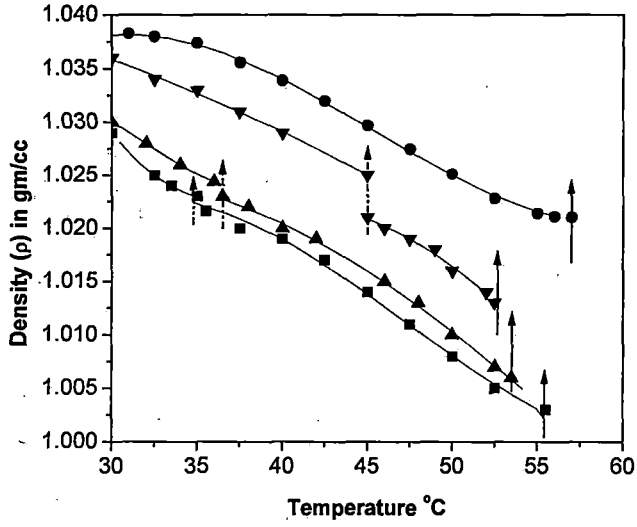

FIGURE 3.2 (a): Temperature dependence of density values for 5CB/ME5O.5 mixtures at different compositions, x = mole fraction of 5CB. ● x = 0.0; ■ x = 0.15; ▲ x = 0.207; ▼ x = 0.305. ↑ indicates S-N and ↑ N-I transition temperature.

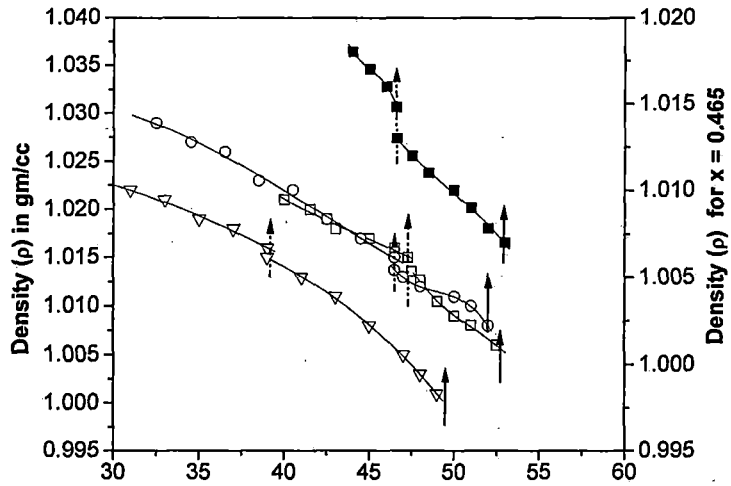

FIGURE 3.2(b): Temperature dependence of density values for 5CB/ME 5O.5 mixtures at different compositions, x = mole fraction of 5CB. □ x = 0.40; ■ x = 0.46; ○ x = 0.501; ▽ x = 0.59. ↑ indicates S-N and ↑ N-I transition temperature.

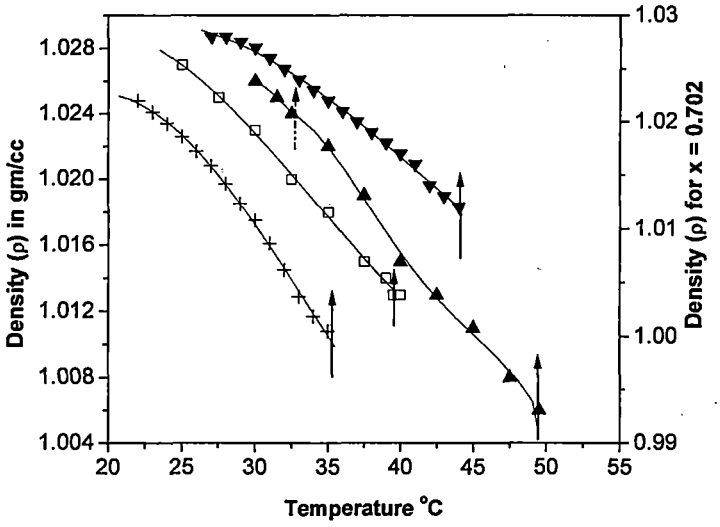

FIGURE 3.2(c): Temperature dependence of density values for 5CB/ME 5O.5 mixtures at different compositions, x = mole fraction of 5CB. ▲ x = 0.645; ▼ x = 0.702; □ x = 0.812; + x = 1.0. ↑ indicates S-N and ↑ N-I transition temperature.

3.3 Birefringence study:

Refractive indices (n_o, n_e) for λ = 5780Å have been measured within ±0.001 by the thin prism method. Experimental set up and the procedure for order parameter determination from refractive indices studies have been described in detail in chapter 2 of this thesis.

In figure 3.3, I have plotted optical birefringence ($\Delta n = n_e - n_o$) values for different mixtures as a function of temperature. Δn and density values of 5CB have already been reported earlier [7,8]. The change in density as well as birefringence (Δn) values at the smectic A to nematic phase transition is discontinuous near x = 0.4 and the discontinuity decreases gradually above and below this concentration, in agreement with the transition entropy and refractive index measurements by Dunmur et al [1]. This indicates that a first order SmA - N phase transition occurs near the center of the phase diagram.

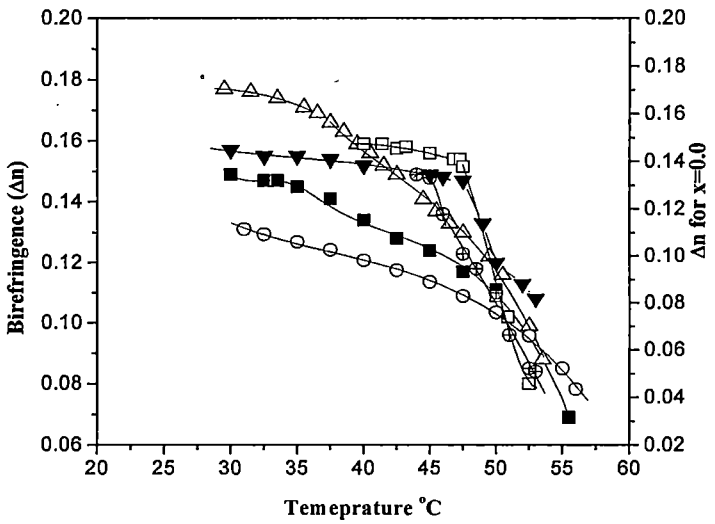

FIGURE 3.3 (a): Birefringence (Δn) values as a function of temperature for different mixtures. ○ x = 0.0; ■ x = 0.15; △ x = 0.207; ▼ x = 0.305; □ x = 0.4; ⊕ x = 0.46.

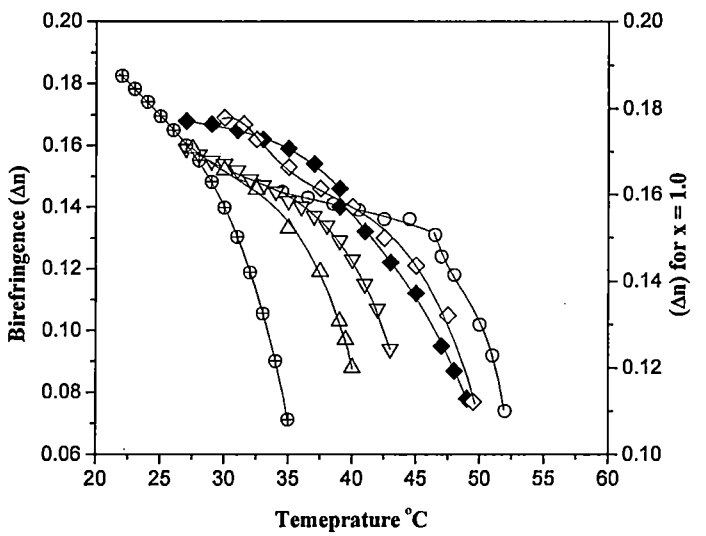

FIGURE 3.3 (b): Birefringence (Δn) values as a function of temperature for different mixtures. ○ x = 0.501;◆ x = 0.59;◇ x = 0.645;▽ x = 0.702;△ x = 0.812; ⊕ x = 1.0 (from Karat et al. [10])

The first order phase transition changes to second order for mixtures of higher and lower concentration of 5CB. The refractive index data have been analyzed to determine the polarizability values (α_e and α_o) using Neugebauer's [9] method. The polarizability anisotropy for a perfectly

ordered sample, i.e., at $<P_2>=1$ was obtained from these data using extrapolation procedure given by Haller et al [10]. Since the temperature variation of $\Delta\alpha$ is large in nematic phase, but in most of the smectic A phase this variation is very small, so I have plotted Haller's extrapolation by taking the values of α_e and α_o in only nematic phase. The order parameter $<P_2>$ is calculated from the well-known relation,

$$< P_2 >= \frac{\alpha_e - \alpha_o}{\alpha_{\parallel} - \alpha_{\perp}} \qquad \textbf{3.1}$$

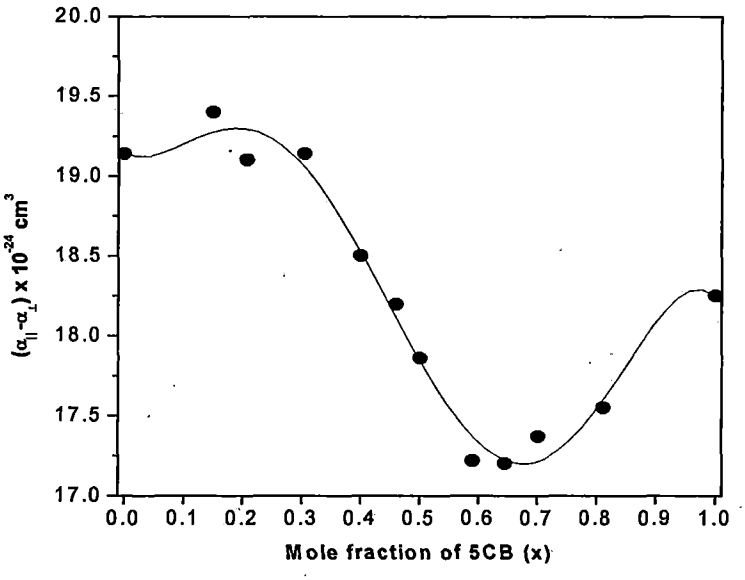

FIGURE 3.4: Polarisability anisotropy ($\alpha_{\parallel}$- $\alpha_{\perp}$) against mole fraction of 5CB. • Neugebauer's method.

As shown in figure 3.4, $\alpha_a = (\alpha_{\parallel} - \alpha_{\perp})$ decreases near equimolar concentration. It is to be noted that from x-ray diffraction studies, Das et al [3] have found a definite minimum in layer spacing or apparent molecular length at the same concentration. Since anisotropy is proportional to the apparent molecular length, the present observation is in agreement with the x-ray results. In figure 3.5(a) to 3.5(f), I have plotted the variation of $<P_2>$ values with temperature. The experimental order parameter values at the smectic A to nematic phase transition appears to be

of the first order in the mixtures for x ≈ 0.45. A second order phase transition is observed for mixtures with x < 0.4 and also x > 0.5. Moreover, in the middle of the phase diagram change in $\langle P_2 \rangle$ is very large at SmA - N phase transition.

I have also fitted the experimentally determined orientational order parameter having an induced smectic phase to McMillan's theory using the mean field potential,

$$V_M(\cos\theta, z) = -v[\alpha\delta\tau \cos\left(\frac{2\pi z}{d}\right) + \{\eta + \alpha\delta \cos\left(\frac{2\pi z}{d}\right)\} P_2(\cos\theta) \qquad \textbf{3.2}$$

where α and δ are adjustable parameters. In fitting $\langle P_2 \rangle$ values to the McMillan's model, it is difficult to vary α and δ independently. Hence, I have assumed that intermolecular pair potential does not change with composition and have taken constant δ values over the entire composition range (δ=0.67). The α values show a broad maximum near x = 0.4. This is expected since near x = 0.4 smectic phases occurs at a relatively higher temperature and is separated from the isotropic phase by narrow temperature range nematic phase.

The order parameter values calculated using Neugebauer's relation do not agree well with Maier-Saupe theory for ME5O.5. But, in case of 5CB and mixtures with x = 0.702 and 0.812, where only nematic phases are present, the agreement with the theory is good (figure 3.5(e)-(f)). However, in all the mixtures as well as in pure compounds the experimental OOP values near N - I transition are significantly lower than the theoretical values. This may be due to the fluctuations of director, which is more pronounced near the clearing point.

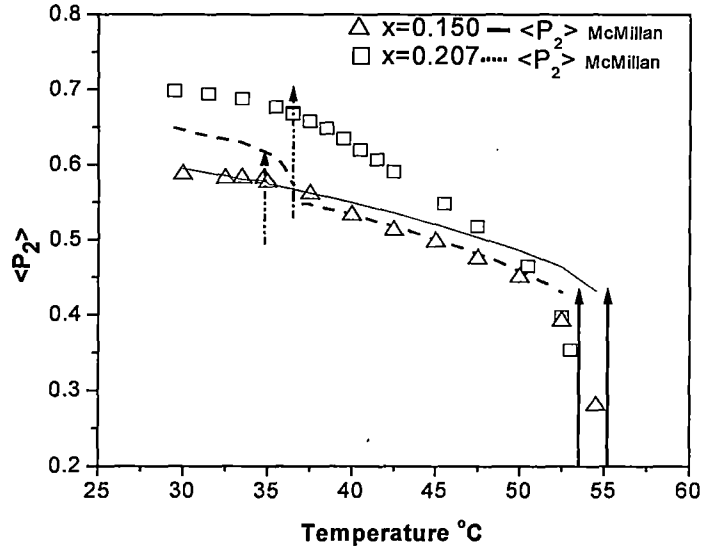

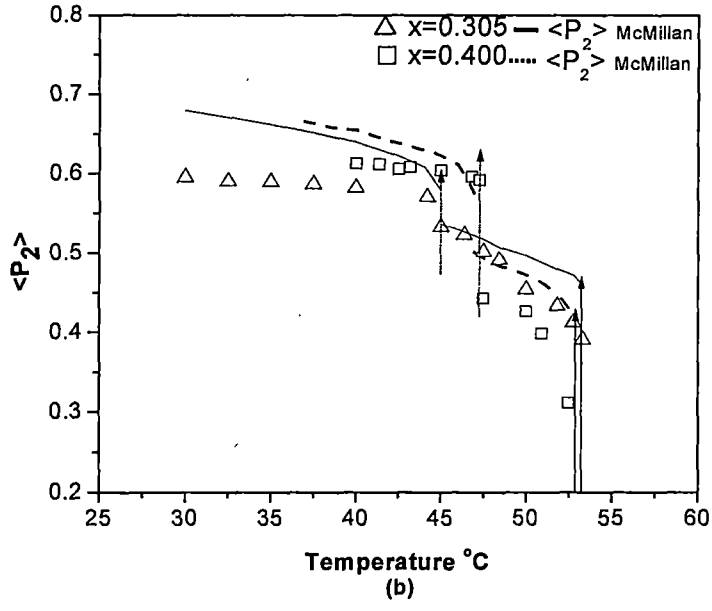

FIGURE 3.5(a) – 3.5(b): Variation of $\langle P_2 \rangle$ with temperature for different mixtures having induced smectic A phase. △ Experimental $\langle P_2 \rangle$ for x = 0.15, 0.305; □ experimental $\langle P_2 \rangle$ for x = 0.207, 0.40; — calculated from McMillan's theory for x = 0.15 (α=0.346, δ=0.67), 0.305 (α=0.424, δ=0.67); and -- calculated from McMillan's theory for x = 0.207 (α=0.39, δ=0.67), 0.40 (α=0.433, δ=0.67). ↑ indicates S-N and ↑ N-I transition temperature.

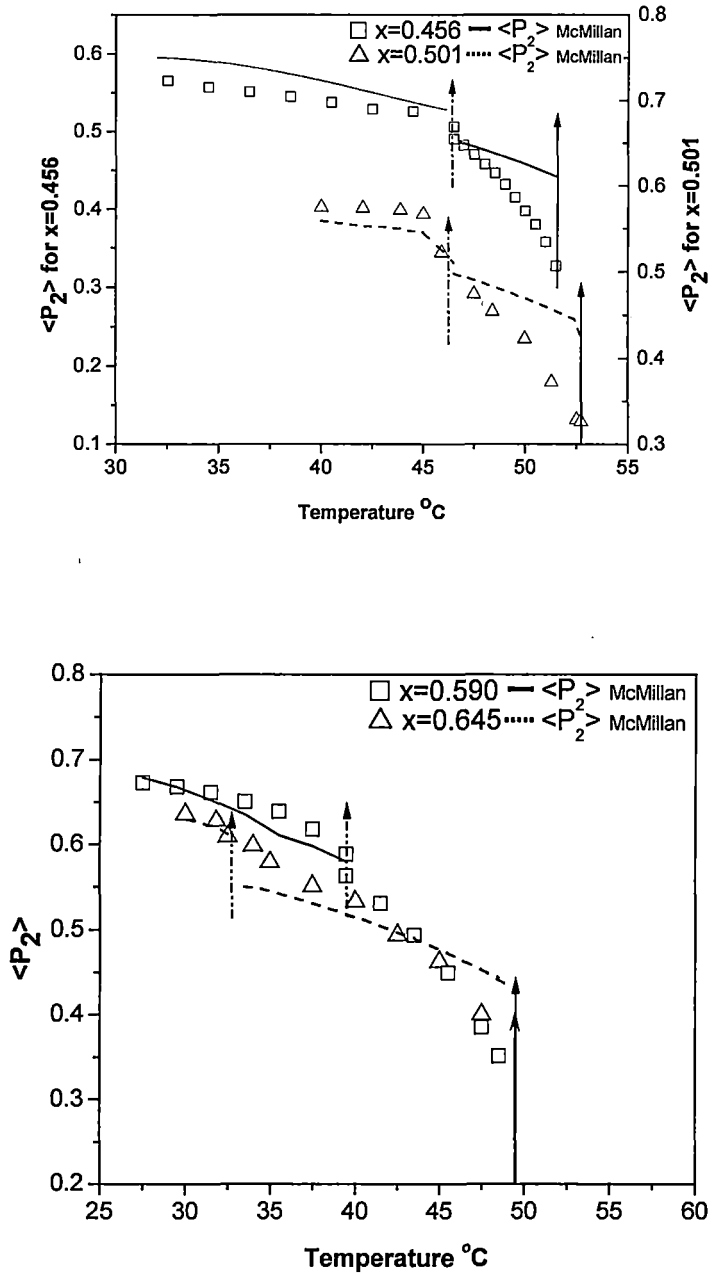

FIGURE 3.5(c) – 3.5(d): Variation of $\langle P_2 \rangle$ with temperature for different mixtures having induced smectic A phase. △ Experimental $\langle P_2 \rangle$ for x = 0.465, 0.59; □ experimental $\langle P_2 \rangle$ for x = 0.501, 0.645; — calculated from McMillan's theory for x = 0.465 (α=0.46, δ=0.67), 0.59 (α=0.346, δ=0.67); and -- calculated from McMillan's theory for x = 0.501 (α=0.433, δ=0.67), 0.645 (α=0.39, δ=0.67). ↑ indicates S-N and ↑ N-I transition temperature.

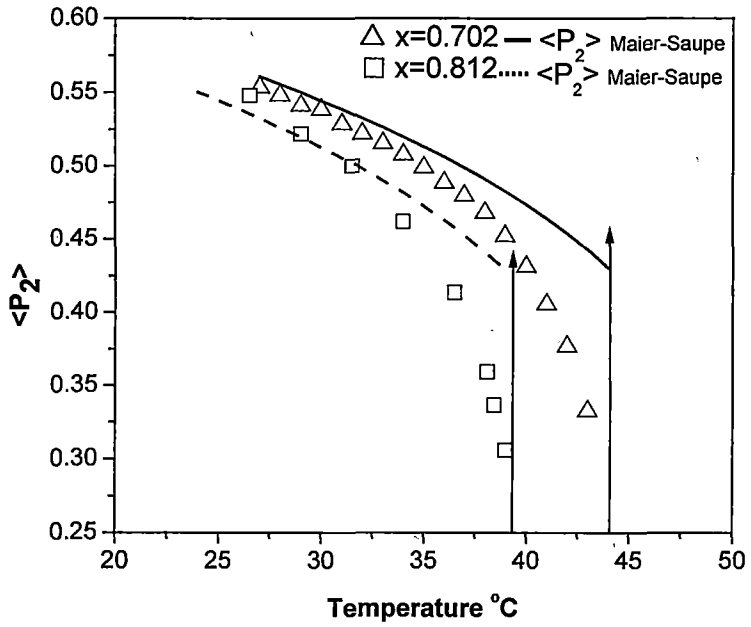

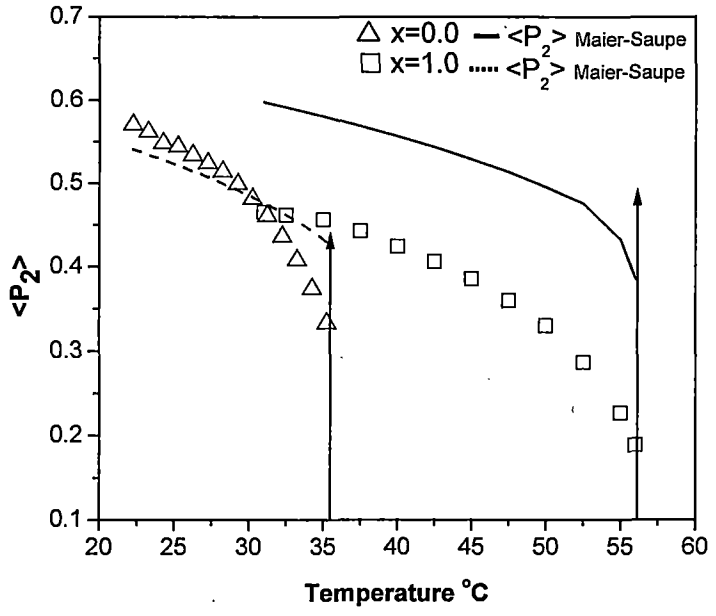

FIGURE 3.5(e)-3.5(f): Variation of $\langle P_2 \rangle$ with temperature for different mixtures having nematic phase only. △ Experimental $\langle P_2 \rangle$ for x = 0.00, 0.702; □ experimental $\langle P_2 \rangle$ for x = 0.812, 1.0; — calculated from Maier-Saupe theory for x = 0.702, 0.812, and -- calculated from Maier- Saupe theory for x = 0.0, 1.0. ↑ indicates N-I transition temperature.

The experimental OOP values in the smectic A phase agree well with those calculated from McMillan's theory for mixtures having x = 0.15, 0.645, in the region of the phase diagram where the experimental order parameter $\langle P_2 \rangle$ values change continuously across the SmA-N phase transition. However, the agreement between the calculated and the experimentally determined OOP values is rather poor for mixtures having x = 0.207, 0.305, 0.465, 0.501, 0.590, where $\langle P_2 \rangle$ values change discontinuously at the smectic A to nematic transition, except for x = 0.207.

3.4 X-ray diffraction measurement:

X-ray diffraction photographs of magnetically aligned samples was taken at a particular temperature T=35°C. The experimental technique employed to obtain x-ray diffraction data and subsequent analysis has also been described in chapter 2.

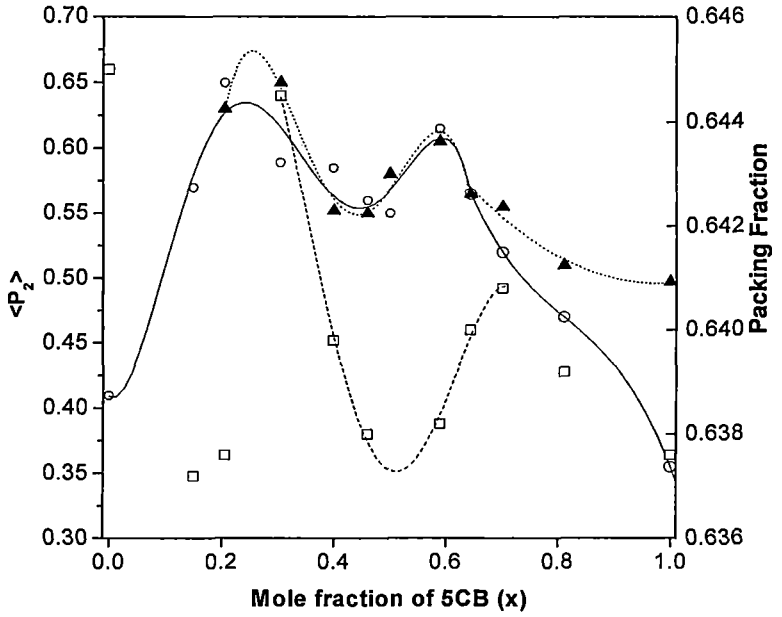

FIGURE 3.6: Variation of $\langle P_2 \rangle$ values obtained from refractive index measurements and that of from X-ray measurements and packing fraction at a temperature T=35°C ○ — <P2> from refractive index measurements, ▲ ····· $\langle P_2 \rangle$ from X-ray measurements, □ packing fraction.

Figure 3.6, shows the variation of orientational order parameters both from refractive index and x-ray diffraction measurements [3] and packing fractions at 35°C. The packing fraction is defined as the ratio of the geometrical volume (Vander waal's volume) to the volume occupied per molecule in the mesophases. Following Kitaigordsky [11], I have calculated the geometrical volume of the pure components V_A and V_B, where A, B refers to 5CB and ME5O.5 molecules respectively. Now, if ρ be the density of a mixture at any temperature and N be the Avogadro's number, then packing fraction

$$= \rho N \frac{(x_A V_A + x_B V_B)}{(x_A M_A + x_B M_B)} \qquad \textbf{3.3}$$

where x_A, x_B and M_A, M_B are the mole fractions and molecular weights of the respective molecules in the mixture.

From figure 3.6 it is clear that the OOP's in the smectic phase and the packing fraction values show definite minimum around x = 0.4. The birefringence (Δn), density (ρ) also follows the same trend indicating that the packing in nearly equimolar mixtures is rather loose. Similar behaviour is also observed in the nematic phase where the smectic A phase is the precursor of the nematic phase (figure 3.7). This may due to the smectic fluctuations presents in the nematic phase.

The OOP values from refractive index measurements agree quite well with the values obtained from X-ray diffraction measurements. The lower values of $\langle P_2 \rangle$ from refractive index measurements near x = 1 may be due to the fact that the temperature T = 35°C is very near to the clearing temperature. Director fluctuations, which are more pronounced in case of refractive index measurements where surface alignment technique has been employed, could

account for such discrepancy as compared with those from magnetically aligned samples used in x-ray diffraction measurements.

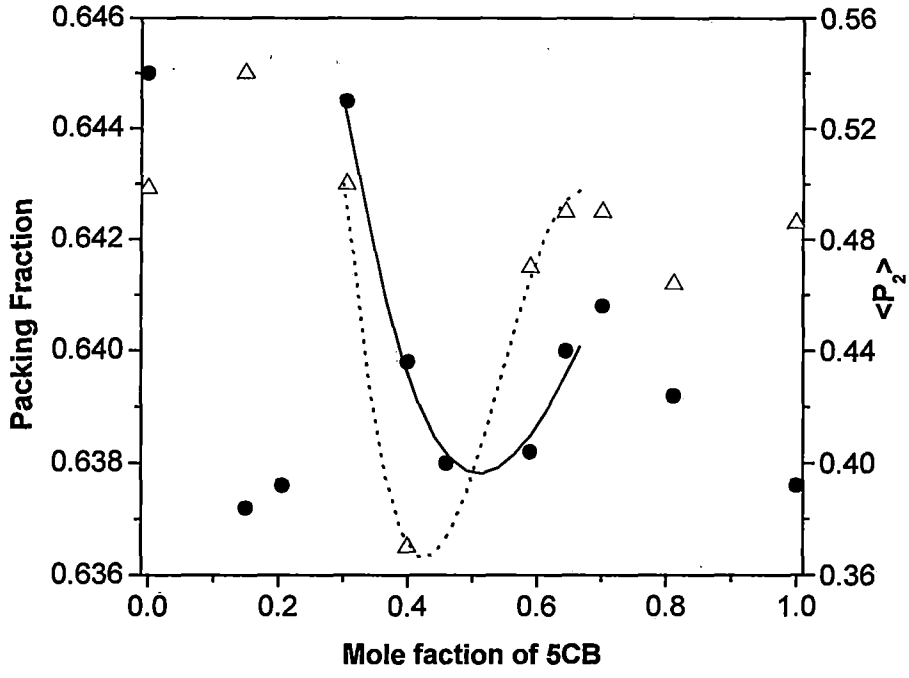

FIGURE 3.7: Variation of orientational order parameter $\langle P_2 \rangle$ and the packing fraction values at a temperature $T=0.98T_{NI}$ ● $\langle P_2 \rangle$, △ packing fraction.

To investigate the minimum in the OOP, packing fraction and other physical properties observed for mixtures around a mole fraction of 0.4, I have analysed the x-ray diffraction data to calculate the average lateral distance between the molecules. The average lateral intermolecular distance D between the molecules can be obtained from the diffraction angle of the outer ring of x-ray pattern by the formula,

$$2D \sin\theta = 1.117\lambda \qquad \textbf{3.4}$$

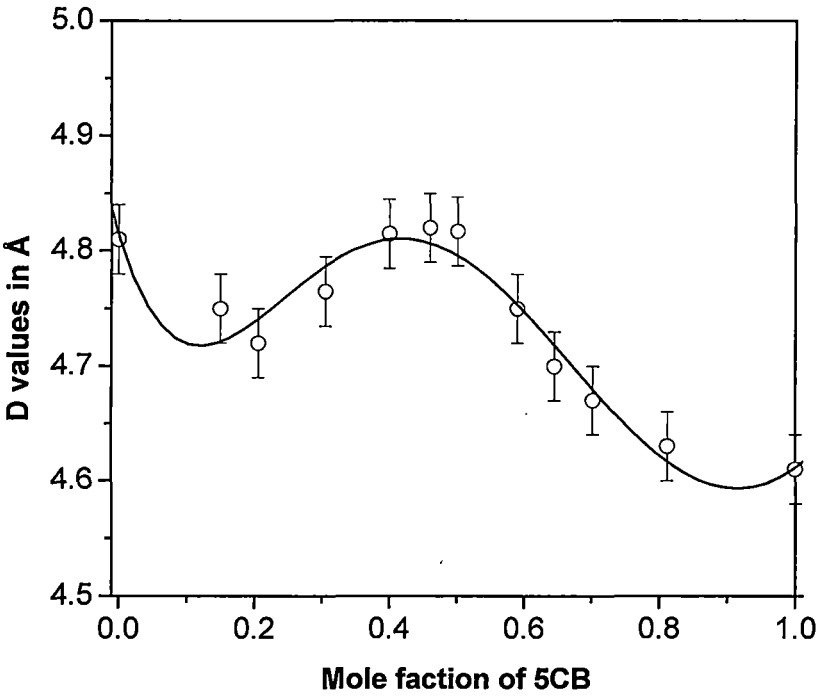

FIGURE 3.8: Variation of D with mole fraction of 5CB at T=35°C. Vertical bar represents estimated errors.

From the figure 3.8, it is clear that the experimental D values, within the smectic phase show an enhancement in their magnitudes near equimolar concentration, whereas the density and layer thickness show a reverse trend i.e., minimum near $x \approx 0.4$. This implies that the packing of the molecules in the smectic layers is poor near $x \approx 0.4$. This variation of D with molar concentration clearly explains why the density of mesogens decreases even when layer thickness is also decreasing near $x \approx 0.4$.

References:

1. D. A. Dunmur, R. G. Walker and P. Palffy- Muhoray, *Mol. Cryst. Liq. Cryst.*, **122**, 321 (1985).
2. P. Palffy-Muhoray, D. A. Dunmur, W. H. Miller and D. A. Balzarini, *Liquid Crystal and Ordered Fluid*, **vol 4**, Ed. A. C. Griggin and J. F. Johonson Plenum, N.Y., p. 615 (1984).
3. M.K. Das, R. Paul and D.A. Dunmur, *Mol. Cryst. Liq. Cryst.*, **285**, 239 (1995).
4. W. L. McMillan, *Phys. Rev.*, **A6**, 936, (1972).
5. W. L. McMillan, *Phys. Rev.*, **A18**, 328, (1973).
6. W. Maier and A. Saupe, Z. Naturforsch, **15a**, 287 (1960).
7. M. K. Das and R. Paul, *Phase Transition*, **46**, 185 (1994).
8. P. P. Karat and N. V. Madhusudana, *Mol. Cryst. Liq. Cryst.*, 36, 51 (1976).
9. J. E. H. Neugebauer, *Can. J. Phys.* **32**, 1 (1954).
10. I. Haller, H. A. Higgin, R. H. Lilienthal and T. R. McGuire, *J. Phys. Chem*, 77, 950 (1973).
11. A. I. Kitaigordsky, Molecular Crystals and Molecules, Chapter 19, Academic press (1973).

Chapter 4

Phase Diagram, Density and Optical Studies on Binary Mixture of a Cyanobiphenyl (11OCB) and a Benzoate Ester (ME6.O5) Showing Enhanced Smectic Phase

4.1 Introduction:

From the study of phase diagram in bicomponent and multicomponent systems, it has been found that smectic A phase can be strongly stabilized in mixtures [1,2]. The clearing temperature is increased compared to the corresponding temperature in the pure state, hence enhancing the respective phases. Some times, it has been observed that although none of the pure compounds is smectic, yet the mixtures of these compounds often show so-called induced smectic phase [3-5]. In many cases smectic phases existing in pure compounds of binary mixtures decrease their smectic stability and new phases of lower order are created. These phases are called 'phase created by depressing smectic stability' [6].

I have observed an enhanced smectic phase from the bicomponent mixtures of undecyloxy cyanobiphenyl (11OCB) and 4-n-hexyl phenyl-4-n'-pentyloxy benzoate (ME6.O5), where 11OCB and ME6.O5 show smectic A and nematic phases respectively. In this chapter, I have reported the phase diagram, density and refractive indices of the binary mixtures of 11OCB and ME6.O5 throughout the entire composition range. For better understanding of this phase, I have also calculated the variation of different physical parameters with molar concentration.

4.2 Phase diagram:

The pure samples 11OCB and ME6.O5 were donated by E. Merck, U.K. and were used without further purification. The phase diagram of this system is obtained by studying the transition temperatures and textures of different

mixtures under crossed polariser with a polarizing microscope equipped with a hot stage (Mettler FP 80/82). The phase diagram of the binary system 11OCB + ME6.O5 are presented in figure 4.1.

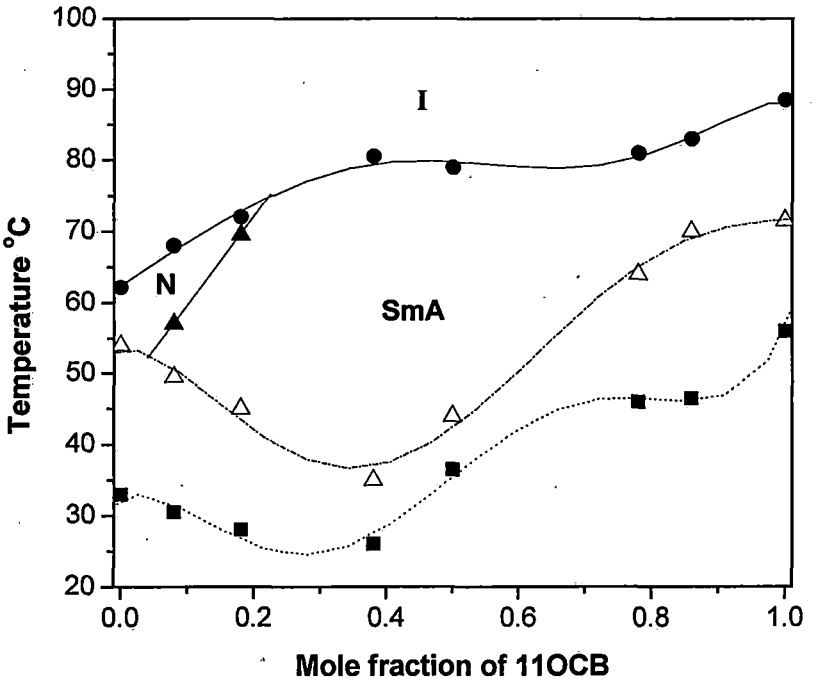

FIGURE 4.1: Phase diagram of the binary mixture of undecyloxy cyanobiphenyl (11OCB) and 4-n-hexyl phenyl-4-n′-pentyloxy benzoate (ME6.O5). x is the mole fraction of 11OCB. ● smectic or nematic to isotropic transition temperature; ▲ smectic to nematic transition temperature; △ melting temperature; ■ super cooled liquid crystal to solid transition.

The pure compounds 11OCB and ME6.O5 show only smectic and nematic phases respectively. From the phase diagram, it has been found that the smectic phase of 11OCB strongly influences the phase behaviour of the system. For mixtures having $x > 0.15$ (x = mole fraction of 11OCB) the nematic phase is completely suppressed. For mixtures with $0.03 < x < 0.15$ both smectic A and nematic phases are found to be present. Only nematic phase is found for $x < 0.03$. A strong positive and a negative deviation from

the linearity in the isotropic transition temperatures are obtained for mixtures with x ≈ 0.4 and 0.8 respectively. Positive deviation from the linearity has also been observed by Das et al [2]. Melting temperature shows a minimum around x ≈ 0.4, where the thermal stability of the smectic A phase is maximum. The mixtures can be super-cooled by about 20°C in the mesomorphic phase before solidification and the solidification curve approximately follows trend of the melting curve.

4.3 Refractive index and density measurements:

The refractive indices of the mixtures and that of the pure compounds were measured throughout the mesomorphic range for λ = 5780Å, having accuracy ± 0.001 with the thin prism method (∠2°) [7], described in chapter 2. The variation of refractive indices (n_o, n_e) with temperature are shown in figure 4.2 (a) – 4.2(c).

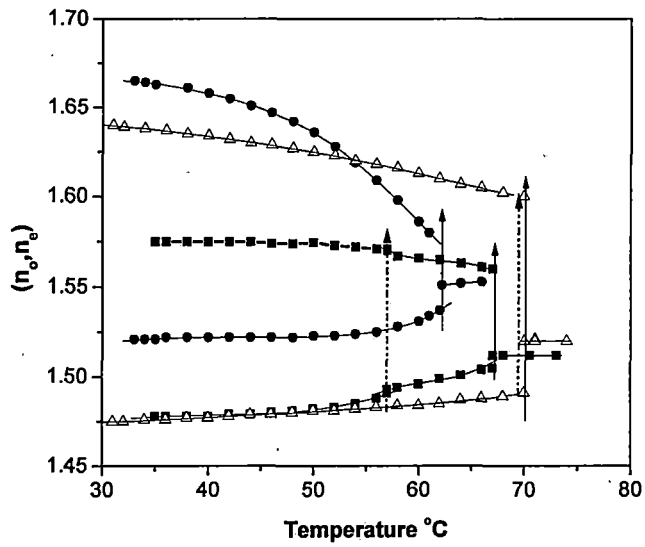

FIGURE 4.2 (a): Refractive indices (n_o, n_e) as function of temperature for pure compounds.● ME6.O5 and mixtures ■ x = 0.08; △ x = 0.18. ↑ represents S-N and ↑ N-I transition temperature.

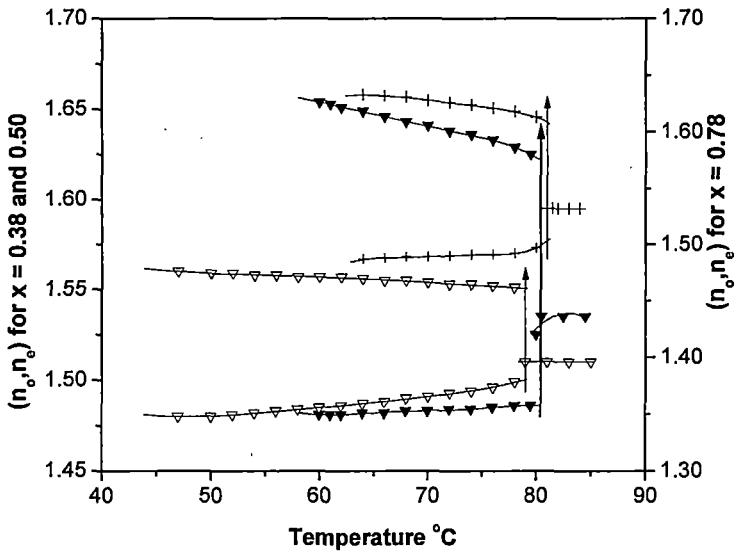

FIGURE 4.2 (b): Refractive indices (n_o, n_e) as function of temperature for mixture ▼ x = 0.38; ▽ x = 0.50 and + x = 0.78. ↑ represents S-I transition temperature.

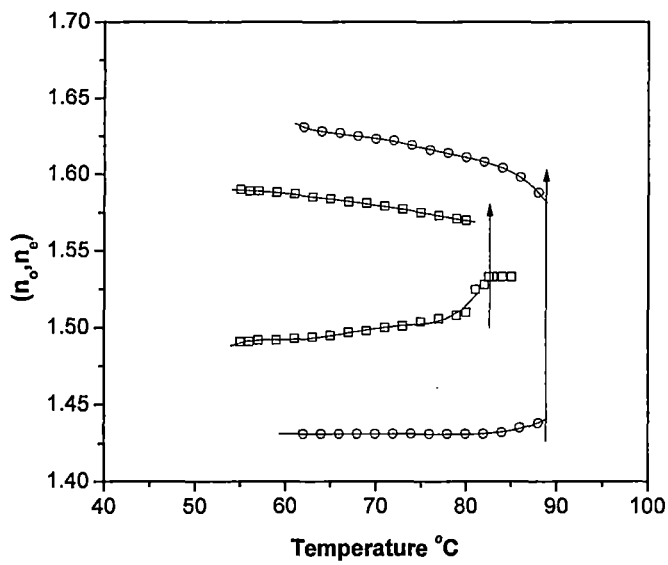

FIGURE 4.2 (c): Refractive indices (n_o, n_e) as function of temperature for mixtures pure compound ○ 11OCB and for mixture □ x = 0.86.↑ represents the S-I transition temperature.

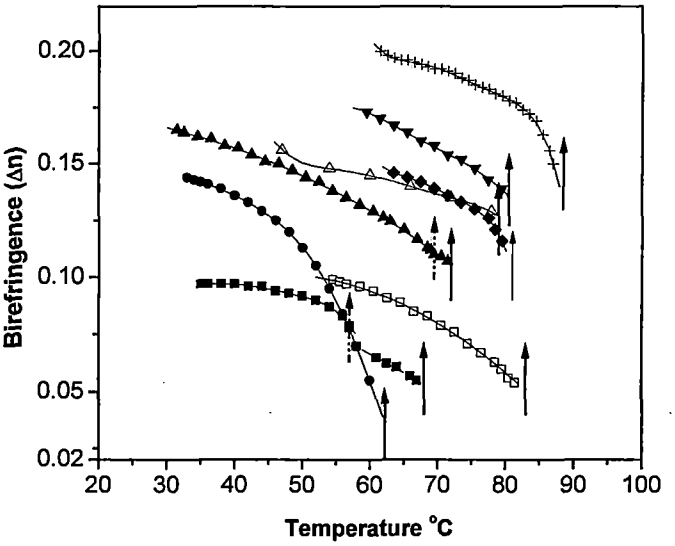

FIGURE 4.3: Birefringence ($\Delta n = n_e - n_o$) as function of temperature for different mixtures and pure compounds. ● ME6.O5; + 11OCB; ■ x = 0.08; ▲ x = 0.18; ▼ x = 0.38; △ x = 0.5; ◆ x = 0.78; □ x = 0.86. ↑ represents S-N and ↑ N-I transition temperature.

I have plotted optical birefringence ($\Delta n = n_e - n_o$) as a function of temperature in figure 4.3. Birefringence values of ME6.O5 are lower than those obtained from 11OCB. This is expected because it is well known that cyanobiphenyl have greater birefringence than ester mesogens. On the other hand density values of ME6.O5 are higher than those obtained from 11OCB. A discontinuity in the density as well as Δn values at the smectic A to nematic phase transition is observed for mixtures having x = 0.08, indicating a first order smectic A to nematic phase transition.

The densities of the mixtures at different temperatures are determined within ± 0.1%, as described in chapter 2 of this thesis. The results of density measurements are presented in figures 4.4(a) and 4.4(b).

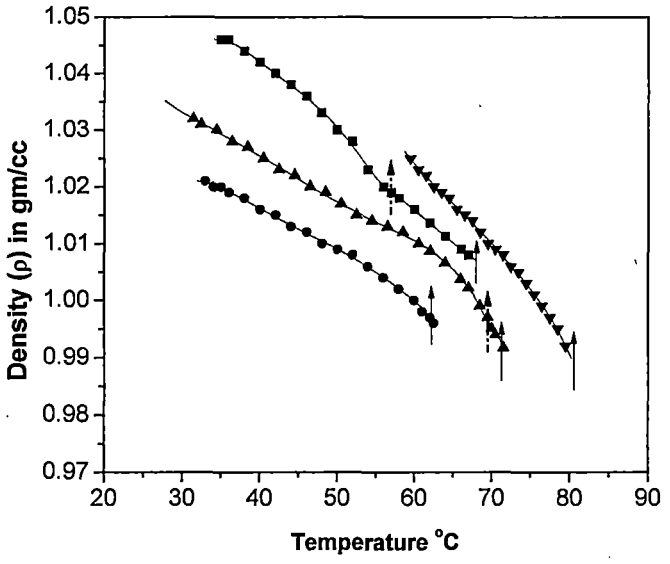

FIGURE 4.4 (a): Temperature variation of density (ρ) of mixtures having mole fraction of 11OCB; ● x = 0.0(ME6.O5); ■ x = 0.08; ▲ x = 0.18; ▼ x = 0.38. ↑ represents S-N and ↑ N-I transition temperature.

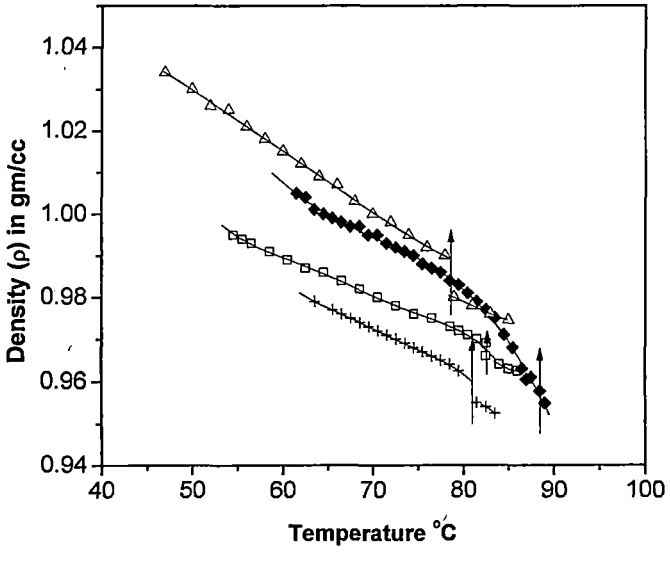

FIGURE 4.4 (b): Temperature variation of density (ρ) of mixtures having mole fraction of 11OCB; △ x = 0.50.+ x = 0.78; □ x = 0.86; ◆ x = 1.0 (11OCB).

At a temperature 5°C below the isotropic transition temperature the density values increases slowly with mole fraction of 11OCB up to x = 0.25 and then decreases continuously having a broad minimum near x ≈ 0.8 (Figure 4.5). On the other hand birefringence values increases up to x ≈ 0.4 and then continuously decreases creating a minimum near x = 0.8. It is to be noted that while density values of 11OCB are lower than the values obtained from ME6.O5, the birefringence values are somewhat higher.

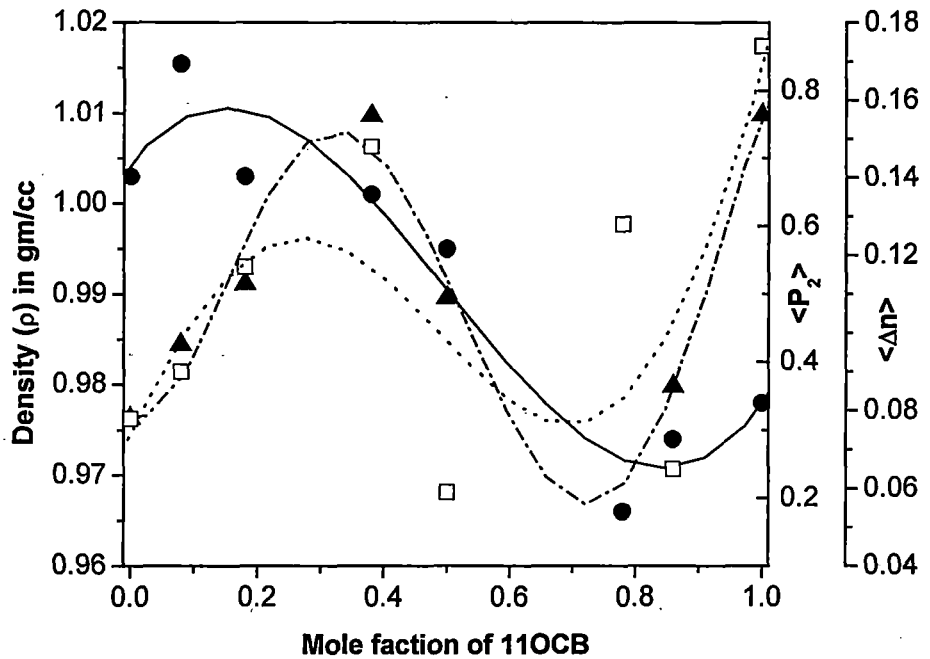

FIGURE 4.5: Density (ρ), $\langle P_2 \rangle$ and Δn against mole fraction of 11OCB at $T=T_{SI}(T_{NI})$ - 5 °C. ● ρ, ▲ $\langle P_2 \rangle$, □ Δn.

In figure 4.6, I have plotted thermal expansivity $\beta = d\rho/dT$ in the smectic A phase along with the relative change of density ($\delta\rho$) during Smectic A (nematic) / Isotropic phase transition. In both the cases the respective values

increases gradually with increase of x having a maximum near equimolar concentration. Similar behaviour is has also been reported by Das et al [2].

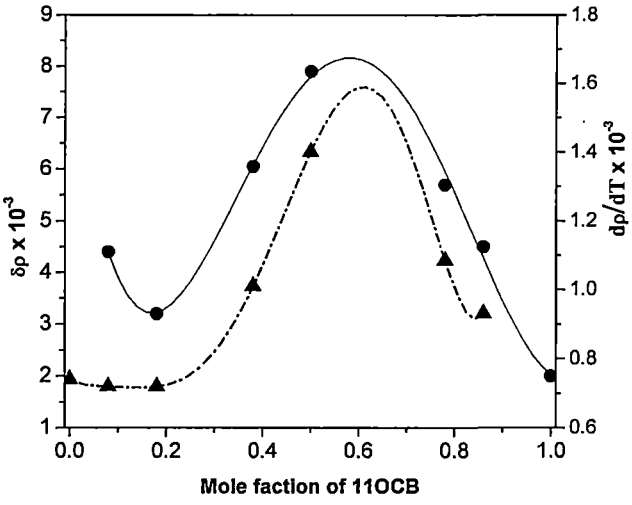

FIGURE 4.6: Change in density (Δρ) during smectic A or nematic to isotropic phase transition and (dρ/dT) in the smectic A phase with mole fraction of 11OCB. ● Δρ and ▲ dρ/dT.

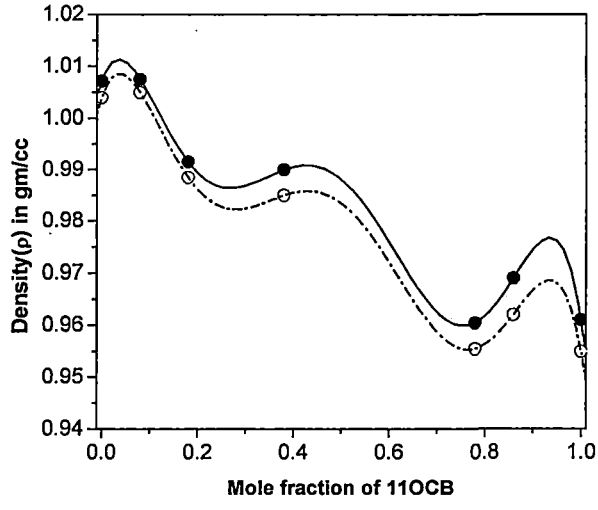

FIGURE 4.7: Density values (ρ) just below (●) and above (○) the clearing temperature with mole fraction of 11OCB (x).

In figure 4.7, I have plotted density values in the mesomorphic and isotropic phase just below and above the mesomorphic to isotropic phase transition

against mole fraction. From this curve it has been found that for both the cases two minima are observed near $x \approx 0.3$ and $x \approx 0.8$, where enhancement and depression of clearing temperature have been observed.

The refractive index data can be used in conjunction with density data to determine the orientational order parameter. The order parameter and optical properties of the system is connected by the relation

$$< P_2 >= \frac{(\alpha_e - \alpha_o)}{\Delta\alpha} \qquad \textbf{4.1}$$

where α_e and α_o are the effective polarizabilities for extraordinary and ordinary rays which are calculated from refractive indices using Neugebauer's method [8]. $\Delta\alpha = (\alpha_{\parallel} - \alpha_{\perp})$ is the polarizability anisotropy, which can be estimated by applying well known Haller's extrapolation procedure [9]. In figure 4.8, I have plotted the polarizability anisotropy values for pure as well as different mixtures. Although polarizability anisotropy values obtained from Haller's procedure are somewhat scattered, a minimum of $\Delta\alpha$ near equimolar concentration has been observed.

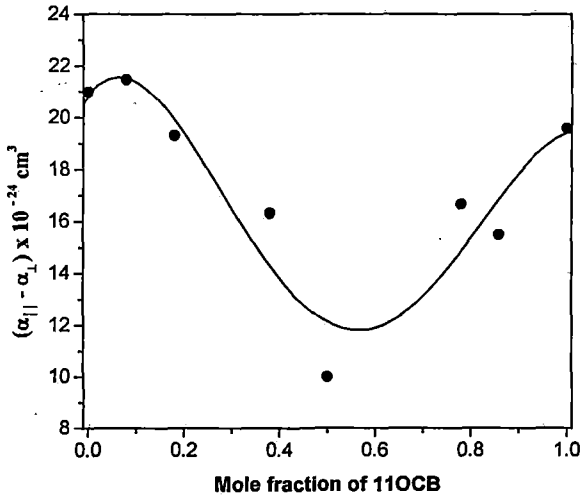

FIGURE 4.8: Variation of $(\alpha_{\parallel}-\alpha_{\perp})$ against mole fraction of 11OCB. ● Neugebauer's method.

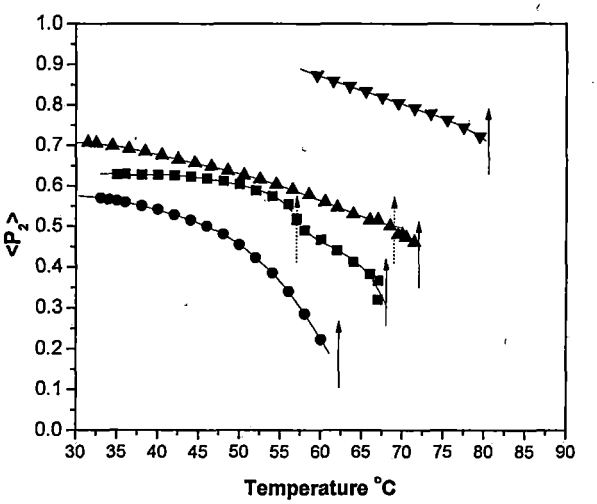

FIGURE 4.9 (a): Temperature variation of order parameter $\langle P_2 \rangle$ for different mixtures and pure compound ● ME6.O5; ■ x=0.08; ▲ x=0.18; ▼ x=0.38. ↑ Represents S-N and ↑ N-I transition temperature.

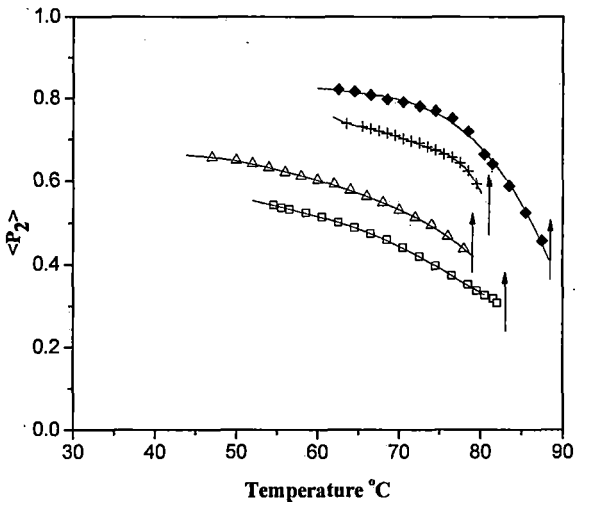

FIGURE 4.9 (b): Temperature variation of order parameter $\langle P_2 \rangle$ for different mixtures and pure compound; △ x = 0.50; + x = 0.78; □ x = 0.86,◆ 11OCB. ↑ Represents the N-I transition temperature.

Figure 4.9(a) - 4.9(b) shows the variation of $\langle P_2 \rangle$ values with temperature for different mixtures as well as for pure components. $\langle P_2 \rangle$ values of ME6.O5 are lower than those obtained from 11OCB. The experimental

order parameter values at the SmA-N phase transition appears to be discontinuous for x = 0.08 implying a first order phase transition. Maximum $\langle P_2 \rangle$ values are obtained for mixtures with x = 0.38 where the stability of smectic phase is maximum. Variations of $\langle P_2 \rangle$ with mole fraction (x) of 11OCB follow the trend as observed from birefringence and density measurements (Figure 4.5).

References

1. B. Engelen, H. Heppke, R. Hopf and F. Schneider, *Ann. Phys.* **3**, 403 (1978).
2. M. K. Das, B. Jha and R. Paul, *Mol. Cryst. Liq. Cryst.*, **261**, 95 (1995).
3. M.K. Das and R. Paul, *Phase Transitions*, **46**, 185 (1994).
4. M.K. Das and R. Paul, *Phase Transitions*, **48**, 255 (1995).
5. D. A. Dunmur, R. G. Walker, P. Palffy Muhoray, *Mol. Cryst. Liq. Cryst.* **122**, 321 (1995).
6. R. Dabrowski, B. Wazynska and B. Sasnnowska, *Liq. Cryst.*, **1**, 415 (1986).
7. A. K. Zeminder, S. Paul and R. Paul, *Mol. Cryst. Liq. Cryst.* **61**, 191, (1980).
8. H.E.J. Neugabauer, *Can. J. Phys.*, **32**, 1 (1954).
9. I. Haller, H.A. Huggins, H.R. Lilienthal, T.R. McGuire, *J. Phys. Chem.* **77**, 900 (1973).

Chapter 5

Physical Properties of a Mesogenic Mixture Showing Induce Smectic A_d Phase I: Refractive Index, Density, X-ray Diffraction and Static Dielectric Permittivity Studies

5.1 Introduction:

The induced Sm A_d phase has been observed in bicomponent mixtures when none of the components of this mixture have smectic phase [1-7]. Generally, induced smectic phases are formed in binary mixtures of nematogenic compounds, one having terminal polar group and other being terminal non-polar one and only in a few cases [8-9], with mixtures of two non-polar mesogens. The strong induction of smectic A_d phase is also possible in binary mixtures of polar nematic compounds as well [10-11]. Although, a considerable volume of work have been reported in the literature on systems involving polar non-polar mixtures of biphenyl compounds showing induced smectic phase, not much work have been done on binary systems of cyclohexane compounds showing induced smectic phase.

In this work, I have chosen a binary mixture of 4-n-pentyl phenyl 4-n′-hexyloxy benzoate (ME6O.5) and p-cyanophenyl trans-4-pentyl cyclohexane carboxylate (CPPCC). The pure compounds show nematic phase only. For a proper understanding of the formation of induced smectic phase and their influence on the adjacent nematic phase the physical properties of the mixture were studied by DSC, refractive index, density, x-ray diffraction and static dielectric permittivity measurements. The details of experimental technique employed are described in chapter 2 of this thesis. Phase transitions were studied by observing textures under a polarizing microscope equipped with Mettler FP80/82 thermo-system.

5.2 Texture study:

The compounds ME6O.5 and CPPCC were gifted by E. Merck, U.K. and were used without further purification. The transition temperatures of the pure compounds, their structural formula and chemical names are as follows:-

Component 1: p-cyanophenyl trans-4-pentyl cyclohexane carboxylate (CPPCC in short)

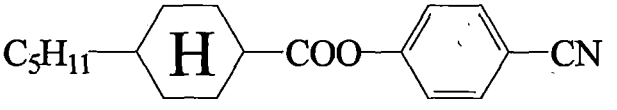

$$K \underset{21.4^{\circ}C}{\overset{48.7^{\circ}C}{\rightleftharpoons}} N \xrightarrow{80.5^{\circ}C} I$$

Component 2: 4-n-pentyl phenyl 4-n'-hexyloxy benzoate (ME6O.5 in short)

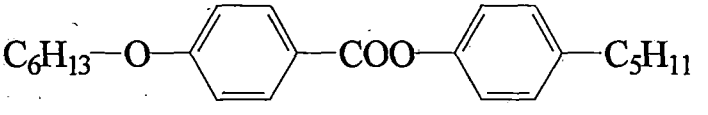

$$K \underset{35.5^{\circ}C}{\overset{49.5^{\circ}C}{\rightleftharpoons}} N \xrightarrow{62.5^{\circ}C} I$$

Of the eight mixtures, two show only nematic phase and all other have both nematic and induced smectic A_d phases. During heating the smectic range is very small. The mixtures show large super-cooling. The induced smectic phase in this system appears mostly in the supercooling temperature region.

5.3 Phase diagram:

The phase diagram of this system is shown in figure 5.1. A detailed study of the phase diagram by microscopic observation revealed that the transition temperatures are reproducible within ±0.5°C between heating and cooling cycles for all the mixtures.

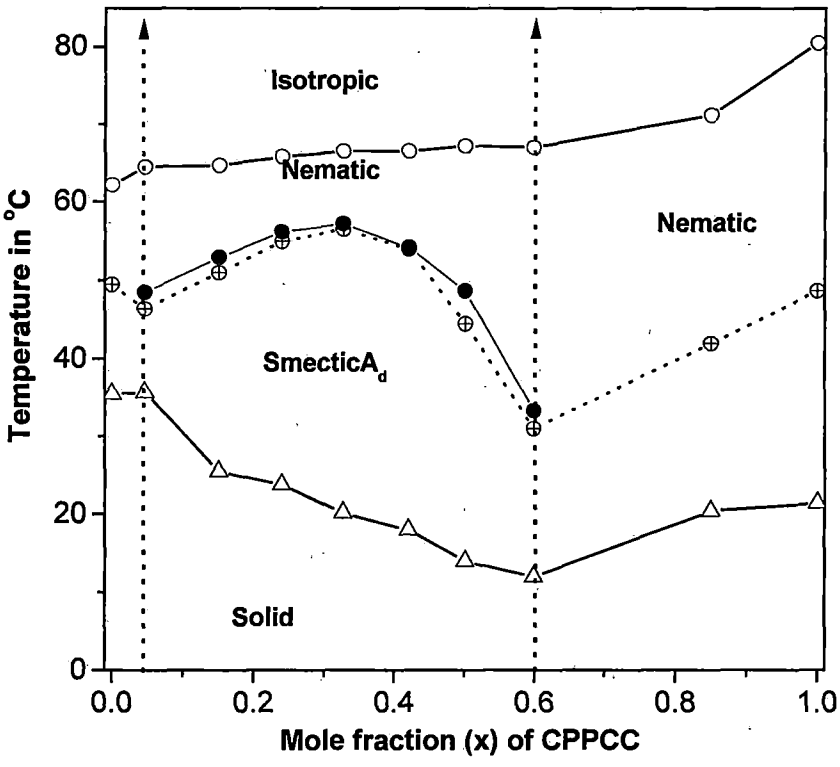

FIGURE 5.1: Phase diagram for the binary system of ME6O.5 + CPPCC. x is the mole fraction of CPPCC. ○ nematic-isotropic transition temperature; ● smecticA$_d$-nematic transition temperature; ⊕ melting temperature; △ super-cooling temperature.

The nematic–isotropic and smecticA–nematic transition temperatures are plotted against concentration. The mixture shows an induced smectic A_d phase in the concentration range $0.03 < x < 0.6$, where x is the mole fraction of CPPCC. Maximum stability of the smectic phase occurs for mixtures

having $x \approx 0.3$. While Das et al for binary systems of similar benzoate esters and bi-phenyl compounds (5CB) [4-6] have found maximum stability of induced smectic phase near equimolar concentration.

The mixtures show large super-cooling. The super cooling temperatures show a minimum near $x \sim 0.6$. During heating the smectic range is very small for the mixtures within the concentration range $0.03 < x < 0.6$. The isotropic transition temperatures for mixtures having $x > 0.15$, lie significantly below the straight line connecting those of the pure compounds. Textures of the pure compounds and their mixtures in nematic phases show typical-marbled type and those in the induced smectic phases are fan-shaped or focal-conic, both typical of smectic A phase. Homeotropic texture studies also confirmed the existence of orthogonal phase in the induced smectic region.

5.4 DSC measurements:

In figure 5.2 the results of the transition entropy are plotted as a function of molar concentration (x_{CPPCC}). The change in entropy during smectic A_d – nematic phase transition (ΔS_{SN}) is larger for $x < 0.33$ compared to mixtures having $x > 0.33$. With increase in concentration of CPPCC above $x = 0.33$ there is a rapid decrease in ΔS_{SN}, which suggest that for $x > 0.33$ the order of S-N phase transition is different from that for $x < 0.33$.

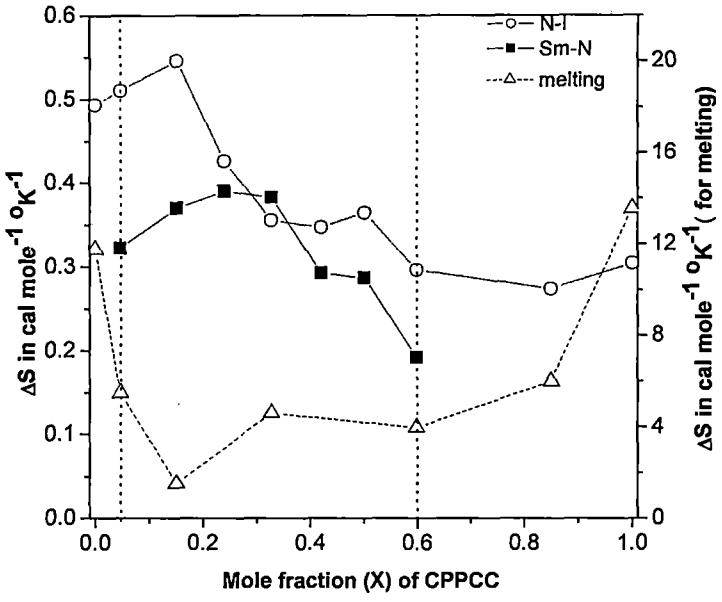

FIGURE 5.2. Transition entropies (ΔS) as a function of mole fraction of CPPCC: ■ smectic A_d - nematic transition, ○ nematic-isotropic transition, and △ crystal-mesomorphic transition.

The entropy change associated with the nematic-isotropic phase transition (ΔS_{NI}) however, decreases with increasing molar concentration (x_{CPPCC}), which indicates that the nematic phase of this system is relatively disordered with increase in the mole fraction of CPPCC. It is to be noted that for all the mixtures ΔS_{NI} values are higher compared to ΔS_{SN}. It appears from the graph that ΔS values for crystal-mesomorphic transition decreases with increasing concentration (x) having a broad minimum near x=0.3.

5.5 Density measurements:

The temperature variation of the density values for the mixtures is shown in figure 5.3(a) – 5.3(b). A small discontinuity in the density values could be observed at the nematic to smectic A_d phase transition for mixtures around a

mole fraction near x ≈ 0.3, consistent with the observed entropies of transition.

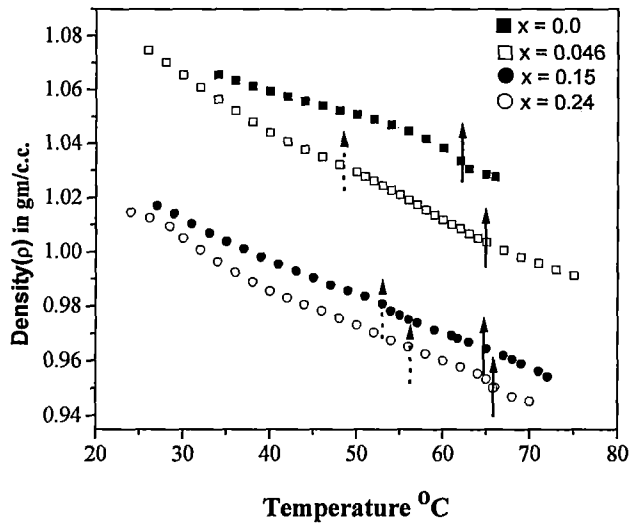

FIGURE 5.3 (a). Variation of density (ρ) as a function of temperature for x = 0.0, 0.046, 0.15, 0.24. ↑ nematic – isotropic and ↑ smectic A_d – nematic transition temperatures.

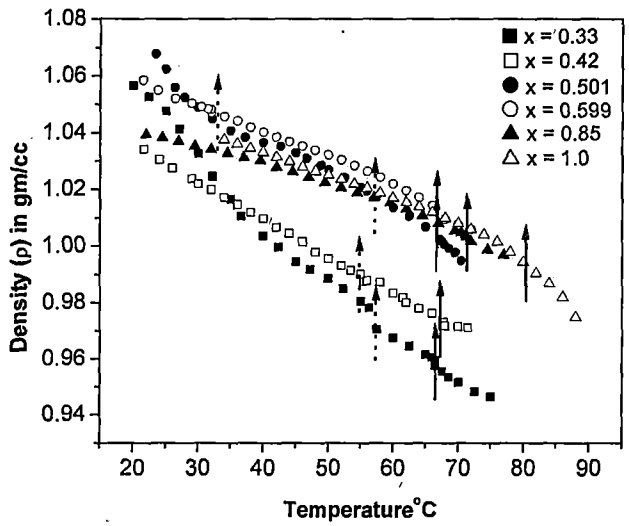

FIGURE 5.3 (b). Variation of density (ρ) as a function of temperature for x = 0.33, 0.42, 0.501, 0.599, 0.85, 1.0. ↑ nematic – isotropic and ↑ smectic A_d – nematic transition temperatures.

5.6 Refractive index measurements:

The temperature dependence of the principal refractive indices n_o and n_e and the refractive index in the isotropic phase (n_{iso}) at wavelength $\lambda = 5780Å$ are shown in figures 5.5(a) – 5.5(e). In general, the change in birefringence is continuous for $x > 0.33$ at the smectic-nematic phase transition which indicates a very weakly first order or a second order phase transition. On the other hand for mixtures with $x < 0.33$ a discontinuity of birefringence ($\Delta n = n_e - n_o$) occurs at the smectic-nematic phase transition which indicates a first order phase transition. This observation is also supported by the density and transition entropy measurements of these mixtures.

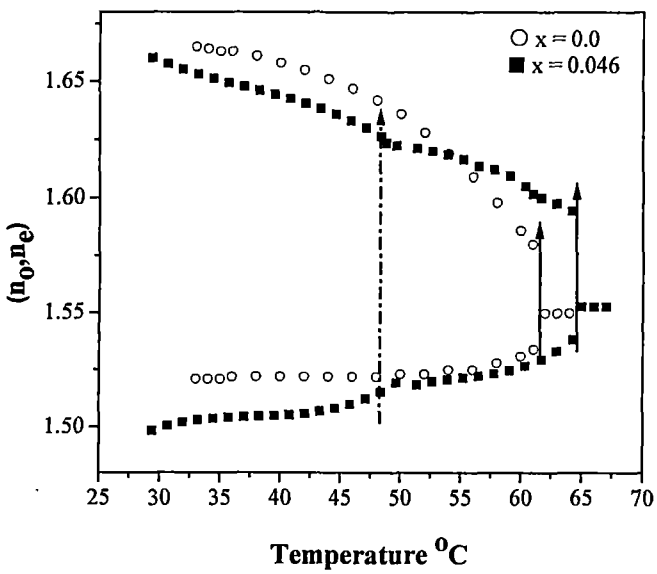

FIGURE 5.5 (a). Temperature variation of refractive indices (n_o, n_e) for ○ x = 0.0, ■ x = 0.046. ↑ nematic – isotropic and ↑ smectic A_d – nematic transition temperatures

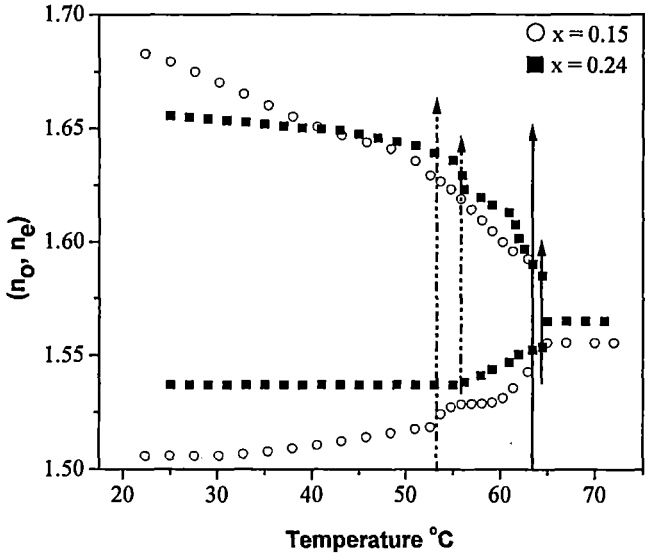

FIGURE 5.5 (b). Temperature variation of refractive indices (n_o, n_e) for ○ x = 0.15, ■ x = 0.24. ↑ nematic – isotropic and ↟ smectic A_d – nematic transition temperatures

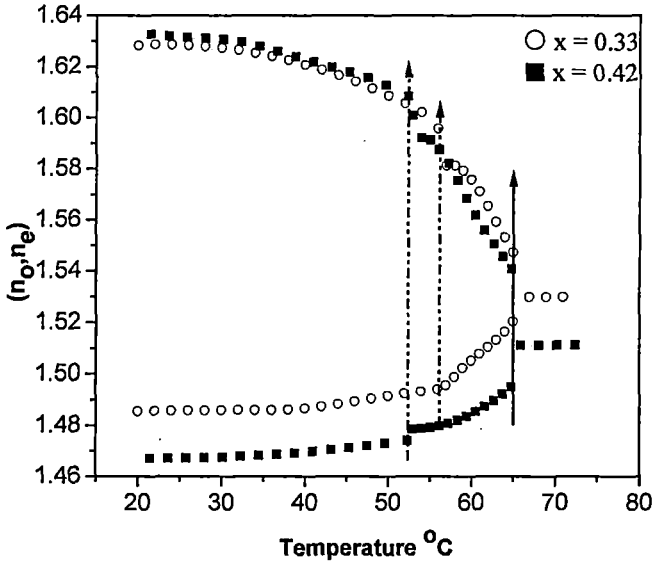

FIGURE 5.5 (c). Temperature variation of refractive indices (n_o, n_e) for ○ x = 0.33, ■ x = 0.42. ↑ nematic – isotropic and ↟ smectic A_d – nematic transition temperatures

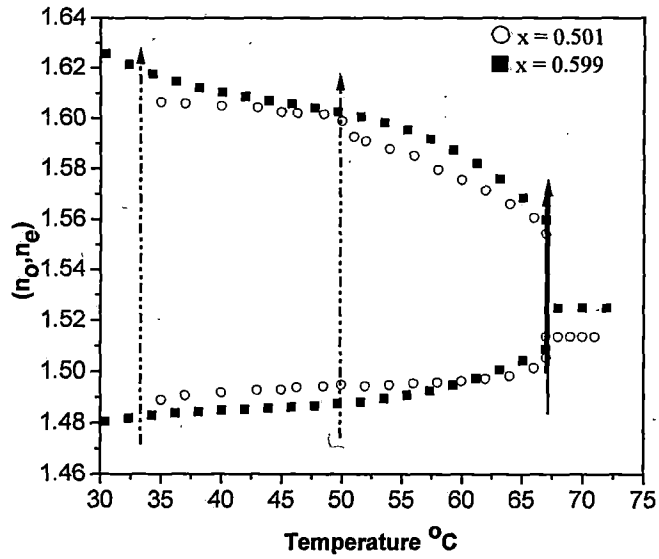

FIGURE 5.5 (d). Temperature variation of refractive indices (n_o, n_e) for ○ x = 0.501,■ x = 0.599. ↑ nematic – isotropic and ↑ smectic A_d – nematic transition temperatures

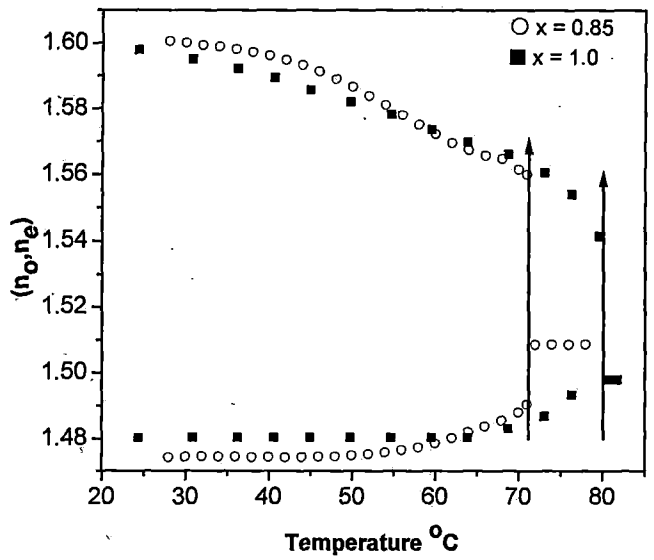

FIGURE 5.5 (e). Temperature variation of refractive indices (n_o, n_e) for ○ x = 0.85, ■ x = 1.0 (CPPCC). ↑ nematic – isotropic and ↑ smectic A_d – nematic transition temperatures

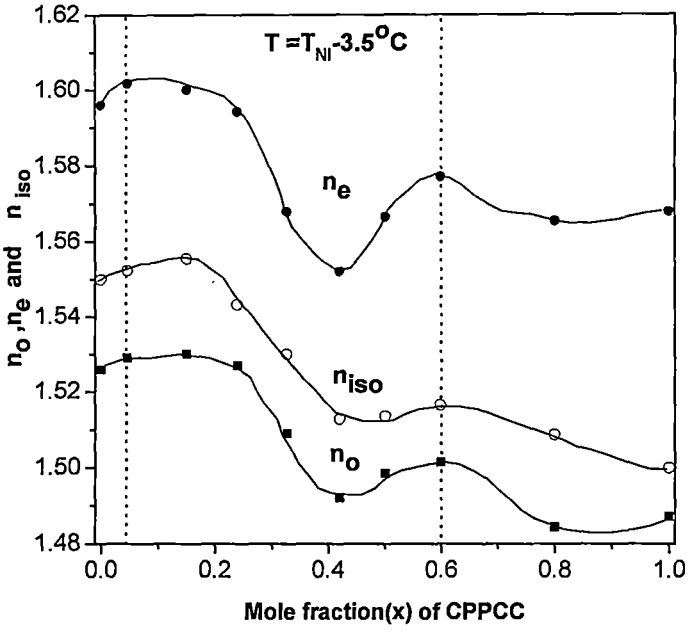

FIGURE 5.6. Variation of refractive indices ■ n_o, ● n_e, and ○ n_{iso} with concentration; ↑ represents the induced smectic A_d concentration range.

The variation of refractive indices n_o, n_e at temperature $T=T_{NI}-3.5°C$ and n_{iso} with mole fraction is shown in figure 5.6. For mixtures with $x < 0.24$ the n_o, n_e and n_{iso} values are more or less constant. However, these values decreases with increase in the molar concentration of $x > 0.24$ and shows a broad minimum near $x = 0.4$.

Principal molecular polarizability (α_o, α_e) is measured from refractive indices (n_o, n_e) by using Neugebauer's method [discussed in chapter 2]. The orientational order parameter $<P_2>$ is calculated using

$$< P_2 >= \frac{\alpha_e - \alpha_o}{\alpha_{\parallel} - \alpha_{\perp}} \qquad \textbf{5.1}$$

where α_o and α_e are respectively the effective polarizability for extraordinary and ordinary rays; and $\alpha_{||}$ and $\alpha_{\perp}$ are the polarizabilities

parallel and perpendicular to the long axis of the molecule. The polarizability anisotropies in the perfectly ordered state are determined by Haller's extrapolation method [as discussed in chapter 2] and the values for different concentrations (x) of this mixture are indicated in Table 5.1.

5.7 X-ray diffraction measurements:

X-ray diffraction patterns were recorded throughout the mesomorphic range. A magnetic field of 0.5T was applied to align the samples. The x-ray diffraction intensity data were analysed to evaluate order parameters using a procedure described in chapter 2. Layer thickness and the apparent molecular length in smectic and nematic phases were also determined from x-ray data. Plate 5.1 shows the x-ray diffraction photographs of the oriented sample of mixture x = 0.501 in the induced smectic (32°C) and nematic phases (44°C). The angular distributions of the x-ray intensity along the outer arc of the diffraction pattern, after necessary background correction, was used to determine orientational order parameter following equation 2.17, which has been described in chapter 2.

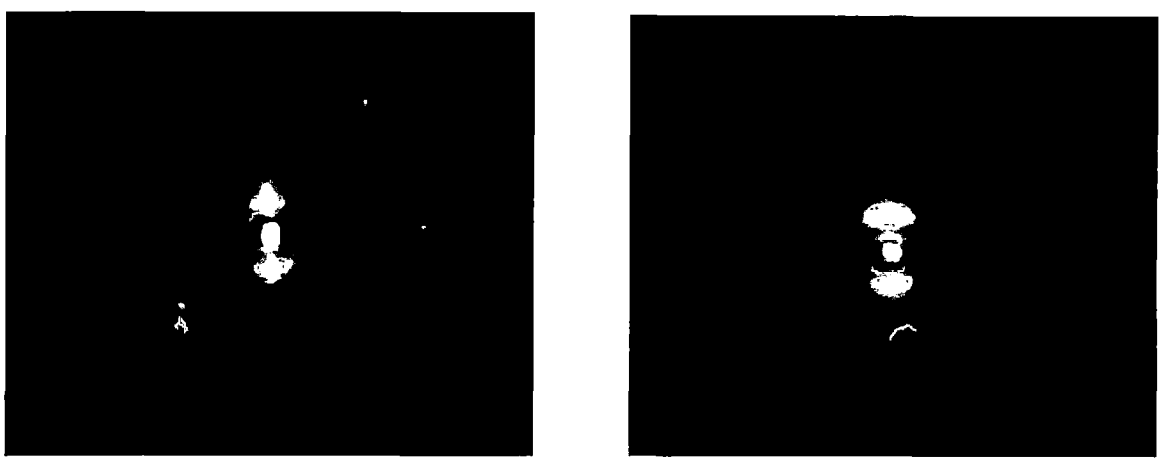

(a) **(b)**

Plate 5.1: X-ray diffraction photograph of the oriented sample **(a)** SmA_d at T=32°C for x=0.501 **(b)** nematic phase at T=44°C for x=0.501.

Figure 5.13 – 5.22 show the variation of experimentally determined orientational order parameters (OOP) $\langle P_2 \rangle$ and $\langle P_4 \rangle$ with temperature for the system studied by x-ray diffraction measurement. In the same figures, I have plotted the $\langle P_2 \rangle$ values obtained from refractive index studies.

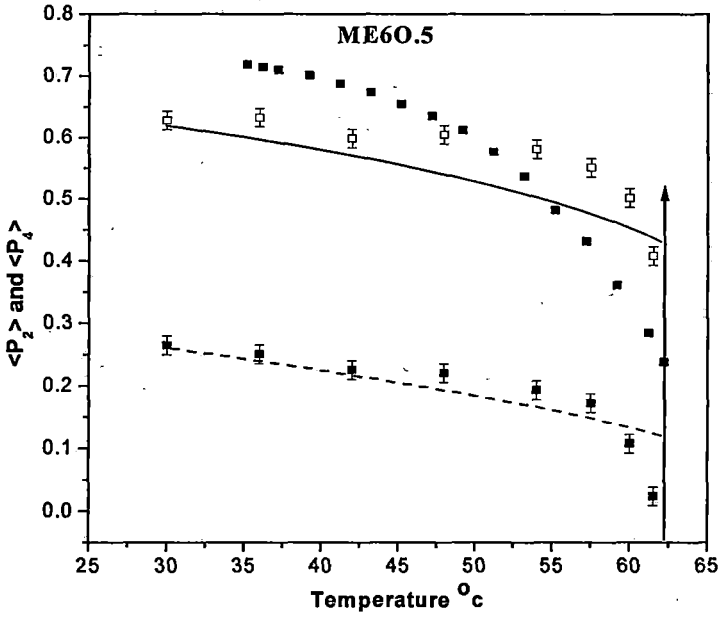

FIGURE 5.13: Temperature variation of $\langle P_2 \rangle$ for ME6O.5 determined from ■ refractive index, □ x-ray measurements; — $\langle P_2 \rangle$ and -- $\langle P_4 \rangle$ from Maier-Saupe theory. ↑ nematic – isotropic transition temperatures.

The $\langle P_2 \rangle$ values measured from x-ray diffraction studies are somewhat smaller than those obtain from refractive index measurements for all the mixtures except near the nematic isotropic phase transition.

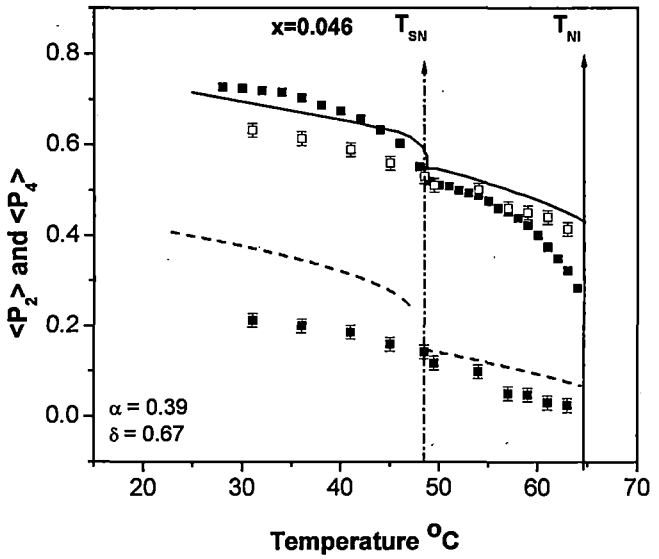

FIGURE 5.14: Temperature variation of $\langle P_2 \rangle$ for x=0.046 determined from ■ refractive index, □ x-ray measurements; — $\langle P_2 \rangle$ and -- $\langle P_4 \rangle$ from McMillan's theory. ↑ nematic – isotropic and ↑ smectic A_d – nematic transition temperatures.

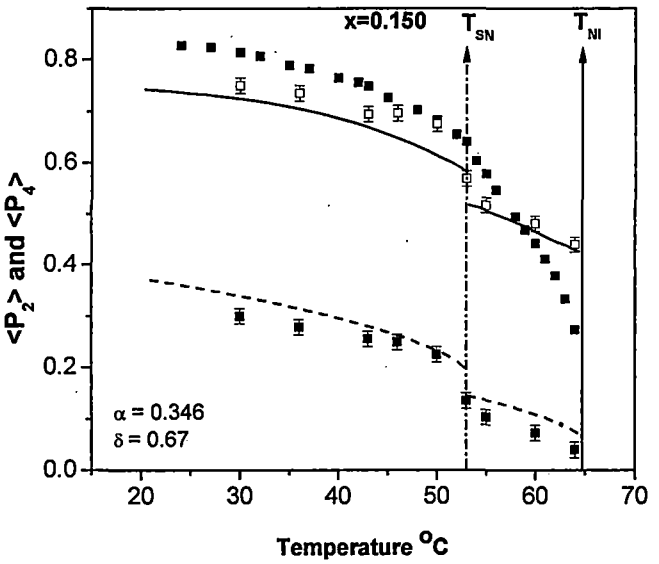

FIGURE 5.15: Temperature variation of $\langle P_2 \rangle$ for x=0.15 determined from ■ refractive index, □ x-ray measurements; — $\langle P_2 \rangle$ and -- $\langle P_4 \rangle$ from McMillan's theory. ↑ nematic – isotropic and ↑ smectic A_d – nematic transition temperatures.

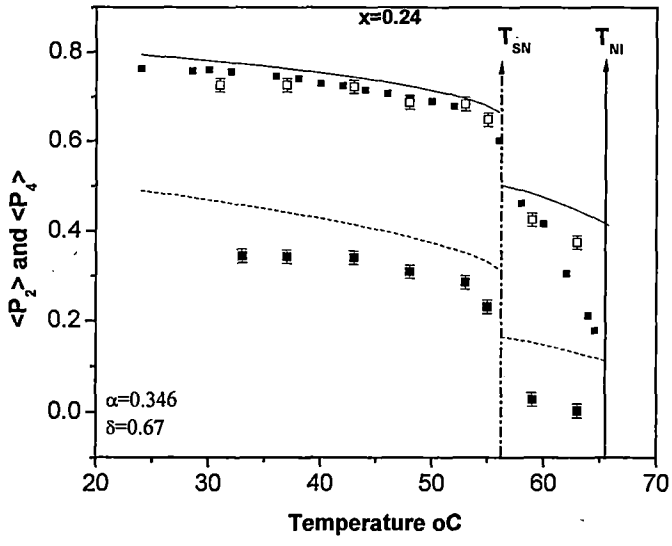

FIGURE 5.16: Temperature variation of $<P_2>$ for x=0.24 determined from ■ refractive index, □ x-ray measurements; — $<P_2>$ and -- $<P_4>$ from McMillan's theory. ↑ nematic – isotropic and ↑ smectic A_d – nematic transition temperatures.

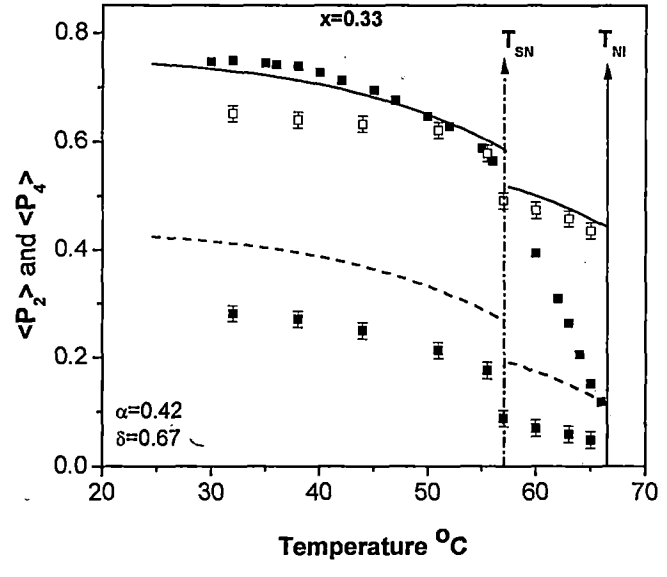

FIGURE 5.17: Temperature variation of $<P_2>$ for x=0.33 determined from ■ refractive index, □ x-ray measurements; — $<P_2>$ and -- $<P_4>$ from McMillan's theory. ↑ nematic – isotropic and ↑ smectic A_d – nematic transition temperatures.

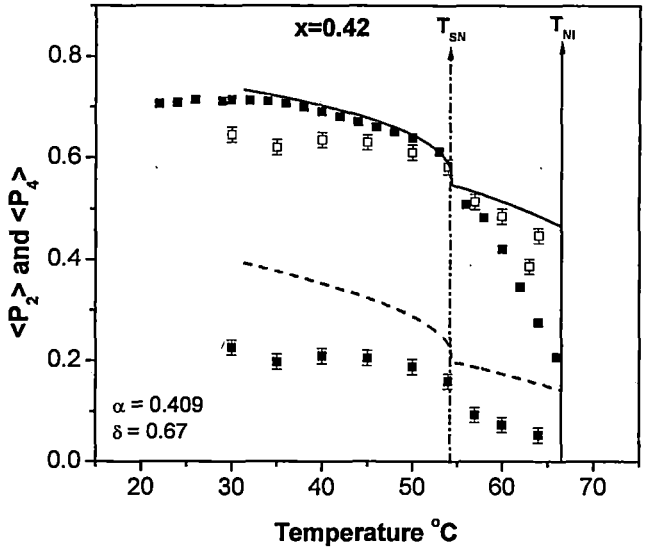

FIGURE 5.18: Temperature variation of <P_2> for x=0.42 determined from ■ refractive index, □ x-ray measurements; — <P_2> and -- <P_4> from McMillan's theory. ↑ nematic – isotropic and ↑ smectic A_d – nematic transition temperatures

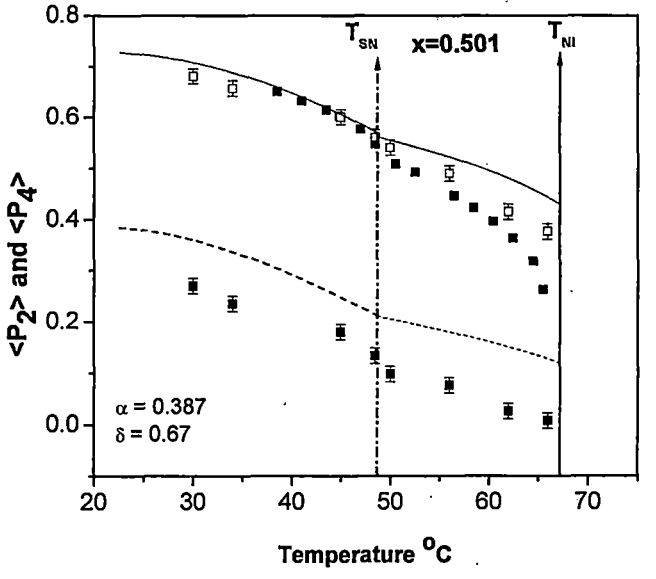

FIGURE 5.19: Temperature variation of <P_2> for x=0.501 determined from ■ refractive index, □ x-ray measurements; — <P_2> and -- <P_4> from McMillan's theory. ↑ nematic – isotropic and ↑ smectic A_d – nematic transition temperatures.

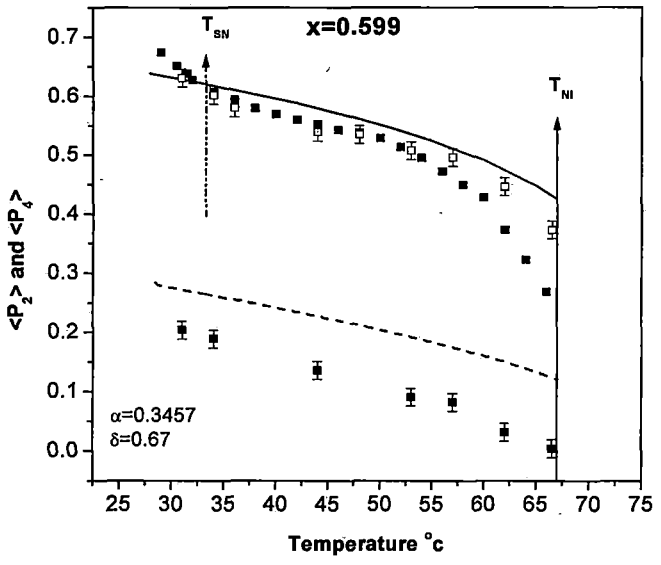

FIGURE 5.20: Temperature variation of $\langle P_2 \rangle$ for x=0.599 determined from ■ refractive index, □ x-ray measurements; — $\langle P_2 \rangle$ and -- $\langle P_4 \rangle$ from McMillan's theory. ↑ nematic – isotropic and ↑ smectic A_d – nematic transition temperatures.

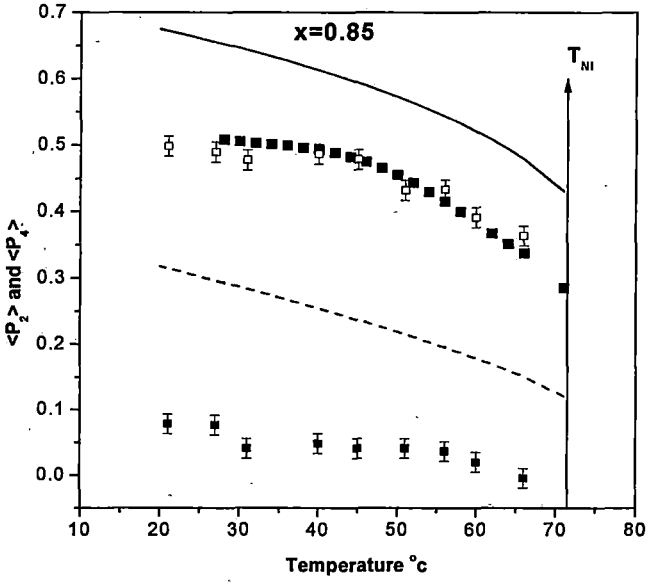

FIGURE 5.21: Temperature variation of $\langle P_2 \rangle$ for x=0.85 determined from ■ refractive index, □ x-ray measurements; — $\langle P_2 \rangle$ and -- $\langle P_4 \rangle$ from Maier-Saupe theory. ↑ nematic – isotropic and ↑ smectic A_d – nematic transition temperatures.

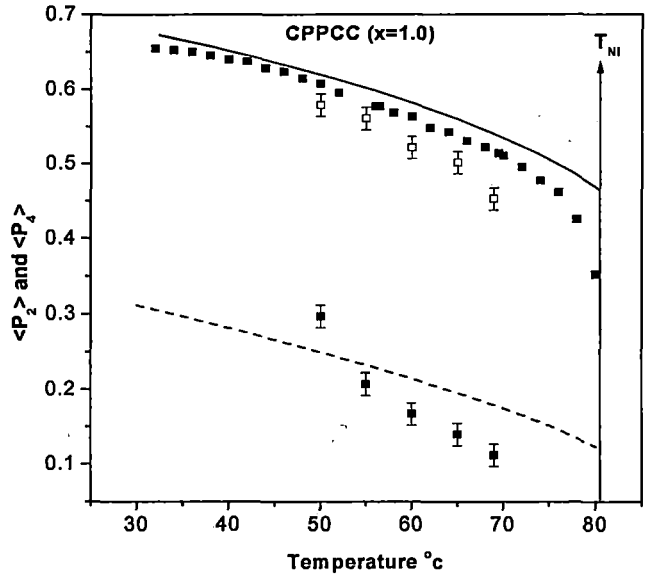

FIGURE 5.22: Temperature variation of $\langle P_2 \rangle$ for CPPCC determined from ■ refractive index, □ x-ray measurements; — $\langle P_2 \rangle$ and -- $\langle P_4 \rangle$ from Maier-Saupe theory. ↑ nematic – isotropic transition temperatures.

From the temperature dependences of the orientational order parameters for mixtures at different concentration it is again observed that there is an appreciable change in the order parameter value at the smectic A_d to nematic phase transition temperature for mixtures around $x \approx 0.33$.

I have also fitted the experimental order parameter values with McMillan's theory [12] for mixtures having smectic A_d phase using α and δ as adjustable parameters in the McMillan potential. It may be mentioned that the order parameter values has been calculated keeping constant δ values over the entire composition range. The best fitted theoretical curve and the values of α and δ used for this calculations are shown in the respective figures. It is to be noted here that, x-ray diffraction photographs of mixtures having 0.15, 0.24 mole fractions of CPPCC were found to exhibit second order

meridional reflections from the smectic layers implying rather high translational order. Orientational order parameter values from x-ray diffraction measurement are also found to be relatively high for these mixtures. The agreement between the experimental $\langle P_2 \rangle$ values from x-ray diffraction measurements with those calculated from McMillan's theory is fair for x = 0.15 and excellent for x = 0.24 (figure 5.15 – 5.16). Also, there is a discrete change in the values of $\langle P_2 \rangle$ and $\langle P_4 \rangle$ at the smectic-nematic phase transition, indicating a first order phase transition for these mixtures.

The mixtures having x = 0.33 and 0.42 do not show second order meridional reflection (as observed from x-ray diffraction photographs) but these mixtures exhibit first order smectic-nematic phase transition as seen from the discontinuity in OOP values at the transition (figure 5.17 – 5.18). The best fitted theoretical curve for the McMillan's theory is also indicated in these figures. For mixtures having mole fraction x = 0.046, 0.501 and 0.599, the experimental order parameter values seem to change continuously at the S/N transition and their agreement with McMillan's theory is fair for x = 0.5 and 0.599; and poor for x = 0.046. Mixture with mole fraction 0.85 has only nematic phase; hence the experimental $\langle P_2 \rangle$ and $\langle P_4 \rangle$ values have been compared with the theoretical Maier-Saupe values.

In the nematic phase of the mixtures which exhibit induced Smectic A_d phase, the experimental OOP values determined from x-ray diffraction study are in closer agreement with the theoretical curve compared to that obtained from refractive index measurement. But there is disagreement near the nematic-isotropic transition temperature. This discrepancy may be due to the fact that different approximations and averaging are involved in calculating

orientational order parameter from experimental data obtained from x-ray studies in one hand and birefringence measurements on the other hand [13]. The $\langle P_4 \rangle$ values obtained from x-ray diffraction measurement however, is always significantly less than the theoretically calculated values in both smectic and nematic phases. Such behaviour of $\langle P_4 \rangle$ has been observed by others [14-16].

Figure 5.23 shows the variation of OOP values at T=35°C against mole fraction from x-ray diffraction measurements. The Δn values at the same temperature are also plotted in this figure. From this figure it is clear that in the smectic phase the OOP values initially increases with molar concentration upto x = 0.24 and then decreases and showing a broad minima around x = 0.4. The Δn values also show similar behaviour. Previous workers have also observed similar trend in the variation of $\langle P_2 \rangle$ and birefringence with mole fraction for a binary mixture ME6O.5 and a

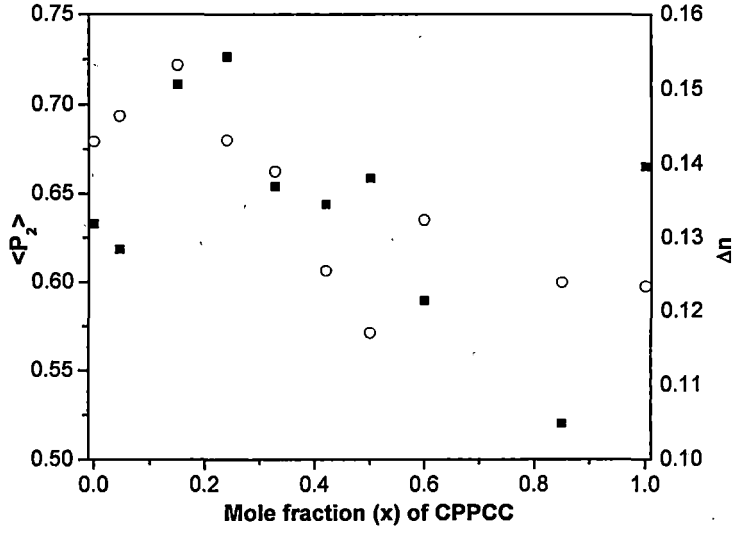

FIGURE 5.23: Concentration variation of $\langle P_2 \rangle$ values obtained form x-ray diffraction measurement and Δn values at T=35°C.

a cyanobiphenyl (5CB) as the individual components. However, for such system this minimum has been observed for nearly equimolar concentration [4].

Regarding the behaviour of entropy change associated with the smectic – nematic phase transition, ΔS_{SN} in this system, I have calculated ΔS_{SN} from McMillan's theory, taking the values of α,δ,η,τ and σ , at either side of the smectic nematic transition temperature obtained from the best fit theoretical curve to the experimental x-ray $\langle P_2 \rangle$ data. The $\Delta S_{SN}=(S_N-S_S)$ is calculated from the following well-known expressions [17].

$$S_S = -\frac{Nk}{T^*}(\eta_S^2 + \alpha\delta\tau_S^2 + \alpha\sigma_S^2) + Nk \ln Z_S \qquad \textbf{5.1}$$

$$S_N = -\frac{Nk}{T^*}\eta_N^2 + Nk \ln Z_N \qquad \textbf{5.2}$$

where $T^* = \frac{kT}{\nu}$

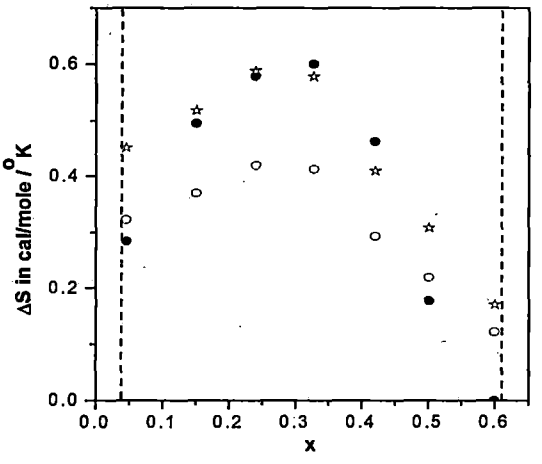

FIGURE 5.24: Entropy change associated with smectic to nematic phase transition of mixture ME6O.5/CPPCC with mole fraction. ○ calculated values of ΔS_{SN} from McMillan's theory. ☆ calculated values multiplied by a factor 1.4; ● experimental values.

Figure 5.24 shows the theoretically estimated and experimentally determined entropy values. It is observed that, although the general trend of the behaviour of entropy change at the smectic A_d – N phase transition, ΔS_{SN}, in the region of the induced smectic phase is reproduced by the theory, the calculated values of the entropy change at the smectic to nematic transition are somewhat 1.4 times larger. The agreement could have been better by changing the values of α and δ, but I have used only those values which give best fit to our experimental order parameter values.

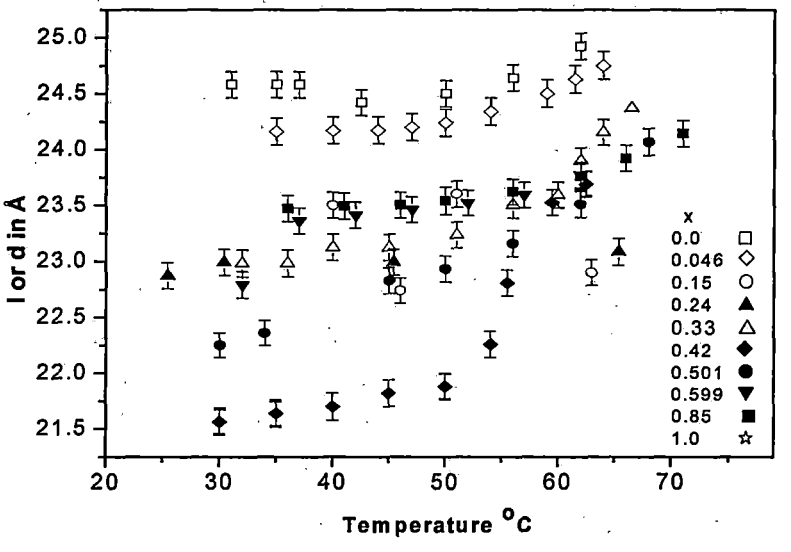

FIGURE 5.23: Temperature variation of apparent molecular length in the nematic phase and the layer thickness in the smectic phase.

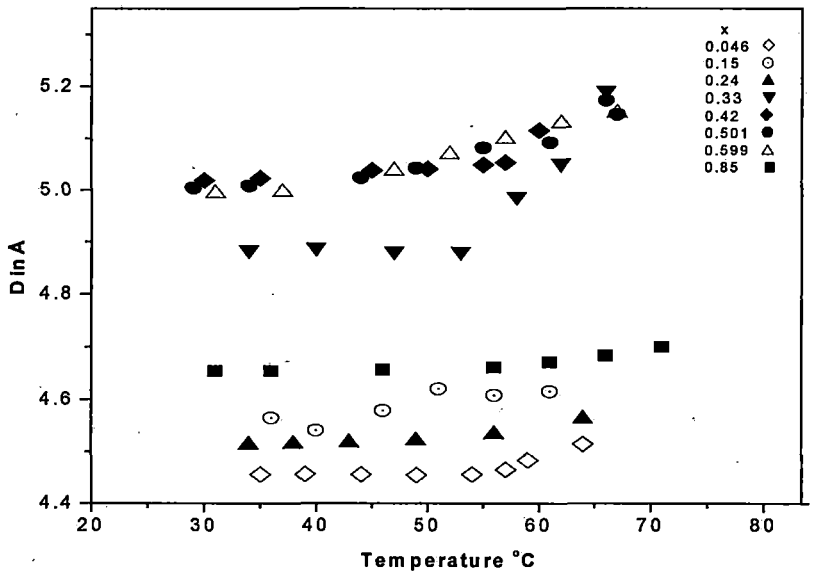

FIGURE 5.24: Lateral intermolecular distance (D) at different temperatures for mixtures of ME6O.5 + CPPCC.

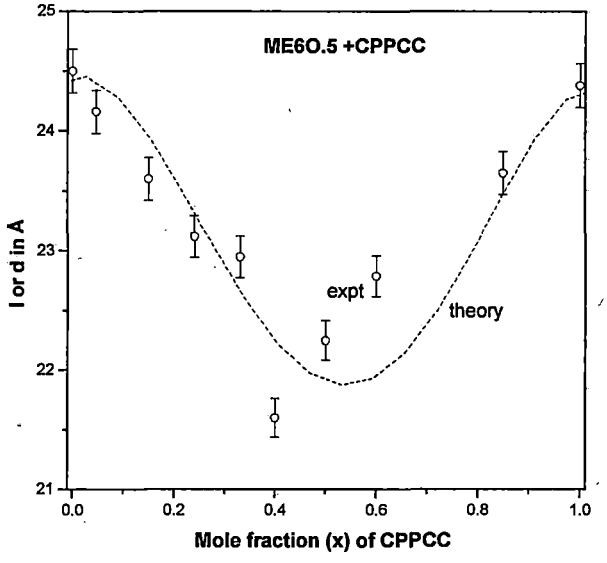

FIGURE 5.25: Variation of layer thickness (d) with molar concentration. Vertical bar represent the estimated error.

The temperature variation of the layer thickness for the mixtures is shown in figure 5.23. It can be seen that the layer thickness (d) values are almost independent of temperature. This is quite common in smectic A phases.

However, the apparent molecular lengths (l) in the nematic phase increases with increasing temperature.

The temperature variation of lateral intermolecular distance (D) for all the mixtures is shown in figure 5.24. It is seen that D values are almost constant throughout the mesophase except near the clearing temperature.

The composition variation of layer thickness at 35°C is shown in figure 5.25. The variation shows a broad minimum of ~21.6Å at about x=0.42 concentration. This behaviour is also observed by Das et al [4-6], where the layer thickness shows a minimum at about equimolar concentration. In order to calculate the variation of layer thickness with molar concentration we assume that the pure CPPCC molecules (molecule A) form association in the nematic phase. The apparent molecular length of CPPCC as determined from x-ray diffraction studies is 24Å, which is much larger than its model molecular length of 17Å. It is considered that the molecules form association and the pure state is a mixture of predominantly associated dimers and monomers, which are in dynamic equilibrium. On the other hand, since the apparent molecular length of ME6O.5 molecule (molecule B), as determined from x-ray studies [4], is almost equal to the model molecular length, so the molecule B exists as a monomer in its pure state. In mixtures we can assume that the terminal polar molecules form homo dimers (AA) as well as hetero dimmers (AB). The possibility of formation of such homo and hetero complexes was proposed earlier by Dabrowski et al. [18]. Garg and Spears from their molecular modeling on a related system showed a strong interaction between two species forming hybrid molecule [19]. Such cross

interaction is also proposed by Kyu et al [20-21] from their theoretical work on induced smectic A phase.

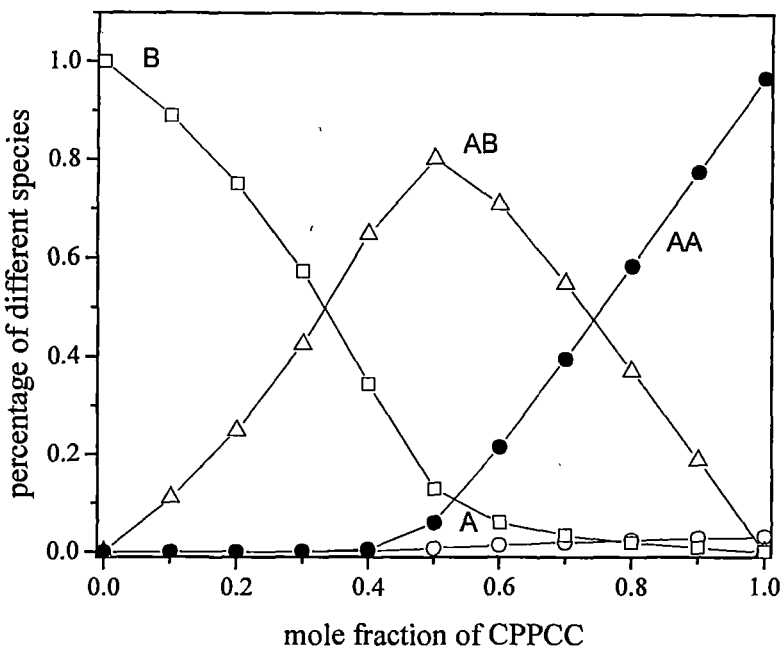

FIGURE 5.26: Percentage of different species A, B, AB and AA as a function of mole fraction of CPPCC.

Hence in the mixtures we can assume that there exist A, B, AA and AB types of molecules in equilibrium. The mole fractions of different species x_A, x_B, x_{AA} and x_{AB} can be determined from the equilibrium constants K_A and K_{AB} for the associations, $A + A \leftrightarrow AA$, $A + B \leftrightarrow AB$, respectively. Using equilibrium constants $K_A = 1000$ and $K_{AB} = 800$, the percentage of different species, A, B, AA and AB as function of mole fraction of CPPCC, have been calculated, which is shown in Figure 5.26. These values of K_A and K_{AB} are typical of similar systems we have studied previously [22].

The average d value may then be written as

$$d = x_A d_A + x_{AA} d_{AA} + x_{AB} d_{AB} + x_B d_B \qquad \textbf{5.3}$$

where x_A, x_B, x_{AA}, x_{AB} are mole fractions of respective components in chemical equilibrium, d_A and d_B are taken to be equal to the lengths of the molecules A and B as obtained from molecular model kit. d_{AB} is taken as the arithmetic mean d_A and d_B, while d_{AA} has been adjusted so that in pure terminal polar compound, which has both A and AA molecules, the apparent molecular length equals ($= x_A d_A + x_{AA} d_{AA}$) the experimentally observed d value. The values of d at T = 35° C, calculated from equation (5.3) is shown in Figure 5.25. It is to be noted that the values of K_A and K_{AB} can be varied by about 15% without much change in the calculated values of d. From figure 5.25 it is seen that the calculated result for the layer thickness is in excellent agreement with the experimental values.

In figure 5.27 I have also plotted the average lateral distance between the molecules at T=35°C with molar concentration. Interestingly, it is seen that D values are more or less constant for $x<0.24$ and then increases showing a maximum near equimolar concentration.

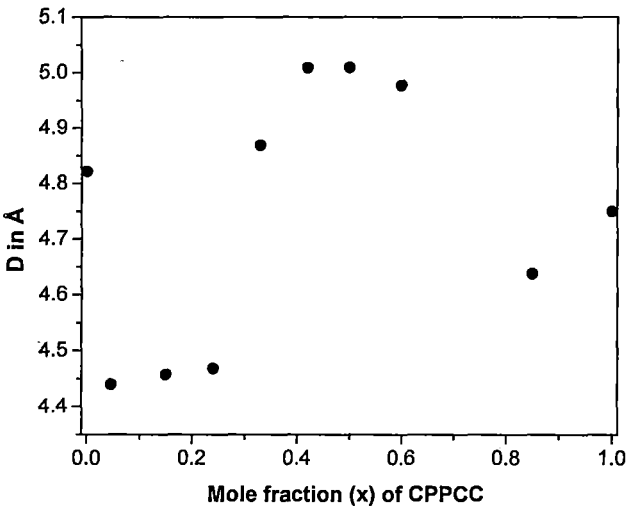

FIGURE 5.27: Variation of lateral intermolecular distance (D) with molar concentration.

5.8 Permittivity measurements:

The temperature variations of the dielectric permittivities ($\varepsilon_{\parallel}$ and $\varepsilon_{\perp}$) are shown in figures 5.28(a)-5.28(c). There is no sharp discontinuity in the measured permittivity components for the mixtures as well as pure compounds at the nematic to isotropic transition. The mixtures and the pure compounds exhibit positive dielectric anisotropy. Dielectric anisotropy ($\Delta\varepsilon$) is large for pure CPPCC and this is due to the terminal polar CN group. On the other hand $\Delta\varepsilon$ for non-polar ME6O.5 is very small. The isotropic dielectric permittivity (ε_{iso}) and the average dielectric permittivity $\bar{\varepsilon} = \{1/3(\varepsilon_{\parallel} + 2\varepsilon_{\perp})\}$ of this mesogen almost coincide at the nematic-isotropic phase transition temperature, as predicted by Madhusudana and Chandrasekhar [23].

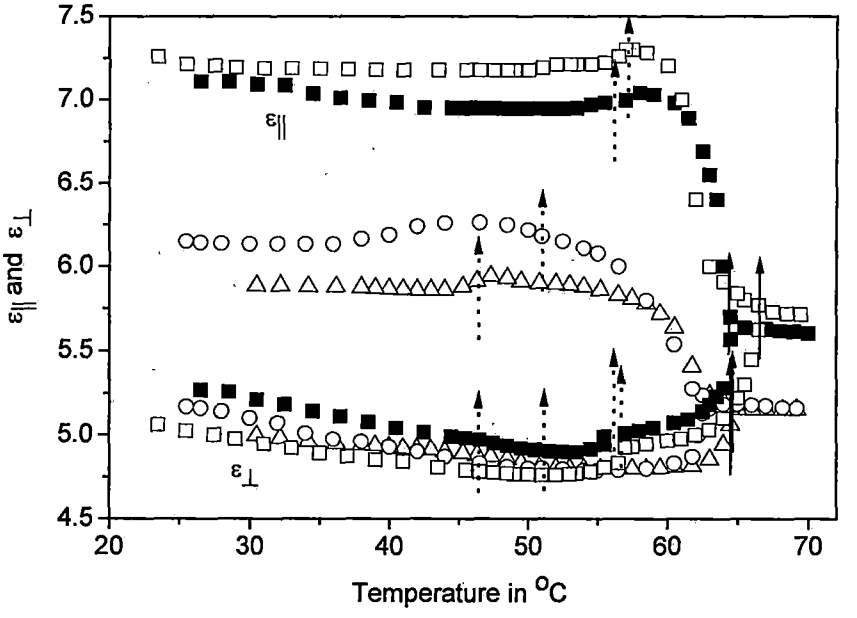

FIGURE 5.28 (a): Variation of electric permittivity as a function of temperature: Δ (x= 0.046); o (x= 0.15); ■ (x= 0.24); □ (x=0.33). ↑ for nematic to isotropic transition; ↑ for smectic A_d to nematic transition.

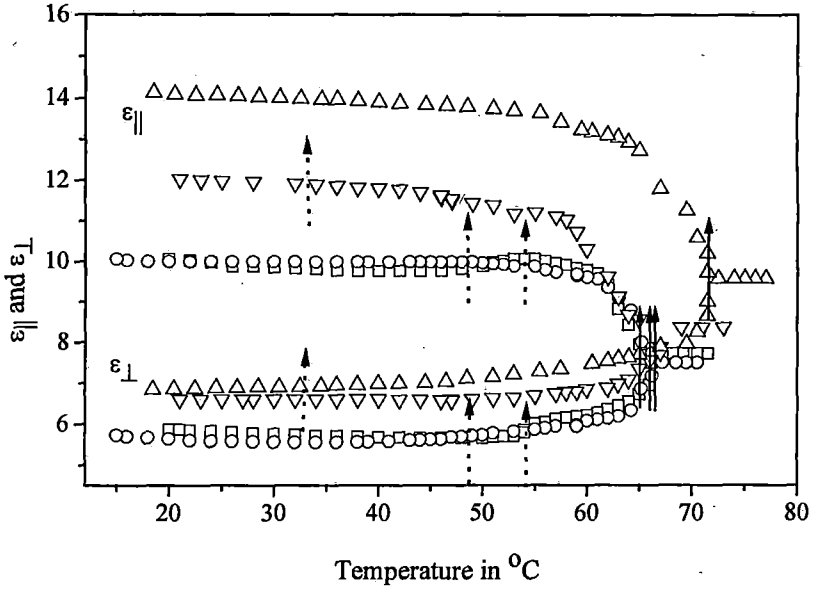

FIGURE 5.28 (b): Variation of electric permittivity as a function of temperature: □ (x= 0.42);o (x= 0.5); ▽ (x= 0.6); Δ (x=0.85). ↑ for nematic to isotropic transition; ↑ for smectic A_d to nematic transition.

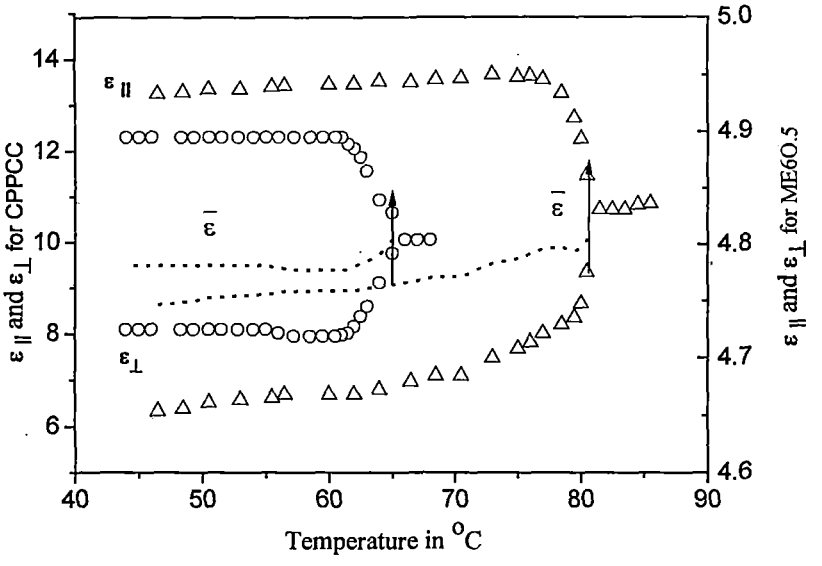

FIGURE 5.28 (c): Variation of electric permittivity as a function of temperature for the pure compounds: o ME 6O.5; Δ CPPCC. ↑ for nematic to isotropic transition.

The value of the isotropic dielectric permittivity (ε_{iso}) of the mixtures extrapolated to the nematic phase is greater than the average dielectric permittivity. Mixtures with mole fraction x in the vicinity of 0.3, show a discontinuity in the permittivity components at the smectic-nematic transitions. The value of both the dielectric permittivity components reduces in the smectic phase. This reduction is maximum when x is near about 0.3. Incidentally, these mixtures correspond to that region of the phase diagram where the induced smectic A_d phase is most stable. Similar effects have been observed in mixtures of 5CB and ME5O.5 [6]. For other mixtures there is no longer such a discontinuity in the permittivity components at the smectic-nematic transitions.

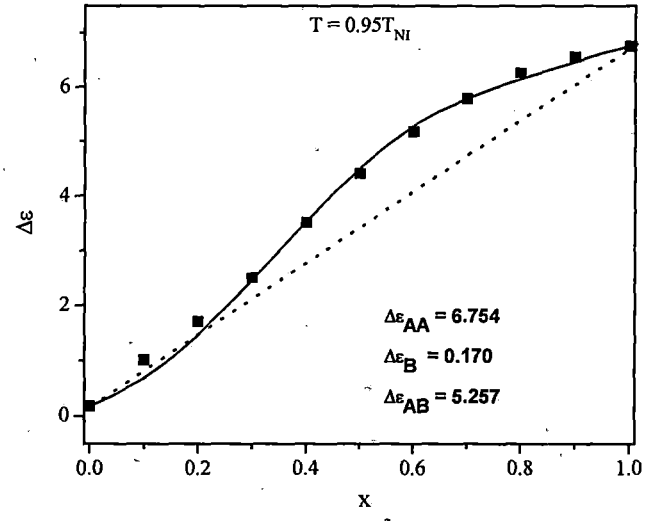

FIGURE 5.29: The permittivity anisotropy Δε plotted against mole fraction (x) at a reduced temperature, $T_R = 0.95$. ■ experimental values, Solid line represents the calculated values. Dotted line represents the average values.

In Figure 5.29 I have plotted Δε as a function of mole fraction of CPPCC corresponding to a reduced temperature $T_R = (T/T_{NI}) = 0.95$. At this reduced temperature all the mixtures with mole fractions $0.03<x<0.6$ show SmA_d phase. The Δε values having mole fractions $x > 0.2$ lie significantly above the average values, shown by a straight line connecting those of the pure compounds.

Similar to the assumptions made in the calculation of the smectic layer spacings (d) as discussed previously in this chapter, in order to calculate the variation of Δε with molar concentration, it is again assumed that the molecules form association and the pure state is a mixture of predominantly associated dimers and monomers, which are in dynamic equilibrium. The percentage of different species has already been shown in figure 5.26.

The average values of $\Delta\varepsilon$ may then be written as

$$\Delta\varepsilon = x_A\Delta\varepsilon_A + x_{AA}\Delta\varepsilon_{AA} + x_{AB}\,\Delta\varepsilon_{AB} + x_B\Delta\varepsilon_B \qquad \textbf{5.4}$$

From 5.26 it is apparent that in pure CPPCC only 3% of A monomers are present. In mixtures this value gradually decreases with decrease in the mole fraction of CPPCC and is nearly absent around $x \approx 0.5$. Since I am not in a position to calculate $\Delta\varepsilon_A$, in this calculation I assumed $\Delta\varepsilon_A \approx \Delta\varepsilon_{AA}=5.57$ (i.e. the experimentally determined $\Delta\varepsilon$ value of pure CPPCC at $T_R = 0.95$). I have assumed $\Delta\varepsilon_B$ is the dielectric anisotropy for ME6O.5 at $T_R = 0.95$. However, I still do not know the value of $\Delta\varepsilon_{AB}$, which may be estimated as follows:- From figure 5.26 it is evident that for mixture with $x \approx 0.4$ there is no A monomer and about 70% of the molecules are forming AB dimer. Knowing the experimental value of $\Delta\varepsilon$ at $T_R = 0.95$, I have estimated $\Delta\varepsilon_{AB}$ for AB dimer from equation 5.4.

$$\Delta\varepsilon = \Delta\varepsilon_{AA}\,x_{AA} + \Delta\varepsilon_{AB}\,x_{AB} + \Delta\varepsilon_B\,x_B \qquad \textbf{5.5}$$

From this calculation, $\Delta\varepsilon_{AB}$ is estimated to be 5.258 at the reduced temperature, $T_R = 0.95$.

The values of $\Delta\varepsilon$ at $T_R = 0.95$, calculated from equation 5.5 is shown in figure 5.29. It is to be noted that the values of K_A and K_{AB} can be varied by about 15% without any appreciable change in the calculated values of $\Delta\varepsilon$. From Figure 5.29 it is seen that the calculated result for the dielectric anisotropy is in excellent agreement with the experimental values.

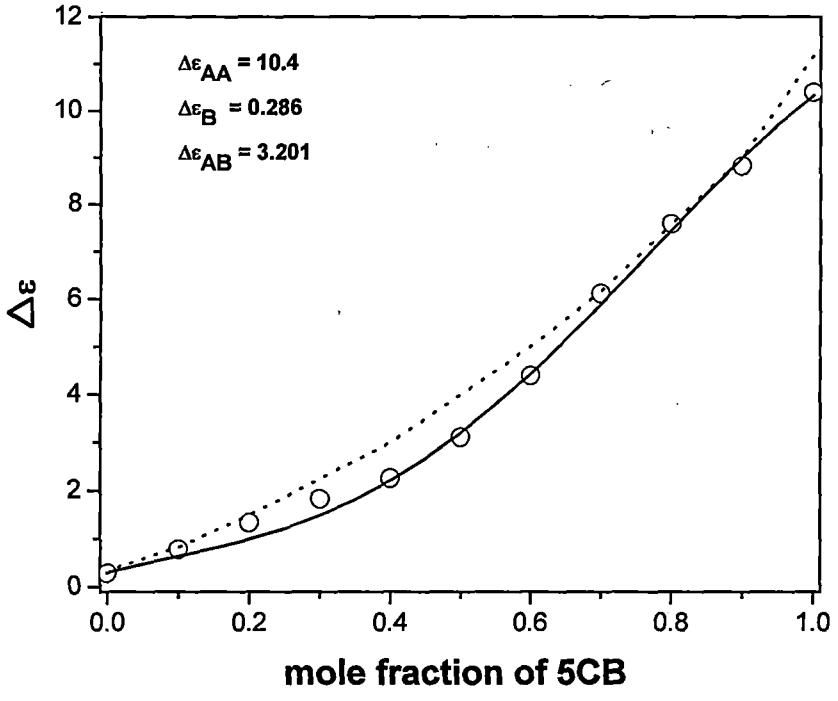

FIGURE 5.30: The dielectric anisotropy Δε in the nematic phase plotted against mole fraction of 5CB (x) at a reduced temperature, T_R = 0.99 for binary mixture ME5O.5 + 5CB. The open circles are experimental points and the solid line represents the calculated values. Dotted line represents the calculated values using additive rule by Dunmur *et al.* [2].

Previously, Das et al have successfully explained the variation of layer thickness with molar concentration by assuming the formation of two types of dimers in a related mixture of 5CB and ME50.5 showing induced smectic A_d phase [6]. Extending this work to explain the molar concentration dependence of the dielectric anisotropy of the same mixture (5CB + ME5O.5) as reported by Dunmur et al [7], it is observed that the results of this calculations using equation 5.5 are also in good agreement with the experimentally determined values as shown in figure 5.30.

These results once again prove the validity of the model of formation of molecular associations in the form of homo and hetero dimers in polar – non polar mixtures exhibiting induced smectic A_d phases [22].

Table 5.1: Polarizability anisotropy calculated from Haller's extrapolation procedure for different mixtures

x	$(\alpha_{\|\|} - \alpha_{\perp}) \times 10^{-24}$
0.046	16.75
0.24	14.26
0.33	14.845
0.42	14.99
0.15	15.50
0.501	15.265
0.599	15.40
0.85	17.508

References:

1. C. S. Oh, *Mol. Cryst. Liq. Cryst.*, **42**, 1(1977).
2. B. Engelen and F. Schneider, *Z. Naturforsch*, **33a**, 1077 (1978).
3. M. Domon and J. Billard, *J. Phys, (Paris)*, **40**, C3-413 (1979).
4. M.K. Das and R. Paul, *Phase Transitions*, **46**, 185(1994), **48**, 255(1994).
5. M.K. Das, R. Paul , *Mol. Cryst. Liq. Cryst.*, **260**, 477(1995).
6. M.K. Das, R. Paul and D.A. Dunmur, *Mol. Cryst. Liq. Cryst.*, **285**, 239 (1995).
7. D.A. Dunmur, R.G. Walker and P. Palffy-Muhoray, *Mol. Cryst. Liq. Cryst.*, **122,** 321(1985).
8. M. Domon and J. Billard, *J. Phys, (Paris)*, **40**, C3-413 (1979).
9. F. Schneider and N.K. Sharma, *Z. Naturforsch.*, **36a**, 62, (1981).
10. K. Araya and Y. Matsunaga, Bull. *Chem. Soc. Jap.*, **53**, 3079 (1980).
11. M. Brodzik and R. Dabrowski, *Mol. Cryst. Liq. Cryst.*, **260**, 361(1995).
12. W. L. McMillan, *Phys. Rev.*, **A4**, 1236 (1971), **A6**, 936 (1972).
13. M.K. Das and R. Paul, *Mol. Cryst. Liq. Cryst.*, 239 107(1994).
14. M. Mitra and R. Paul, *Mol. Cryst. Liq. Cryst.*, 177, 71 (1989).
15. M. Mitra, S. Paul and R. Paul, *Liq. Cryst.*, **3**, 123 (1988).
16. P. Mandal, M. Mitra, S. Paul and R. Paul, *Liq. Cryst.*, **2**, 183 (1987).
17. P. J. Wojtowicz, "*Introduction to Liquid Crystals*", (Eds.) E. B. Priestely, P. J. Wojtwicz and P. Sheng, Plenum Press, New York, p. 95 (1947).

18. R. Dabrowski, K. Czuprynski, "*Modern topics in Liquid Crystals - from Neutron Scattering to Ferroelectricity*", (Ed.) Agnes Buka, World Scientific, 1993 (London).
19. Shila Garg and Tom Spears, *Mol. Cryst. Liq. Cryst.*, 409, 335 (2004).
20. Thein Kyu, Hao-Wen Chiu and Tisato Kajiyama, *Phy. Rev.* **E55**, 7105 (1997).
21. Hao-Wen Chiu and Thein Kyu, *J. Chem. Phys*, **103**, 7471 (1995).
22. M. K. Das, R. Paul , *Mol. Cryst. Liq. Cryst.*, **260**, 477 (1997).
23. N. V. Madhusudana, K.L. Savithramina and S. Chandrasekhar, *Pramana*, **8**, 22 (1977).

Chapter 6

Physical Properties Of A Mesogenic Mixture Showing Induce Smectic A_d Phase II: Diamagnetic Susceptibility Anisotropy And Splay And Bend Elastic Constants

6.1 Introduction:

In chapter 5, I have reported some physical properties of a binary system (ME6O.5 + CPPCC) showing induced smectic phase from x-ray diffraction, refractive index and dielectric anisotropy measurements. In this chapter the results of magnetic susceptibility anisotropy measurements on the same mixture, throughout their mesomorphic and concentration range is reported. The splay (K_{11}) and bend (K_{33}) elastic constants, for this binary system have also been determined by observing Freedericksz transition [1] in magnetic field. It is to be noted that, although the formation of induced smectic phase is undesirable in LCD materials, its presence at a lower temperature than the working temperature of the LCD may be helpful under certain conditions [2-4]. The performance of liquid crystal materials in LCD's depends critically on the temperature dependence of the dielectric, optical, elastic constants and the viscosity coefficients of the materials to be used. Measurements of Frank elastic constants [5] play an important role in characterizing liquid crystal display devices and this information is important from display manufacturing point of view [6-8]. Again, precise determination of the elastic constant requires knowledge of the corresponding diamagnetic anisotropy of the material.

6.2 Magnetic susceptibility measurement:

The details of the experimental techniques involved have already been described in chapter 2 of this thesis. The experimental data for magnetic susceptibility anisotropy have been analysed to calculate the order parameter of the system.

The phase diagram of this mixture has been reported and discussed in chapter 5. As observed earlier, this mixture shows an induced smectic A_d

phase in the concentration range $0.03<x<0.6$, where x is the mole fraction of CPPCC. Refractive indices (n_o, n_e) as well as birefringence (Δn) show a minimum near x=0.4. The orientational order parameters as calculated from refractive index and x-ray diffraction studies of this mixture, when plotted against composition, show a minimum near the x=0.3. The layer thicknesses also show a minimum near x=0.4. It is of interest to investigate whether the magnetic susceptibility anisotropy $\Delta\chi$ and orientational order parameter $\langle P_2 \rangle$ as determined from magnetic susceptibility studies, also follow a similar trend. Moreover, the experimental magnetic susceptibility anisotropy $\Delta\chi$ data, which has been analyzed to calculate the temperature variation of the order parameter [9-10] of the system, is widely accepted to be one of the best methods.

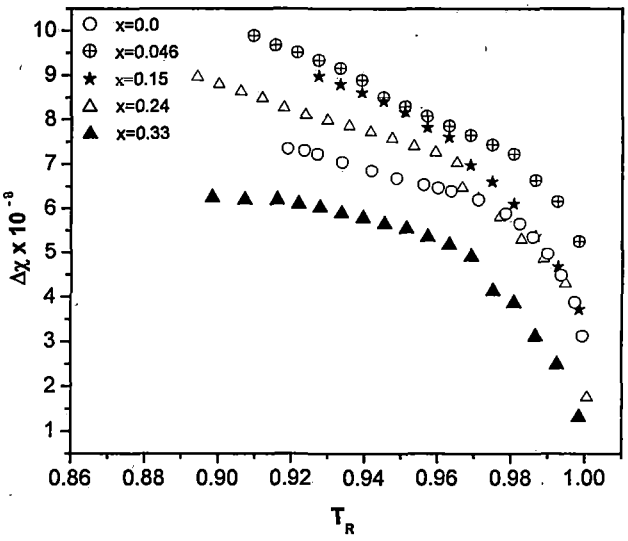

FIGURE 6.1: Variation of magnetic susceptibility ($\Delta\chi$) with reduced temperature for different mixtures and pure compounds.

The mass diamagnetic susceptibility as a function of temperature for eight different concentrations of this mixture has been measured. Both the pure compounds and their mixtures are found to be diamagnetic in nature. Our

experiment gives, therefore, the principal susceptibility parallel to the director. The diamagnetic susceptibility anisotropy as a function of reduced temperature for all the eight mixtures as well as pure compounds are shown in figure 6.1 – 6.2.

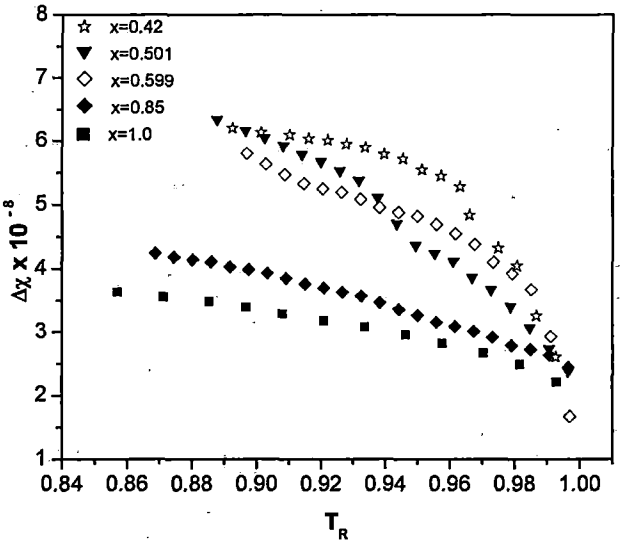

FIGURE 6.2: Variation of magnetic susceptibility ($\Delta\chi$) with reduced temperature for different mixtures and pure compounds.

For all the mixtures as well as pure compounds, $\chi_{\|}$ and hence $\Delta\chi$ increases with decrease in temperature in nematic and smectic phases. Anisotropy of diamagnetic susceptibility values of ME6O.5 are higher than those obtained from CPPCC. This is expected because ME6O.5 contains two phenyl rings with terminal alkyl chains and hence gives large diamagnetic anisotropy. On the other hand CPPCC molecule contains one cyclohexane ring and one benzene ring in its core. As expected, the replacement of one aromatic benzene ring by cyclohexane leads to a decrease in anisotropy. Presence of the terminal CN group in CPPCC with a negative magnetic anisotropy reduces the anisotropy further [11]. Since this system exhibits induced smectic phase and the behaviour of physical parameters is more or less

complex compared to the pure compounds, additional interactions between the constituent molecules may play an important role on the physical properties of the mixtures.

In the isotropic state, χ_{iso} remains practically independent of temperature similar to the ordinary diamagnetic substances. In the solid phase the susceptibility χ also remains independent of temperature and its value is nearly equal to that in the isotropic phase. This happens due to the fact that during this transition a large amount of energy is released in the form of latent heat, which overcomes the magnetic energy. Hence in going through this, the completely oriented ensemble of molecules is broken into almost randomly oriented crystallites in the solid phase. This loss of alignment may be regarded as the cause of observed decrease in χ and hence $\Delta\chi$ [12]. The changes in $\Delta\chi$ values at the SmA_d - N transition are more pronounced for mixtures with x = 0.24 and 0.33. Similar behaviour is also observed in birefringence (Δn) as well as in the density values of these mixtures [13].

The experimental data for $\Delta\chi$ have been analyzed to calculate the order parameter of the system. As discussed in chapter 2, the determination of order parameter from equation 2.48 requires knowledge of the absolute susceptibility anisotropy values ($\Delta\chi_o$). Since the experimental data on $\Delta\chi_o$ are not available, one can derive from equation 2.37 only the relative temperature dependence of $\langle P_2 \rangle$. However, $\Delta\chi_o$ can be estimated using well-known Haller's extrapolation method [14].

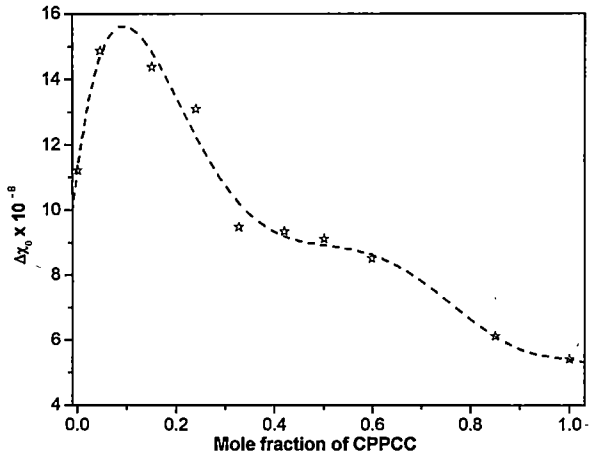

FIGURE 6.3: Variation of $\Delta\chi_o$ with reduced temperature for different mixtures and pure compounds.

In figure 6.3 I have plotted the absolute susceptibility anisotropy values estimated from Haller's method in the most ordered crystalline phase against mole fraction of CPPCC. The $\Delta\chi_o$ values decreases with increase in mole fraction of CPPCC. From the figure it is clear that inspite of the inaccuracies involved in this calculation and the arbitrariness of the Haller's procedure, there appears to be a minimum of $\Delta\chi_o$ values near x=0.4.

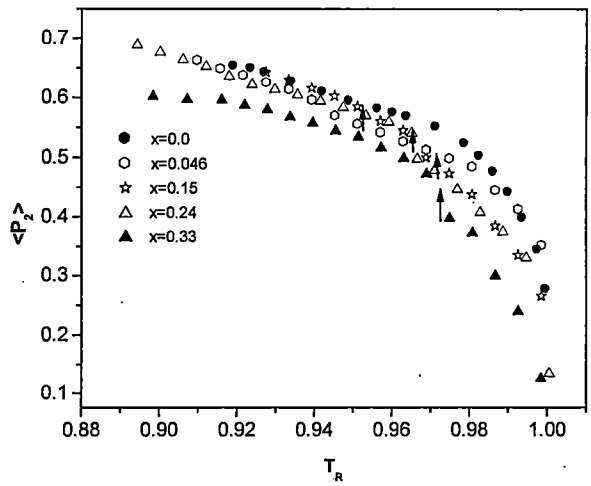

FIGURE 6.4: Temperature variation of order parameter $\langle P_2 \rangle$ with reduced temperature for different mixtures and pure compounds.↑ SmA_d-N transition.

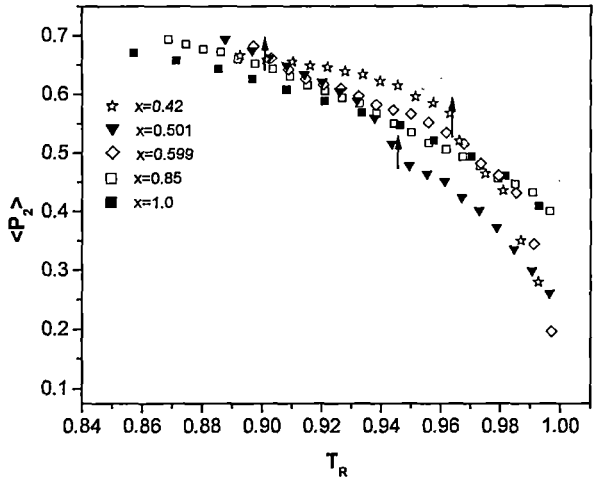

FIGURE 6.5: Temperature variation of order parameter $<P_2>$ with reduced temperature for different mixtures and pure compounds.↑ SmA_d-N transition.

The temperature variations of order parameter values for all the eight mixtures and pure components are shown in figures 6.4 – 6.5. From the temperature dependences of the orientational order parameters for mixtures at different concentration it is again observed that there is an appreciable change in the order parameter value at the smectic A_d to nematic phase transition temperature for mixtures in the range $0.15<x<0.42$.

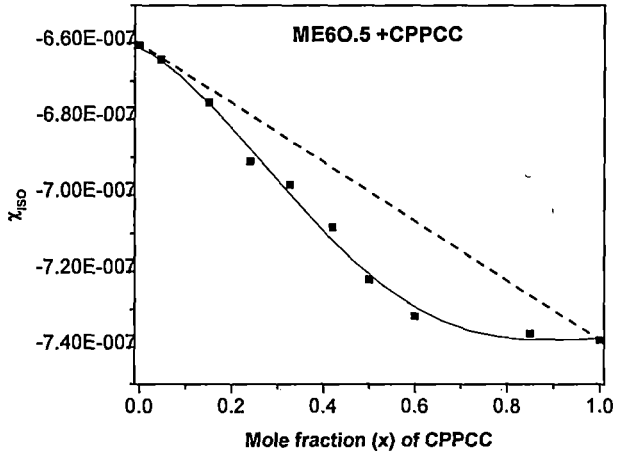

FIGURE 6.6: Variation of χ_{iso} for binary mixture of ME6O.5+CPPCC with mole fraction. Dotted line represents the average value.

The composition variation of the magnetic susceptibility in the isotropic phase, χ_{iso}, of all the mixtures is shown in figure 6.6. The experimental values of the pure components ME6O.5 and CPPCC are also plotted in the same figure. It has been found that the χ_{iso} values decreases with molar concentration and deviates from linearity (shown by straight line connecting those of the pure compounds). This deviation is maximum near $x \approx 0.6$.

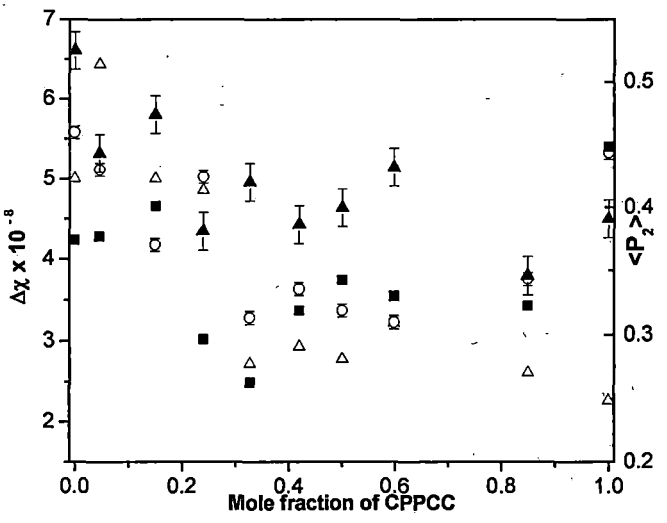

FIGURE 6.7: Variation of $\Delta\chi$ and order $\langle P_2 \rangle$ of CPPCC + ME6O.5 mixture with mole faction of CPPCC at a fixed reduced temperature $T_R = 0.99\ T_{NI}$. △ $\Delta\chi$ values, ○ $\langle P_2 \rangle$ from magnetic susceptibility, ▲ $\langle P_2 \rangle$ from x-ray diffraction and ■ $\langle P_2 \rangle$ from refractive index measurements.

Figure 6.7 shows the composition variation of $\Delta\chi$ in the mixture CPPCC + ME6O.5 at a reduced temperature of $T_R = 0.99T_{NI}$. The order parameter values from magnetic susceptibility measurement are also shown in this figure. The $\Delta\chi$ values are higher for mixtures having mole fraction $x<0.3$ in comparison to the both the pure compounds. In the concentration range $x>0.04$, $\Delta\chi$ values decreases with increase in molar concentration and shows a broad minimum near $x=0.3$. The orientational order parameter $\langle P_2 \rangle$ also shows a minimum there. The magnetic susceptibility data therefore is found

to agree quite well with the findings from refractive index as well as x-ray diffraction studies on this system. The maximum in the stability of smectic A_d phases (x=0.33) corresponds to the minimum of the order parameter. The birefringence shows a minimum nearly the same composition range [13]. This lowering in the order parameter values has also been confirmed from the present magnetic susceptibility studies done on this system.

6.3 Elastic constants measurement:

In this section, I present the results of the splay and bend elastic constants measurement of this mixture. The experimental set up and the techniques adopted have been given in detail in chapter 2. The values of splay (K_{11}) and bend (K_{33}) elastic constants as functions of reduced temperature ($T_R=T/T_{NI}$) are given in figures 6.8 and 6.9 respectively.

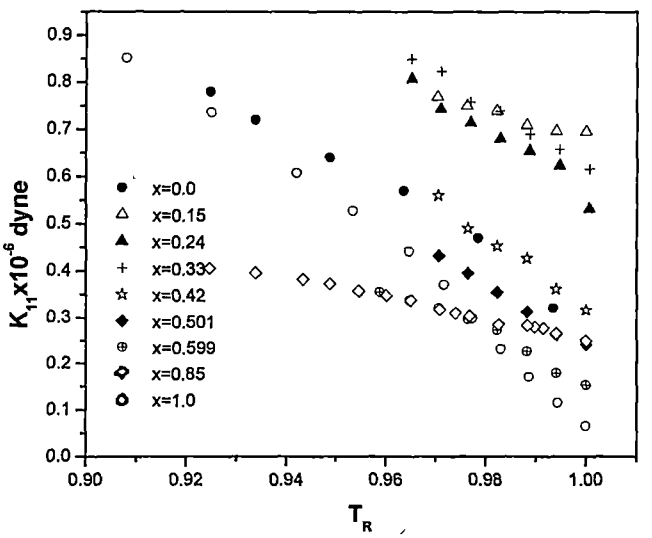

FIGURE 6.8: The splay (K_{11}) elastic constant as a function of reduced temperature ($T_R=T/T_{NI}$).

Figure 6.10 shows the K_{33}/K_{11} ratios for the pure compounds as well as their mixtures as a function of reduced temperature. It is observed that the K_{33}/K_{11} values decreases with increasing temperature as is expected. For mixtures exhibiting the induced smectic phase, the K_{33}/K_{11} values in the nematic shows a sharp increase particularly near the SmA-N transition. This increase of the bend to splay has also been reported by Bradshaw et al [2] in hybrid mixtures containing phenyl benzoate esters. Possible reason for this may be formation of smectic clusters as pre-transitional effects. Whereas such rapid increase is not found in the mixture (x=0.85), possibly because this mixture was studied in the concentration range which is far away from the induced phase region.

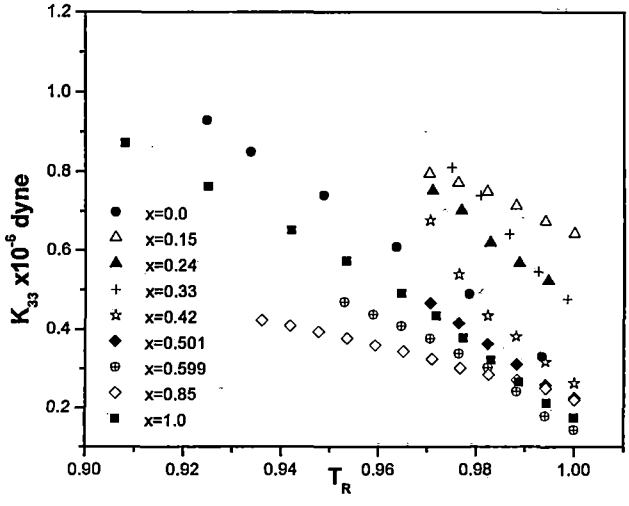

FIGURE 6.9: The bend (K_{33}) elastic constant as a function of reduced temperature ($T_R=T/T_{NI}$).

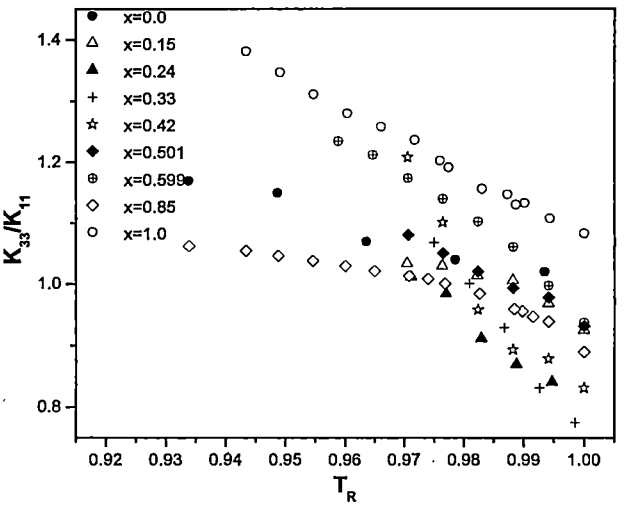

FIGURE 6.10: The splay to bend elastic constant ratios (K_{33}/ K_{11}) as a function of reduced temperature ($T_R=T/T_{NI}=0.99T_{NI}$).

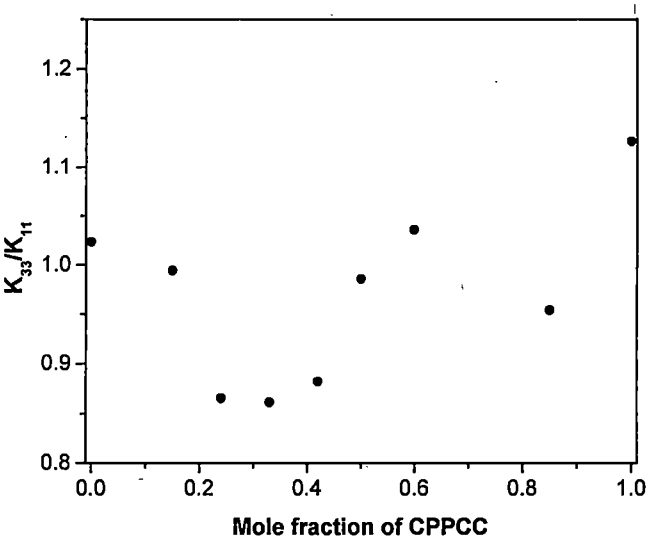

FIGURE 6.11: The splay to bend elastic constant ratios ● K_{33}/K_{11} as a function of mole fraction of CPPCC at reduced temperature ($T_R=T/T_{NI}=0.99T_{NI}$).

In Figure 6.11, I have plotted the K_{33}/K_{11} values at $T=0.99T_{NI}$ against mole fraction of CPPCC. The variation of K_{33}/ K_{11} shows a minimum near x=0.33 where the maximum stability of induced smectic A_d is observed in the mixtures.

The values of (K_{33}/K_{11}) for all the mixtures are lower than those of the pure compounds. Low values of (K_{33}/K_{11}) were observed in the binary mixtures [15-17] of strongly polar compounds containing terminal cyano groups together with weakly polar or non-polar esters [2]. This may be a consequence of the reduction in anti-parallel ordering of the cyano molecules (CPPCC) as the non-polar esters (ME6O.5) are added.

References:

[1] W. H. de Jue, *"Physical Properties of Liquid Crystalline Materials"*, Gordon Breach, NY, p. 24 (1980).

[2] M. J. Bradshaw and E. P. Raynes, *Mol. Cryst. Liq. Cryst.*, **138**, 307 (1986).

[3] M. K. Das, R. Paul, D. A. Dunmur, *Mol. Cryst. Liq. Cryst.*, **258**, 239 (1995).

[4] N. V. Madhusudana, *"Liquid Crystals: Application and uses"*, (Ed. B. Bahadur), World Scientific, **1** (1991).

[5] C. Frank, *Discussion Faraday Soc.*, **25**, 19 (1958).

[6] M. Schadt, M. Petrzilka, P. R. Gerber and A. Villiger, *Mol. Cryst. Liq. Cryst.*, **122**, 241 (1985).

[7] M. Schadt, R. Buchecker, F. Leenhouts, A. Boller, A. Villiger and M. Petrzilka, *Mol. Cryst. Liq. Cryst.*, **139**, 1 (1986).

[8] M. Schadt, R. Buchecker, and K. Muller, *Liq. Cryst.*, **5**, 1239 (1989).

[9] M. Mitra and R. Paul, *Mol. Cryst. Liq. Cryst.*, **148**, 185 (1987).

[10] W. Kuczyński, B. Żywuchki and J. Matecki, *Mol. Cryst. Liq. Cryst.*, **381**, 1 (2002).

[11] D. Demus, J. Goodby, G. W. Gray, H.-W, Spiess, V. Vill (Eds.), *"Handbook of Liquid Crystals: Low Molecular Weight Liquid Crystals -I"*, **2A**, 221-226 Wiley-VCH Verlag, Germany (1998).

[12] B. Bahadur, *J. Chem. Phys.*, **67**, No7 (1977).

[13] P. D. Roy, Chapter-5 of current thesis.

[14] I. Haller, H. A. Huggins, H. R. Lilienthal and T. R. McGuire, *J. Phys. Chem.*, **77**, 950 (1973).

[15] B. S. Scheuble, G. Baur and G. Meier, *Mol. Cryst. Liq. Cryst.*, **68**, 57 (1981).

[16] M. Schadt and P. R. Gerber, *Z. Naturforsch*, **A37**, 165 (1982).

[17] M. J. Bradshaw and E. P. Raynes, *Mol. Cryst. Liq. Cryst.*, **91**, 145 (1983).

Chapter 7

Phase Transitions and Physical Properties of a Binary Mixture of Bicyclohexane Compounds: Refractive Index and X-ray Diffraction Measurements

7.1 Introduction:

Liquid crystal material research have contributed significantly both to the development of liquid crystal display (LCD) technology and also at the same time to the better understanding of the phase behaviour of soft condensed matter systems. Thus, attempts are being continuously made to study the material properties of both pure compounds as well as their mixtures for a better insight into the basic understanding of liquid crystalline behaviour, so that better display devices can be made.

In this chapter, I present the phase diagram, DSC, birefringence, density and x-ray diffraction measurements of a binary mixture of two isomeric non-polar bicyclohexane compounds containing alkenyl side chains. So far, there are only a few liquid crystal classes described in the literature whose core consists of two cyclohexane rings. The physical properties of the pure components have been studied previously in our laboratory [1-4]. These two compounds, one comprising of only nematic phase ($1d(3)CCO_2$) and the other only smectic B phase ($0d(4)CCO_2$), are characterized by similar molecular structure, except for a shift in the position of the double bond. It has been shown by Schadt et al [5] that, the introduction of a double bond at specific side chain positions markedly affects the physical properties of liquid crystals. With a view to study the effect of the position of double bond in the alkenyl side chain on the mesomorphic properties, mixtures of these compounds have been prepared. Physical properties of these mixtures have been studied at seven different compositions. Phase diagram for this system shows the presence of mixtures with only smectic B phase, only nematic phase and mixtures with both smectic B and nematic phases. A two phase (smectic B - nematic) co-existing region (~2-3°C) has also been observed for

a small concentration range for these mixtures. Differential scanning calorimetric studies on these mixtures have been done and the entropy changes associated with the smectic B - nematic and nematic - isotropic phase transition have been calculated. Densities and refractive indices (n_o, n_e) have been measured for these mixtures. The refractive index data have been analyzed to yield orientational order parameters. From the DSC, density and birefringence measurements, the nature of the smectic B - nematic phase transition for these mixtures and the behaviour of these phase transitions with concentration has been assessed.

For x-ray diffraction measurements we have selected a few compositions of this mixture, which show both the smectic B and nematic phases. Two mixtures with molar concentration of 1d(3)CCO$_2$ = 0.6 (Mixture A) and 0.73 (Mixture B) have been studied thoroughly throughout the entire mesomorphic range. DSC studies for these two mixtures show a weakly first order or a second order phase transition in going from the smectic B to the nematic phase.

According to Birgeneau and Lister [6], the smectic B phase is a realization of the stacked hexagonal phase possessing BOO found in two dimensions. The order parameter associated with a system having six-fold symmetry, as in the case of smectic B liquid crystals is the Bond Orientational Order, defined to be the thermal average of the quantity

$$\psi(r) = \langle \exp (i6\theta(r)) \rangle \qquad \textbf{7.1}$$

where, the bond angle $\theta(\mathbf{r})$ is the orientation, relative to any fixed laboratory axis, of a bond between two nearest neighbour molecules. The x-ray

diffraction patterns have been analysed to determine the temperature dependence of the Bond Orientational Order (BOO) in the smectic B phase of only mixture A, where it has been possible to obtain a good mono-domain sample.

Orientational order parameters have also been studied throughout the entire mesomorphic range for mixtures A and B. The intermolecular distance, layer thickness and apparent molecular lengths of several mixtures (x = 0.3, 0.4, 0.5, 0.6 and 0.73, where x is the mole fraction of 1d(3)CCO_2)) have also been studied. Although x-ray [7-13] and electron diffraction [14,15] studies on smectic B phase have been reported so far, not much work has been done to determine the BOO and OOP in smectic B phase of bicyclohexane compounds. The BOO values obtained have been utilized to characterize the SmB phase which is found to be of the crystal B type. The BOO values of mixture A are found to be nearly independent of temperature in the SmB phase but increases with temperature within the co-existing SmB-N phase. The transverse correlation length diverges near the vicinity of the two-phase co-existing SmB-N region indicating a second order phase transition.

7.2 Experimental:

Phase diagram and texture study:

The compounds were donated by M/S Hoffmann-La-Roche and Co., Basel, Switzerland and were used without further purification. Phase transitions of the pure samples as well as their mixtures were studied by observing textures under crossed polariser with a polarizing microscope equipped with

a Mettler FP80/82 Thermo-system. The structural formula, transition temperatures and chemical name of the pure compounds are as follows:

Compound 1:

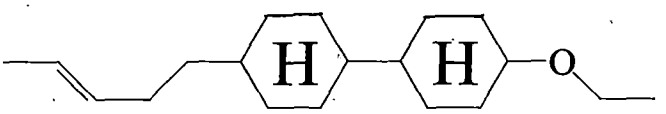

$$K \underset{24.5^{\circ}C}{\overset{44^{\circ}C}{\rightleftharpoons}} N \xrightarrow{76.5^{\circ}C} I$$

4(3″- pentenyl) 4′(ethoxyl) 1,1′ bicyclohexane (1d(3)CCO_2)

Compound 2:

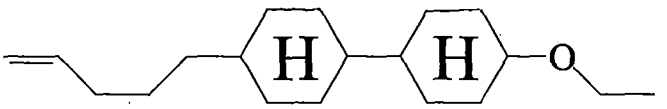

$$K \xrightarrow{11^{\circ}C} Sm\ B \xrightarrow{43^{\circ}C} I$$

4-ethoxy, 4′ - pent - 4″- enyl bicyclohexane (0d(4)CCO_2)

The phase diagram of this system is shown in figure 6.1. The nematic-isotropic and smectic B-nematic transition temperatures are plotted against mole-fraction (x) of 1d(3)CCO_2 in figure 6.1. It has only been possible to measure the supercooling temperature for mixture with x = 0.71 and the pure compound 1d(3)CCO_2 due to lack of cooling facilities in our laboratory. Texture study of these mixtures showed typical marbled texture in the nematic phase and a mosaic texture in smectic B phase.

DSC measurements:

Transition entropies ΔS (J $mol^{-1}K^{-1}$) were obtained from DSC studies (at a heating rate of 1°C/min) using a Mettler FP84HT TA Cell.

Density measurements:

The densities of all the binary mixtures were measured with the help of dilatometer of the capillary type. Density measurement of the pure compounds has already been done in our laboratory [1-2]. Temperature during the experiment is controlled to about ± 0.5°C by a temperature controller. Experimental uncertainty of the density measurement is 0.1%.

Refractive Index measurements:

The ordinary and extraordinary refractive indices (n_o, ne) for wavelength λ = 5780Å of mercury vapour lamp were measured within ± 0.001 by thin prism method (refracting angle < 2°) [16]. Details of the experimental technique used have been described in chapter-2 of this thesis. From the density and refractive index values, I have calculated the principal polarizabilities ($\alpha_{\|}$,$\alpha_{\perp}$) using Neugebauer's anisotropic internal field model [17] and Haller's extrapolation procedure [18].

X-ray diffraction Measurements:

X-ray diffraction patterns are recorded using a flat plate camera at several temperatures within the mesomorphic phase using Ni filtered CuK_{α} radiation of wavelength λ = 1.542Å. For x-ray diffraction study, the pure compounds as well as their mixtures could not be aligned even in a magnetic field of about 0.6T. The magnetic susceptibility anisotropy, $\Delta\chi$ for these compounds being almost zero, it is not possible to obtain monodomain samples by application of magnetic field. However, I succeeded in obtaining very good

monodomain samples in which the hexagonal symmetry of the SmB phase extended throughout the bulk sample by controlled cooling (at the rate of 0.1°C/min) of the samples kept in 0.5mm diameter glass capillaries, from the isotropic state to room temperature (~20°C). By trial a monodomain sample was selected and the capillary is rotated in such a way that the layer normal coincided with the direction of the x-ray beam. At this position of the capillary x-ray photographs are recorded. Photographs for orientational order parameter measurements are taken after rotating the sample filled capillary 90 degrees with respect to the previous position such that the smectic layer is now parallel to the direction of x-ray beam.

The x-ray diffraction photographs are scanned by a Mustek 1200 UB scanner. The gray mode scan is used and the resolution was set at 600 dpi. Optical densities of the pixels are calculated and then converted to X-ray intensities with the help of a calibration curve following the procedure of Klug and Alexander [19]. The Origin 7.0 software is used for data analysis purpose.

7.3 Results And Discussions:

From a detailed study of the phase diagram by microscopic observations, it is observed that for mixtures within the concentration range $0.2 < x < 0.8$ (x = mole fraction of 1d(3)CCO2), both smectic B and nematic phases are present. Mixtures with $x < 0.2$ show smectic B phase only and for $x > 0.8$ show only nematic phase.

For mixtures with mole fraction between x ≈ 0.5 to x ≈ 0.8 a two-phase (SmB- N) co-existing region of 2-3°C is observed. The phases could be identified distinctly under polarizing microscope and the co-existing phases are quite stable. All the mixtures show large super cooling.

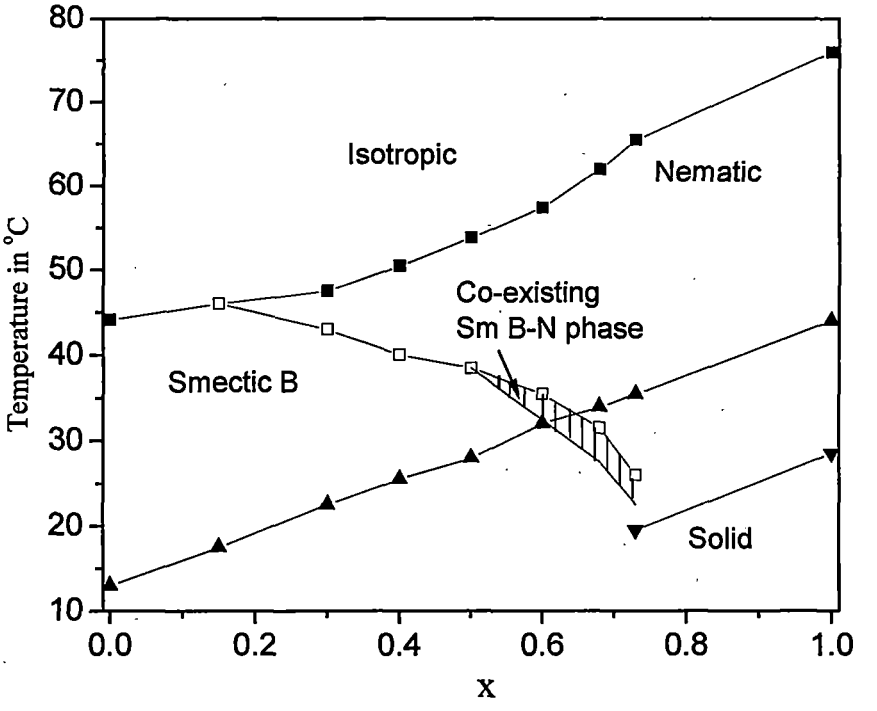

FIGURE 7.1: Phase diagram for the binary system of 1d(3)CCO_2 and 0d(4)CCO_2 . x is the mole fraction of 1d(3)CCO_2. ■ nematic (smectic B) - isotropic transition temperature. □ smectic B- nematic transition temperature; ▲ melting temperature; ▼ super- cooling transition temperature; shaded region represent the co-existing smectic B - nematic phase.

The isotropic transition temperature for these mixtures lie significantly below the straight line connecting those of the pure compounds and a fairly deep minimum is observed in the clearing curves for x ≈ 0.4. The melting temperatures for these mixtures however follow the additive rule.

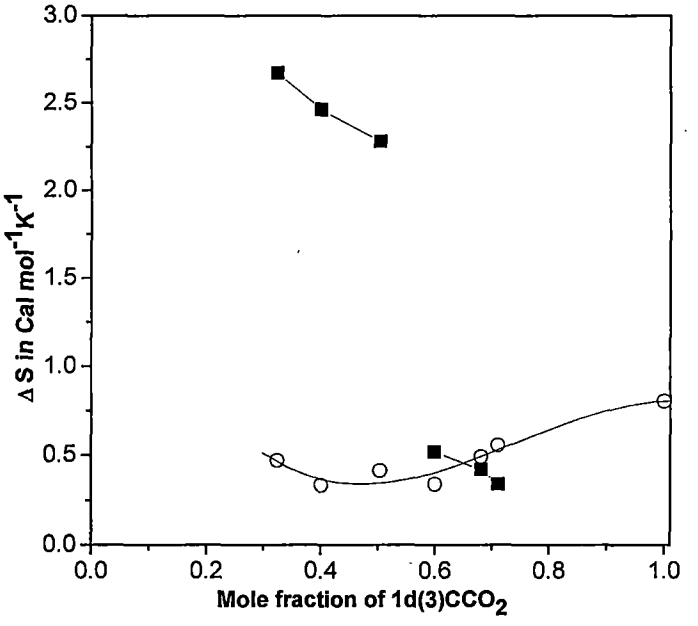

FIGURE 7.2: Transition entropies (ΔS) as a function of mole fraction of 1d(3)CCO_2 : ■ smectic B/nematic transition, ○ nematic/isotropic transition.

Figure 7.2 shows the entropy change associated with the smectic B - nematic and nematic - isotropic phase transition plotted against mole fraction of 1d(3)CCO_2. From the figure it is evident that the entropy change associated with the smectic B - nematic phase transition for these mixtures decreases linearly in the region x = 0 to x = 0.55 and then falls rapidly at x = 0.6. This clearly implies a change in the order of this phase transition from discontinuous to continuous at this value of x (= 0.6). The nematic-isotropic entropy change shows a minimum near equimolar concentration.

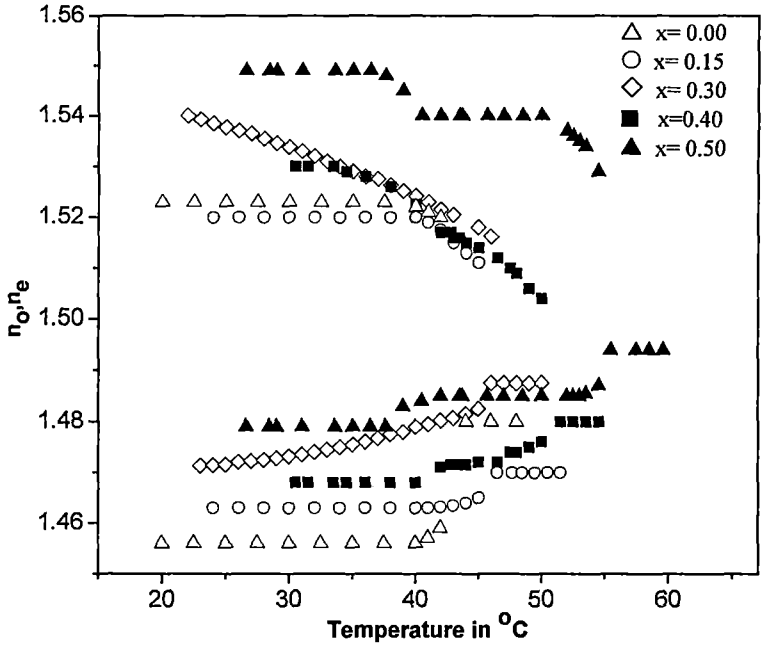

FIGURE 7.3 (a): Refractive indices as a function of temperature for mole-fractions (x) of 1d(3)CCO$_2$. △ (x= 0.0); ○ (x= 0.15); ◇ (x= 0.3); ■ (x= 0.4); ▲ (0.5).

The variation of ordinary (n_o) and extraordinary (n_e) refractive indices with temperature are shown in figures 7.3(a) – 7.3(b) for λ = 5780Å. The ordinary as well as the extraordinary refractive indices are found to be nearly independent of temperature in the smectic B phase, except very near to the smectic B-nematic (or isotropic) transition temperatures for all the mixtures. The n_e and n_o values are however quite sensitive to temperature in the nematic phase. In the co-existing smectic B - nematic phase, I have been able to measure simultaneously the refractive indices of both the smectic B and the nematic phases. The ordinary refractive indices for smectic B and nematic phases are the same, whereas the extraordinary refractive index for the nematic phase (n_{en}) and smectic B phases (n_{es}) are different. The

temperature dependence of n_{es} is large, but n_{en} is more or less independent of temperature.

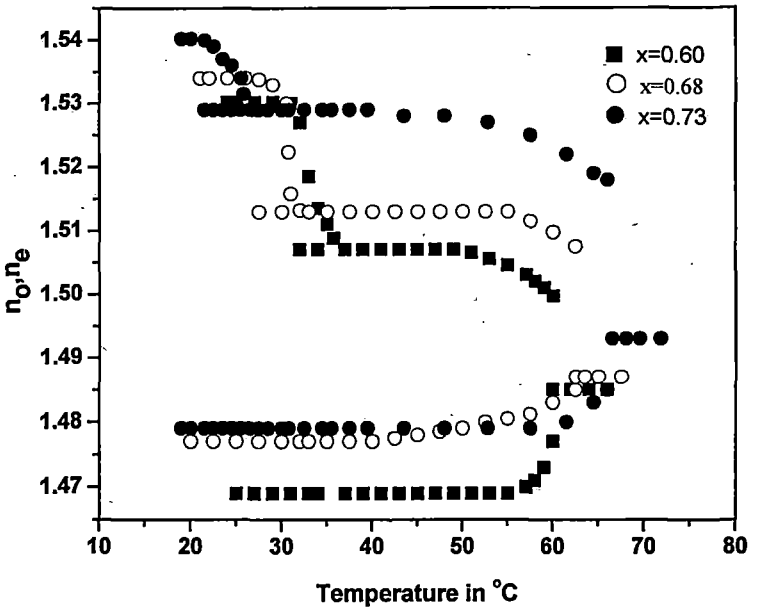

FIGURE 7.3 (b): Refractive indices (n_o, n_e) as function of temperature for different mixtures. ■ x=0.6; ○ x=0.68 ; ● x=0.73.

The optical birefringence Δn (= n_e-n_o) are shown in figures 7.4 (a) – 7.4 (b) for these mixtures, which are found to be very low and is less than 0.1 even in the smectic B phase. The temperature dependence of the density values for different mixtures as well as the pure compounds are plotted in figure 7.5. The change of birefringence as well as density values at the smectic B-nematic phase transition seems to be continuous for $x \geq 0.55$ which indicate a weakly first order or second order phase transition.

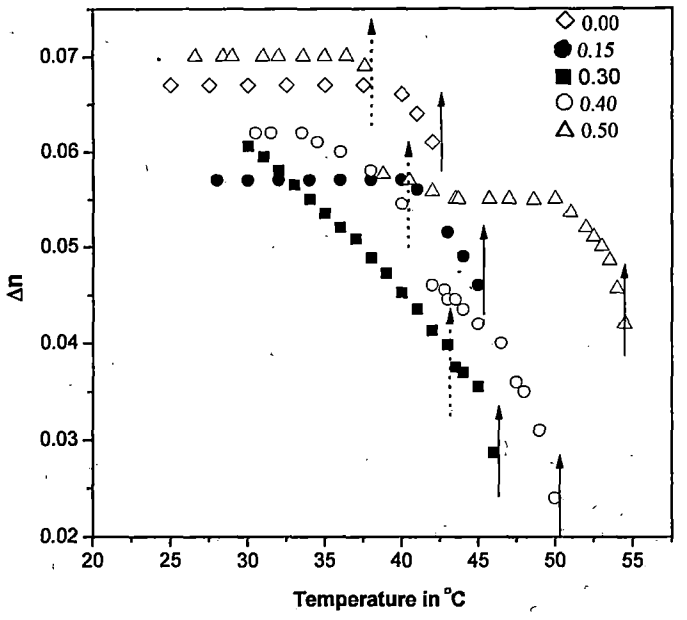

FIGURE 7.4 (a): Birefringence ($\Delta n = n_e - n_o$) as a function of temperature for different mixtures and a pure compound. ◇ (x= 0.0); ● (x= 0.15); ■ (x= 0.30); ○ (x= 0.4); △ (x= 0.5) ; ↑ for nematic to isotropic transition; ↑ for smectic B to nematic transition.

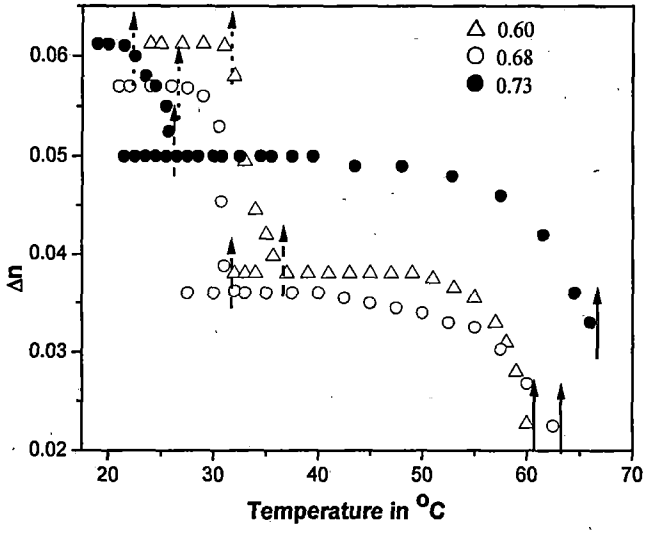

FIGURE 7.4 (b): Birefringence ($\Delta n = n_e - n_o$) as a function of temperature for different mixtures: △ (x= 0.6); ○ (x= 0.68); ● (x= 0.73); ↑ for nematic to isotropic transition; ↑ for coexisting SmB-N to nematic transition; ↑ for SmB to SmB – N coexisting transition.

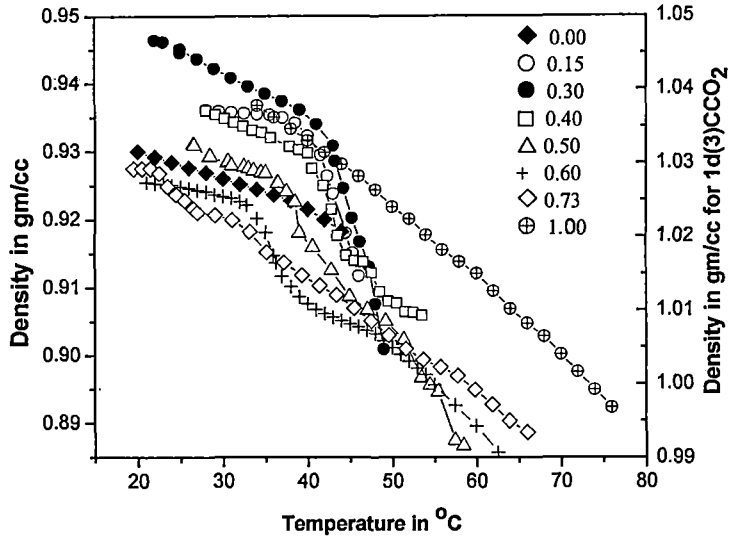

FIGURE 7.5: Density (ρ) values as a function of temperature for different mixtures and pure compounds. ◆ (x= 0.0); ○ (x= 0.15); ● (x= 0.3); □ (x= 0.4); △ (x= 0.5); +(x = 0.6); ◇ (x= 0.73); ⊕ (x= 1.0).

Both birefringence (Δn) and density values changes sharply with temperature within the co-existing smectic B-nematic phase. Also, the temperature dependences of the density values in the smectic B phase are much higher for mixtures with $x \leq 0.55$ than in the smectic B phase for those mixtures with $x \geq 0.55$. Incidentally the two-phase smectic B - nematic co-existence region is present for mixtures with $x \geq 0.55$. The temperature dependences of the density values show a steep variation within the co-existing phase in comparison to its dependence within its nematic and smectic B neighbours. I also observe similar behaviour of birefringence values for these mixtures (figure 7.4).

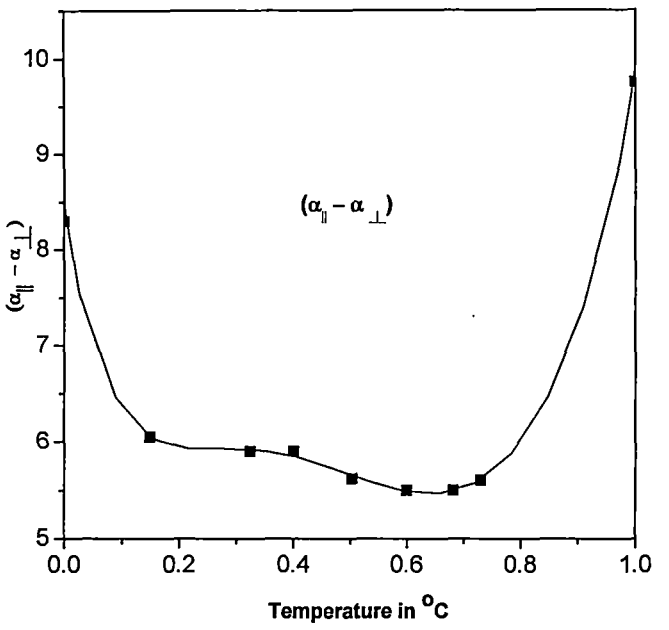

FIGURE 7.6: Variation of $(\alpha_{||} - \alpha_{\perp})$ against mole fraction of 1d(3)CCO_2.
■ Neugebauer's method.

In figure 7.6, I have plotted the polarizability anisotropy ($\Delta\alpha$) values for the pure compounds as well as for the different mixtures. I have observed that a decrease in the values of $\Delta\alpha$ with mole fraction of 1d(3)CCO_2 which shows a broad minimum near $x \approx 0.6$.

The temperature variations of orientational order parameter $\langle P_2 \rangle$ for the different mixtures are shown in figures 7.7(a) – 7.7(b). Similar to the observed trends in the temperature dependences of the density and birefringence, the $\langle P_2 \rangle$ values drops sharply at the nematic – smectic B phase transition for mixtures with $x < 0.5$ once again indicating the order of the nematic-smectic B phase transition for these mixtures to be of first order (figure 7.7(a)).

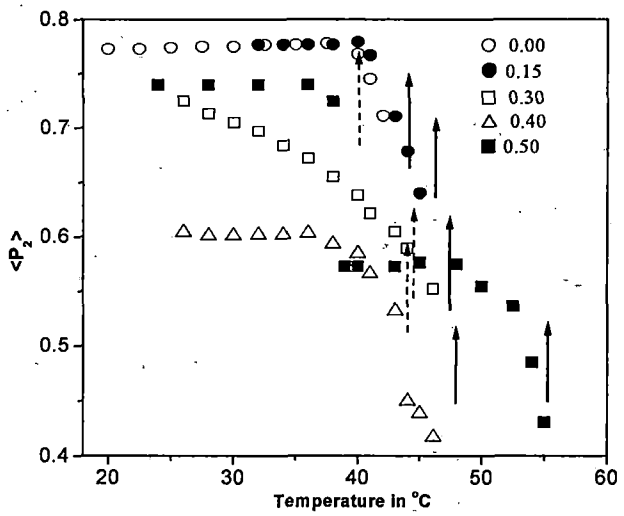

FIGURE 7.7 (a): Orientational order parameter $\langle P_2 \rangle$ as a function of temperature for mole-fractions (x) of ○ 1d(3)CCO_2 (x= 0.0) ; ● (x= 0.15) ; □ (x= 0.3); △ (x= 0.4) ; ■ (x= 0.5) ; ↑ for nematic to isotropic transition; ↑ for smectic B to nematic transition.

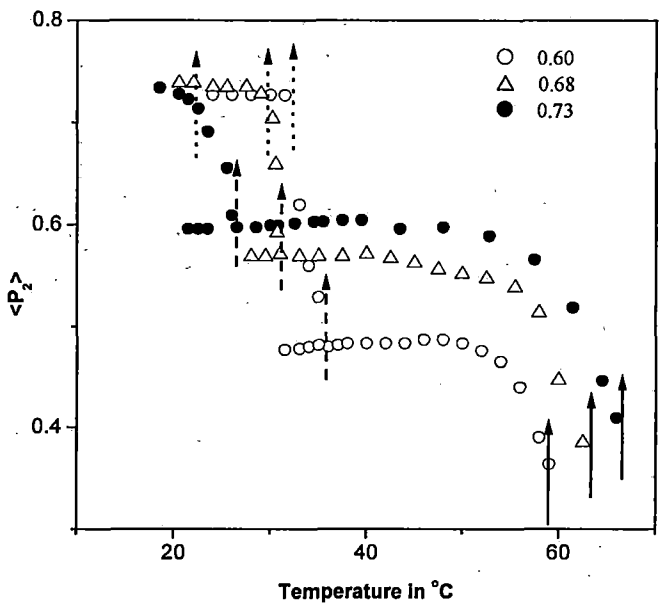

FIGURE 7.7(b): Orientational order parameter $\langle P_2 \rangle$ as a function of temperature for different mixtures with mole-fractions (x) of 1d(3)CCO_2 .○(x= 0.6) ; △ (x= 0.68) ; ● (x= 0.73); ↑ for nematic to isotropic transition ; ↑ for coexisting SmB-N to nematic transition ; ↑ for SmB to SmB – N coexisting transition.

The order parameter values however changes continuously across the nematic – smectic B transition temperatures for mixtures with molar concentration x > 0.5 as indicated in figure 7.7(b). It is also observed that within the co-existing phase the temperature variation of $\langle P_2 \rangle$ is quite sharp which corroborate the results of density and refractive index measurements.

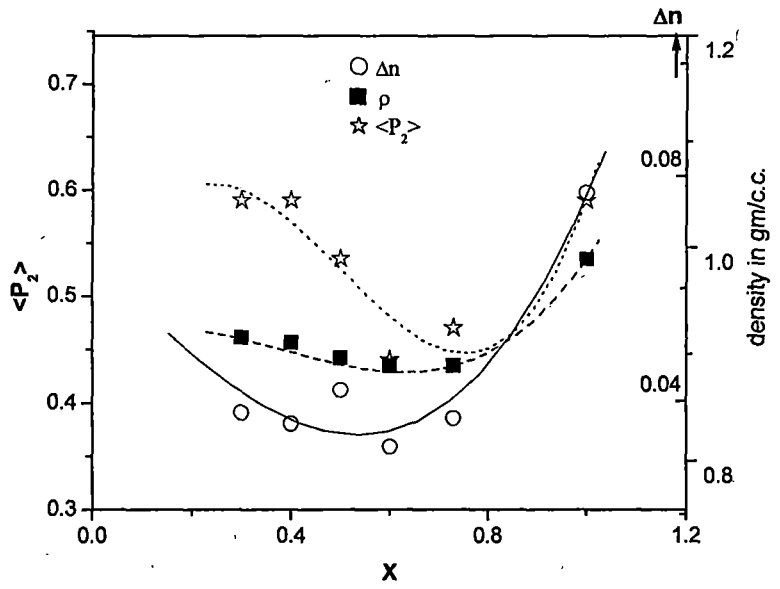

FIGURE 7.8: Density (ρ), $\langle P_2 \rangle$ and Δn against mole fraction of 1d(3)CCO2 at $T = T_{NI}(T_{SI}) - 2\ ^{\circ}C$. (■ ρ, ☆ $\langle P_2 \rangle$, ○ Δn).

Figure 7.8 shows the variation of $\langle P_2 \rangle$, Δn and density with mole fraction of $1d(3)CCO_2$ at a temperature $T = T_{NI}(T_{SI})-2^{\circ}C$. The $\langle P_2 \rangle$, Δn and density values in the nematic phase show a minimum near $x \approx 0.6$.

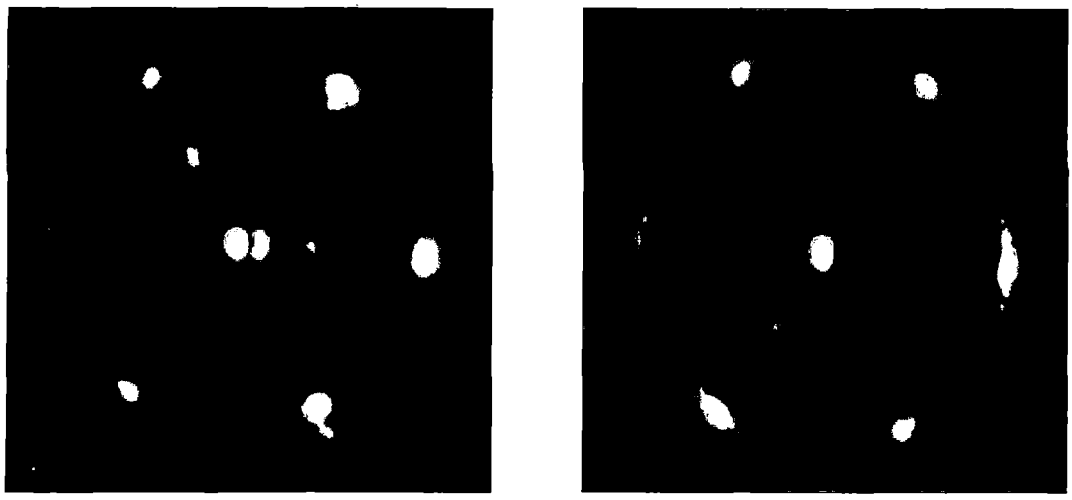

(a) (b)

FIGURE 7.9: X-ray diffraction photograph from an aligned sample of mixture A (x= 0.6001), where the incident x-ray beam parallel to the layer normal. (**a**) Smectic B phase 25°C (**b**) Co-existing SmB-Nematic phase at 35.5° C

Figure 7.9(a) shows the x-ray diffraction photograph of the aligned sample in the smectic B phase of mixture A at 25°C where the incident x-ray beam is parallel to the layer normal. The outer diffraction ring is split up into six spots, clearly showing the hexagonal molecular arrangement within the layers. Almost identical photographs have been observed from room temperature up to the smectic B to nematic phase transition except in the co-existing SmB-N phase. The co-existing phase is marked by the appearance of relatively sharp x-ray diffraction spots exhibiting the hexagonal symmetry of the SmB phase, superimposed on the diffuse liquid like outer ring characteristic of the nematic phase with the direction of the incident beam parallel to the nematic director (figure 7.9(b)), indicating the presence of both nematic and smectic B domains. Similar behaviour of these mixtures has also been observed from refractive index measurements, where I have

been able to observe and measure the refractive indices for both the smectic B and nematic phases in the co-existing region.

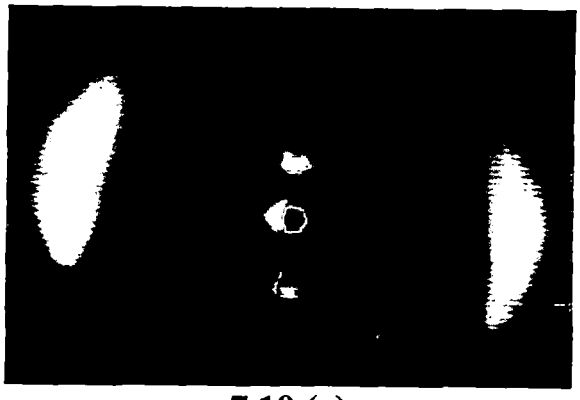

7.10 (a)

7.10(b)

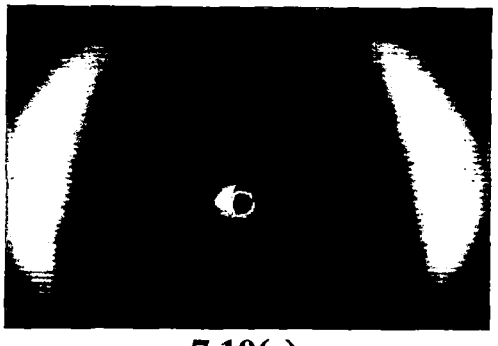

7.10(c)

FIGURE 7.10: X-ray diffraction pattern of an aligned sample of mixture A, where x-ray beam is incident perpendicular to the layer normal: (**a**) x = 0.6 SmB at T = 23°C; (**b**) smectic B-nematic co-existing phase at 35° C; (**c**) nematic phase at 38° C.

The x-ray diffraction pattern of a well oriented monodomain sample of mixture A in the smectic B, smecticB-nematic co-existing phase and nematic phases are shown in figures 7.10(a) - 7.10(c) respectively. These photographs are obtained after slow cooling of a drop of the liquid crystal placed on a glass plate with the x-ray beam incident parallel to the glass plate. The x-ray patterns are recorded using a 2-D area detector (HI – Star, Siemens AG).

The bond orientational order has been calculated by evaluating the expression,

$$\langle \cos(6\theta) \rangle = \int_0^{\pi/6} \cos(6\theta) f(\theta) d\theta \,/\, \int_0^{\pi/6} \cos f(\theta) d\theta \qquad \textbf{7.2}$$

where, f(θ) is the angular distribution function of centre of mass of the neighbouring molecules with respect to a central molecule and the angular distribution function has a maximum at $\theta = 0$. The above equation can be approximated by the following expression,

$$\langle \cos(6\theta) \rangle \approx \int_0^{\pi/6} \cos(6\theta) I(\theta) d\theta \,/\, \int_0^{\pi/6} I(\theta) d\theta \qquad \textbf{7.3}$$

where I(θ) is the azimuthal distribution of the x-ray diffraction intensity. According to Vainshtein [20] it has been assumed that I(θ), the intensity distribution, is proportional to f(θ) the distribution function and consequently has its maximum at $\theta = 0$. BOO is calculated for each peak and finally the average over six peaks are taken. The intensity values plotted against azimuthal angular positions have been corrected for the background (scattered) intensity values.

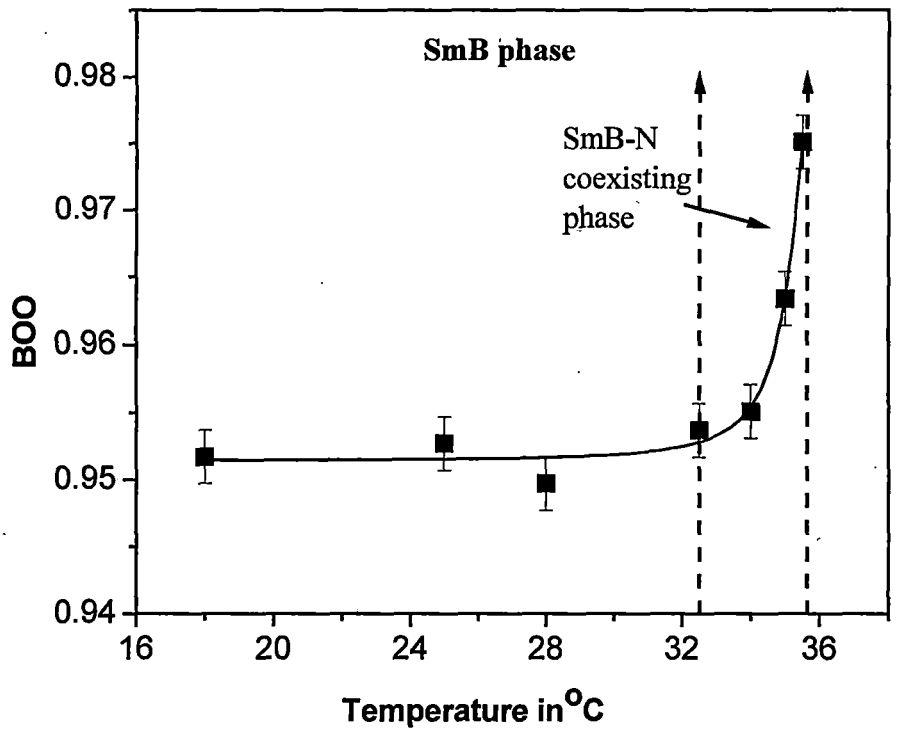

FIGURE 7.11: Temperature variation of bond orientational order (BOO) for mixture A.

Figure 7.11 shows the Bond Orientational Order (BOO) values at different temperatures in the smectic B phase for mixture A. The BOO in the smectic B phase of this mixture is found to be ~ 0.96 and independent of temperature throughout the SmB phase. This result seems to indicate that the smectic B phase for this mixture is of the crystal B type in the sense that the molecular positions exhibit long-range bond orientational order throughout the phase. Interestingly it is found that the BOO values increases rapidly with temperature in the co-existing SmB-N phase. This increase may be due to the pretransitional effect of the SmB-N second order phase transition.

The transverse correlation length in the SmB as well as in the nematic phase of mixtures A and B has been determined from a linear scan of the x-ray diffraction peaks. X-ray intensities are at first corrected for the use of a flat plate camera. This corrected intensity data are then deconvoluted for finite width of the collimator. The deconvoluted intensity profile I(q) is fitted to a Lorentzian form with a quadratic background viz.,

$$I(q) = \frac{a_1}{a_2 + (q - q_o)^2} + a_3 q^2 + a_4 q + a_5 \qquad \textbf{6.4}$$

q being the magnitude of the scattering vector. The transverse correlation length is defined as $\xi = 2\pi(a_2)^{-1/2}$. The in-plane transverse resolution (FWHM) for this instrument is $\Delta q = 6 \times 10^{-3}$ Å^{-1}.The values of the correlation lengths obtained in this way varied from 35Å to 50Å in SmB phase and 18Å to 25Å in nematic phase for these mixtures. For Crystal B phase the correlation lengths are expected to be much longer. One reason for this discrepancy may be due to the use of Ni filtered CuK_α radiation, which contains a white background radiation in addition to the CuK_α peak. No correction for this white radiation, which broadens the diffraction peaks considerably, is made here. Hence the experimental values of correlation lengths as obtained above are much shorter than the theoretically expected values.

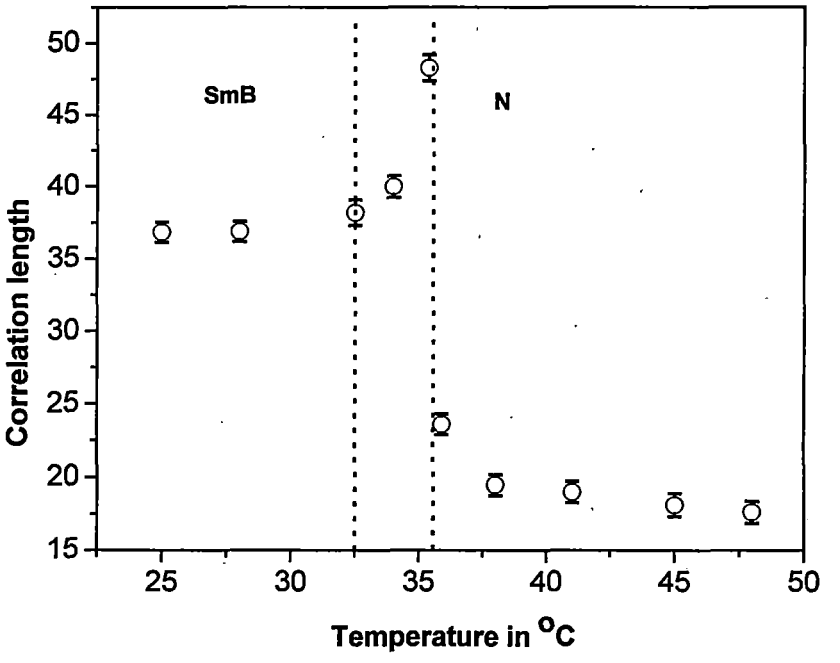

FIGURE 7.12: Temperature variation of transverse correlation length of mixture A.

Figure 7.12 shows the measurements of transverse correlation length over the entire mesomorphic temperature region for mixture A. These values are found to diverge as the co-existing phase region is approached from either side, indicating a second order phase transition. This has been supported by entropy, density, refractive index and OOP measurements. The temperature variation of transverse correlation length for mixture B also shows a similar trend.

The angular distribution of the x-ray diffraction intensities for mixtures A and B are used to measure the orientational distribution function $f(\theta)$ and hence the orientational order parameter $\langle P_2 \rangle$ and $\langle P_4 \rangle$ throughout their entire mesomorphic range following a procedure described in chapter 2.

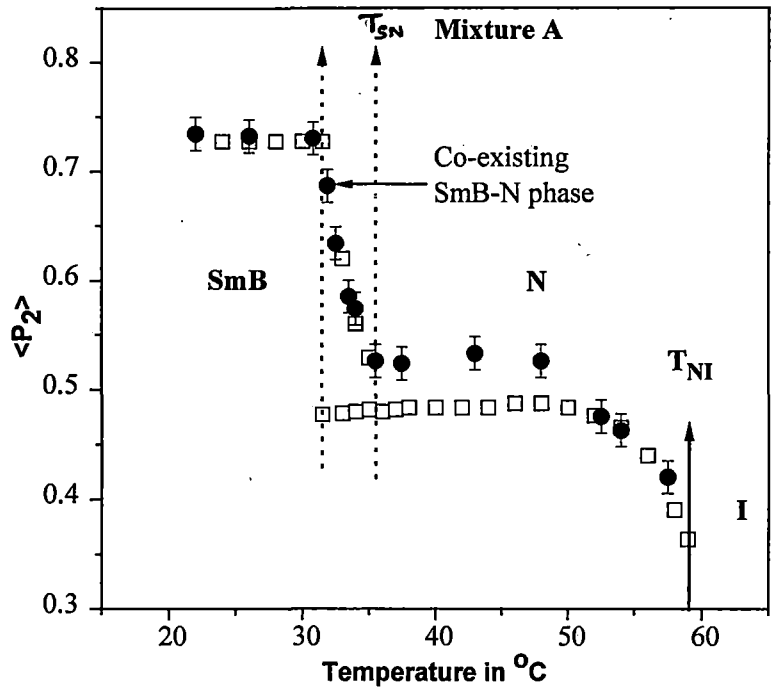

FIGURE 7.13: Temperature dependences of <P_2> values for mixture A. □ <P_2> from refractive index data, ● <P_2> from x-ray data. T_{NI} = nematic – isotropic transition temperature. T_{SN} = smectic B – nematic transition temperature.

Figures 7.13 and 7.14 show the variation of the experimentally determined OOP's with temperature for the two mixtures A and B respectively. The experimental <P_2> and <P_4> values are relatively high in the smectic B phase, showing the phase to be much more orientationally ordered than its neighbouring nematic phase. In the coexisting SmB-N phase a very sharp decrease of the OOP values is observed with increase in temperature. This OOP is in effect the weighted mean OOP of the two phases. This is due to the fact that in this two-phase region, the SmB domains rapidly reduce in size with increasing temperature, so that the weighted mean OOP decreases rather rapidly. Similar results are also observed in the OOP values obtained

from the refractive index measurements, which are also indicated in the respective figures.

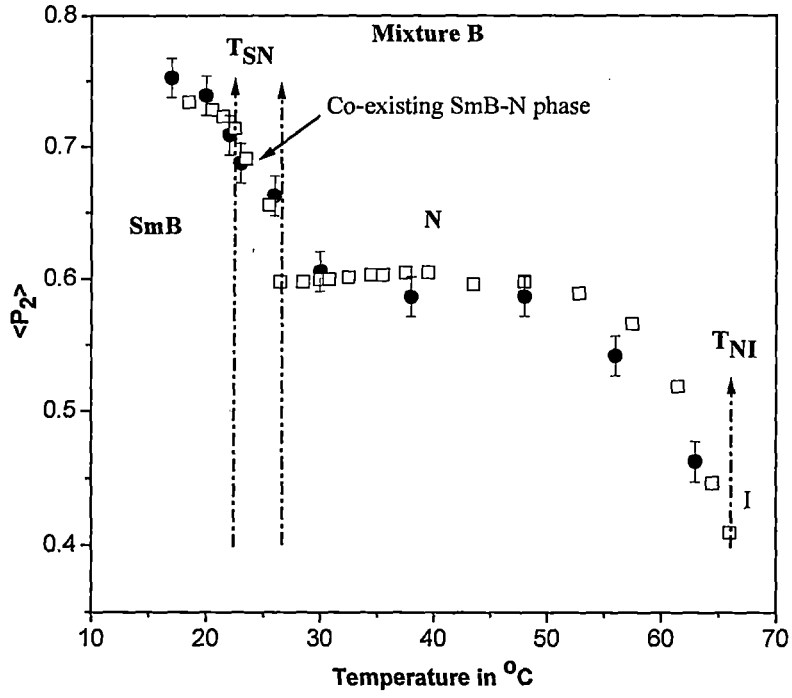

FIGURE 7.14: Temperature dependences of $<P_2>$ values for mixture B. □ $<P_2>$ from refractive index data, ● $<P_2>$ from x-ray data. T_{NI} = nematic – isotropic transition temperature. T_{SN} = smectic B – nematic transition temperature.

The values of the apparent molecular length or layer thickness (d) and the intermolecular distance (D), at different temperatures are also measured for mixtures with x = 0.3, 0.4, 0.5, 0.6, 0.73. The temperature variation of the intermolecular distance, D, for mixtures A and B throughout the mesomorphic range are shown in figure 7.15. There is an increase in the D values from the Smectic B to nematic phase transition. This increase is most sharp at the transition to the co-existing phase and these values also continue to increase within this phase. The reason for this is the same as stated for the variation of OOP in the two-phase region. As observed from figure 7.15, the

variation of D with temperature in the nematic phase is quite appreciable, caused due to the increasing thermal vibrations of the chain parts of these flexible molecules.

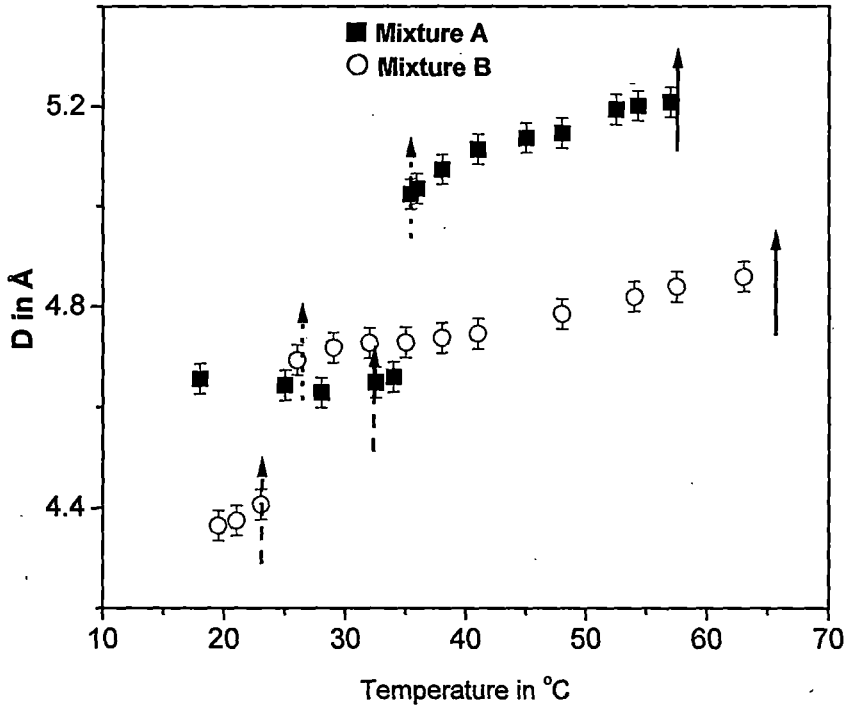

FIGURE 7.15: Temperature dependences of D values for mixtures A and B. Key to symbols: ■ Mixture A ○ Mixture B

As expected, the temperature variation of d in the smectic phase is slight. However, for all the mixtures the apparent molecular lengths (l) increases with increasing temperature and the effect is pronounced near the nematic-isotropic phase transition (figure 7.16). This increase before the phase transition is once again due to the increasing thermal vibrations of their chain parts just before the transition.

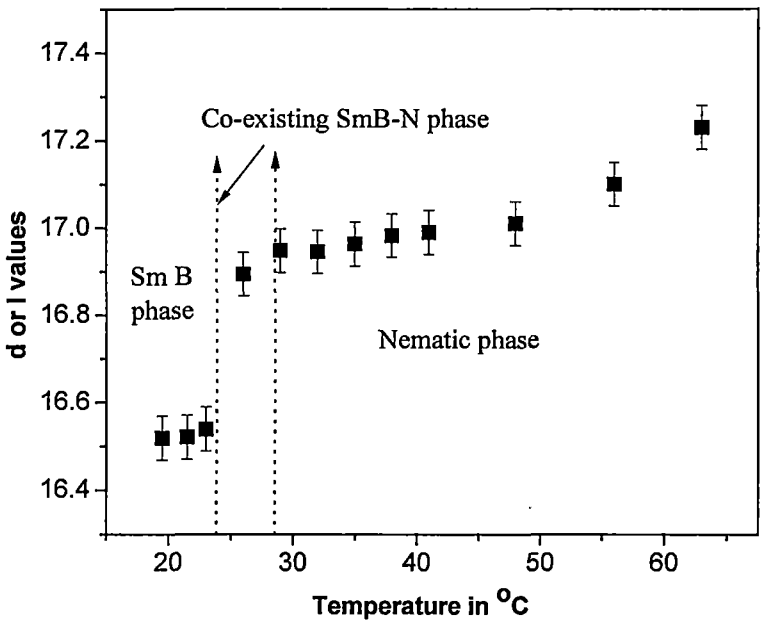

FIGURE 7.16: Temperature variations of apparent molecular length (l) or layer thickness (d) values.

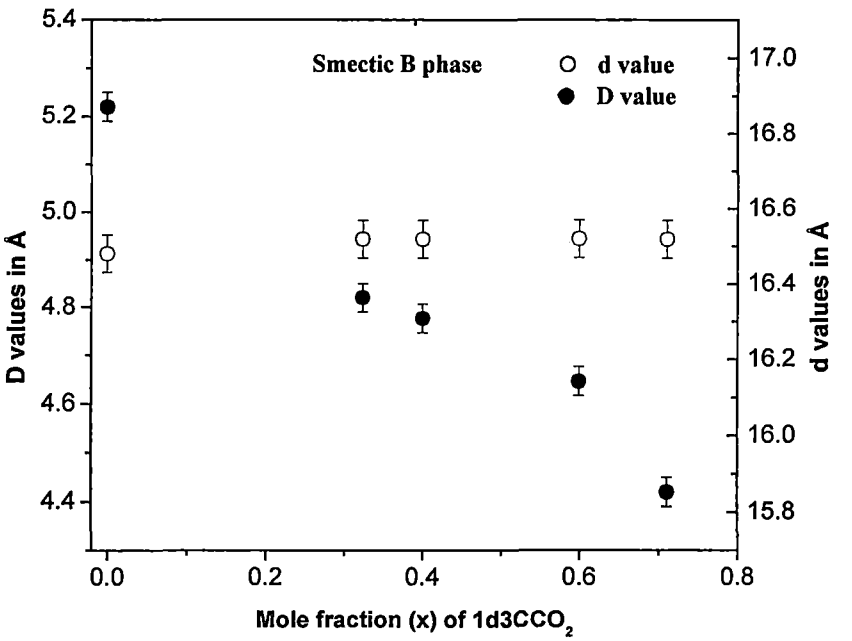

FIGURE 7.17: Variations of D (●) and d (○) values with mole fraction (x) in smectic B phase.

The d values in the smectic B phase are more or less the same for all the mixtures (figure 7.17) and are almost equal to the respective model molecular lengths of the isomeric pure components. However, the D values in the smectic B phase decreases with the increase in mole fraction of 1d(3)CCO_2 . At a temperature T = T_{NI}-2.5°C, in the nematic phase of this system, the D values show an enhancement in their magnitudes near x≈0.6 (figure 7.18), whereas the density and order parameter show a reverse trend. This implies that the packing of the molecules in nematic phase is rather poor near this region. The l values in the nematic phase however, slightly increases with increase in the mole fraction of 1d(3)CCO_2.

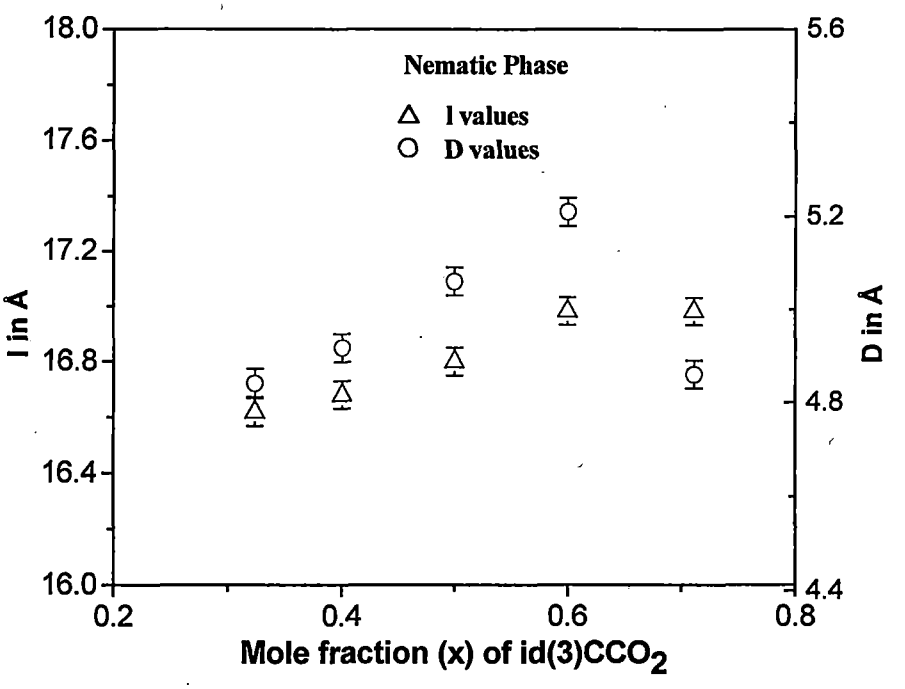

FIGURE 7.18: Variations of l (△) and D (○) values with mole fraction (x) in nematic phase.

REFERENCES:

[1] A. Nath, B. Chaudhury and S. Paul, *Mol. Cryst. Liq. Cryst.* **265**, 699 (1995).

[2] B. Adhikari and R. Paul, *Phase transitions*, **56**, 165 (1996).

[3] A. Nath, S. Gupta, P. Mandal, S. Paul and H. Schenk, *Liq. Cryst.*, **20**, 765 (1996).

[4] A. Nath, Chaudhury, B. Paul and S. Paul, *Mol. Cryst. Liq. Cryst.*, **265A**, 699 (1995).

[5] M. Schad, R. Buchecker and K. Müller, *Liq. Cryst.*, **5**, 293 (1989).

[6] R. J. Birgeneau and J. D. Lister, *J. Phys. Lett.*, **39**, L-399 (1978).

[7] C. C. Haung and T. Stoebe, *Adv. Phys.*, **42**, 343 (1993).

[8] G. J. Brownsey, & A. J. Leadbetter, *Phys. Rev. Lett.* **44**, 1608 (1980).

[9] P. A. C. Gane and A. J. Leadbetter, *J. Phys. C.: Solid State Phys.*, **16**, 2059 (1983).

[10] C. V. Lobo, S. Krishna Prasad and D. S. Shankar Rao, *Phy. Rev. E*, **69**, 051706 (2004).

[11] D. E. Moncton and R. Pindak, *Phy. Rev. Lett.*, **43**, 701 (1979).

[12] C. C. Haung and K. J. Strandburg, (Ed.), *"Bond Orientational Order in Condensed Matter Systems"*, Springer-Verlag, Berlin, pp 78 (1992).

[13] J. Doucet, A. M. Levelut and M. Lambert, *Ann. Phys.*, **3**, 157 (1978).

[14] A. J. Kim, M. Veum, T. Stoebe, C. F. Chou, , J. T. Ho, , S. W. Hui, , V. Surendranath and C. C. Haung, *Phy. Rev. Letts.*, **74**, no24, 4863 (1995).

[15] M. Cheng, J. H. Ho, S. W. Hui and R. Pindak, *Phys. Rev. Letts.*, **59**, 1112 (1987).

[16] A. K. Zeminder, S. Paul, and R. Paul, *Mol. Cryst. Liq. Cryst.*, **61**, 191 (1980).

[17] H. E. J. Neugabauer, *Can. J. Phys.*, **32**, 1 (1954).

[18] I. Haller, H. A. Huggins, H. R. Lilienthal and T. R. McGuire, *J. Phys. Chem.* **77**, 900 (1973).

[19] H. P. Klug and L. E. Alexander, *"X-ray diffraction procedure for polycrystalline and amorphous materials"*, John Wiley and Sons, New York, page 114 and 473 (1974).

[20] B. K. Vainshtein, *"Diffraction of x-rays by chain molecules"*, Elsevier Pub. Co., London (1966).

Chapter 8

Summary And Conclusion

The dissertation entitled *"Study of Physical Properties of Binary Mixtures of Liquid Crystals"* submitted for the degree of doctor of philosophy (Science) of the University of North Bengal embodies the results of experimental investigation of the physical properties of a few binary mixtures of liquid crystals. The thesis comprises of eight chapters.

In chapter 1, I have given a brief introduction to Liquid Crystals, especially thermotropic liquid crystals. I have described only those phases which have been studied by me namely nematic, smectic A and smectic B. A brief review, which covers all other aspects of liquid crystal research, is also given in this chapter.

In chapter 2, I have described the experimental techniques in details to study the physical properties of liquid crystals and the theories, which support the experimental results, are given at the beginning. The experimental techniques adopted are - phase identification by texture studies, x-ray diffraction studies, the interpretation of the x-ray results, density, refractive index, magnetic susceptibility, static dielectric permittivity and elastic constants measurements. Methods of calculation of orientational order parameters, apparent molecular length, intermolecular distance, refractive indices, molecular polarizabilities etc have been outlined.

In chapter 3, I have given the phase diagram, reported the experimental values of density and refractive index measurement of a binary mixture of 4-n-pentyl 4′-cyanobiphenyl (5CB) and 4-n-pentyl phenyl 4 n′- pentyloxy benzoate (ME5O.5) showing the presence of an induced smectic A phase. The density and refractive indices are used to calculate molecular

polarizability values parallel and perpendicular to the molecular long axes using Neugebauer's method. Orientational order parameters as a function of temperature and concentration are determined. The relative change in density at the SmecticA-nematic phase transition shows a maximum near equimolar concentration. The orientational order parameter values and calculated packing fraction show a minimum around $x \approx 0.4$ at a temperature $T = 35^{\circ}C$. Similar behaviour is also observed at a temperature $T = 0.98T_C$, in the nematic phase where the smectic A phase is the precursor of the nematic phase. Average lateral distance (D) between the molecules is measured from the analysis of x-ray diffraction data. The variation of D with molar concentration in smectic A phase shows a maximum near equimolar concentration.

Chapter 4 deals with the study of binary mixture of undecyloxy cyanobiphenyl (11OCB) and 4-n-hextyl phenyl-4-n'-pentyloxy benzoate (ME6.O5) which shows enhanced smectic A phase, where 11OCB has smectic A and ME6.O5 has nematic phase only. The phase diagram, experimental results of refractive index and density measurements; and calculation of orientational order parameter throughout the entire temperature and concentration range have been reported. At a reduced temperature, density values increase with mole fraction (x) of 11OCB up to $x = 0.25$ and then decreases continuously having a minimum near $x=0.8$. The birefringence and $\langle P_2 \rangle$ values follow the same trend showing a maximum near $x = 0.4$ and a minimum near $x = 0.8$.

The results of the study of the binary mixtures of 4-n-pentyl phenyl 4-n'-hexyloxy benzoate (ME6O.5) and p-cyanophenyl trans-4-pentyl

cyclohexane carboxylate (CPPCC) are presented in chapter 5. It includes the phase diagram, DSC values, the values of refractive indices and densities. The result of x-ray diffraction study and static dielectric permittivity measurements are also reported in this chapter. The binary mixture ME6O.5 and CPPCC shows the presence of induced smectic A_d phase in a certain concentration range $0.03 < x < 0.6$, where x is the mole fraction of CPPCC. Maximum stability of the smectic phase occurs for mixtures having $x \approx 0.3$. The change in entropy during smectic A_d – nematic phase transition (ΔS_{SN}) is larger for the mixture having $x < 0.33$ than the mixture having $x > 0.33$. A small discontinuity in the density values could be observed at the nematic to smectic A_d phase transition for mixtures around a mole fraction near $x = 0.3$, consistent with the observed entropies of transition.

In general, the change in birefringence is continuous for mixtures with $x>0.33$ at the S/N transition which indicates a weakly first order or a second order phase transition. On the other hand for mixtures with $x < 0.33$ a discontinuity of birefringence ($\Delta n = n_e - n_o$) occurs at the smectic-nematic phase transition which indicates a first order phase transition. This is consistent with the density and transition entropy measurements. The $\langle P_2 \rangle$ values measured from x-ray diffraction studies are somewhat smaller than those obtain from refractive index measurement in the induced smectic phase for all the mixtures. In the smectic phase the OOP values initially increases with molar concentration upto $x = 0.24$ and then decreases and showing a broad a minima around $x = 0.4$. The variation of layer thickness in the induced smectic phase with composition has been successfully explained by assuming formation of homo and hetero dimers. The variation

of dielectric anisotropy with molar concentration in the nematic and smectic phases has also been successfully explained.

In chapter 6 the results of magnetic susceptibility anisotropy study on the same mixture (ME6O.5 + CPPCC), as given in chapter 5 is reported. The experiment is carried out over the entire mesomorphic and concentration range. The splay (K_{33}) and bend (K_{11}) elastic constants for this system have also been reported by observing Freedericksz transition in magnetic field. The experimental data for magnetic susceptibility anisotropy have been analysed to calculate the order parameter of the system. The changes in $\Delta\chi$ values at the SmA_d - N transition are more pronounced for mixtures with x = 0.24 and 0.33. Similar behaviour is also observed in birefringence (Δn) as well as in the density values of these mixtures.

From the temperature dependences of the orientational order parameters for mixtures at different concentration it is again observed that there is an appreciable change in the order parameter value at the smectic A_d to nematic phase transition temperature for mixtures around x $\approx$0.33. The K_{11} and K_{33} values decrease with increasing temperature as is expected. The K_{33}/K_{11} values for all the mixtures in the nematic phase are less than those of the pure compounds. The variation of K_{33}/K_{11} against mole fraction at $T=0.99T_{NI}$ shows a minimum near a concentration where the maximum stability of smectic phase occurs.

The chapter 7 is concerned with the phase diagram of a binary mixtures of two alkenyl bicyclohexane compounds, one having of nematic phase (1d(3)CCO_2) and the other smectic B phase (0d(4)CCO_2) only. These two compounds are characterized by similar molecular structure, except for a

shift in the position of the double bond in the side chain. An interesting observation in the phase diagram is the occurrence of two phase (smectic B - nematic) co-existing region (≈ 2.5-3°C) for a small concentration range (x = 0.55 – 0.8) of the mixture. Density and refractive indices (n_o, n_e) have been measured for the mixtures having different concentration. The refractive indices have been measured in the co-existing smectic B - nematic region and also in the region having nematic phase only. The refractive index data have been analyzed to yield orientational order parameters. From the DSC, density and birefringence measurements the nature of the smectic B - nematic phase transition for these mixtures and the behaviour of these phase transitions with concentration has been discussed.

X-ray diffraction data for the same binary mixture have been analysed to determine the Bond Orientational Order (BOO), Orientational Order Parameters (OOP), layer thickness (in Smectic B phase), apparent molecular length (in nematic phase) and lateral molecular distance, D, as a function of temperature. The OOP values drop sharply with increase in temperature within the co-existing phase, which is due to the fact that the observed OOP value is the weighted mean OOP of the two phases. Interestingly, the BOO values are found to increase with increase in temperature in the co-existing smectic B-nematic phase. The transverse correlation lengths in the smectic, co-existing and nematic phases have also been estimated. These values are found to diverge as the co-existing smectic B – nematic phase region is approached indicating a second order phase transition. This result has also been supported by entropy, density, refractive index and OOP measurements.

List Of Publications

Paper published:

1. Orientational order parameter of a binary liquid crystal mixtures showing induced smectic phase. P. D. Roy, N. K. Pradhan and M. K. Das, *Mol. Cryst. Liq. Cryst.*, **365**, 593(2001).

2. Phase diagram, density and optical studies on binary mixture of a cyanobiphenyl (11OCB) and a benzoate ester (ME6.O5) showing enhanced smectic phase, P. D. Roy, M. K. Das and R. Paul, *Mol. Cryst. Liq. Cryst.*, **365**, 607(2001).

3. Phase Transitions and Physical Properties of a Binary Mixture of Bicyclohexane Compounds: Refractive Index Measurements, Prithwi Dev Roy, Malay Kumar Das, Sukla Paul, Ranjit Paul and Banani Das, accepted for publication in *Mol. Cryst. Liq. Cryst.* (2005). [Article ID: 144695, Journal ID: PP231].

4. Phase Transitions and Physical Properties of a Binary Mixture of Bicyclohexane Compounds II: X-ray Diffraction Measurements, Malay Kumar Das, Prithwi Dev Roy, Sukla Paul, Ranjit Paul and Banani Das, accepted for publication in *Mol. Cryst. Liq. Cryst.* (2005).[Article ID: 144697, Journal ID: PP232].

5. Dielectric permittivity studies of nematogenic compounds and their binary mixtures showing induced smectic A_d phase. Prithwi Dev Roy, Malay Kumar Das and Sukla Paul, accepted for publication in *Phase Transitions*, (2005). [vol. 79, No.4 (2006)].

Papers presented:

1. Orientational order parameter of a binary liquid crystal mixtures showing induced smectic phase. P. D. Roy, N. K. Pradhan and M. K. Das, 18th International Liquid Crystal Conference, Sendai (Japan), 2000, Proc. Page-220 (2000).

2. Phase diagram, density and optical studies on binary mixture of a cyanobiphenyl (11OCB) and a benzoate ester (ME6.O5) showing enhanced smectic phase, P. D. Roy, M. K. Das and R. Paul, 18th International Liquid Crystal Conference, Sendai (Japan), 2000, Proc. Page-221 (2000).

3. Phase transition and physical properties of a binary mixture of bicyclohexane compounds. B. Adhikari, P. D. Roy, M. K. Das, S. Paul and R. Paul, 18th International Liquid Crystal Conference, Sendai (Japan), 2000, Proc. Page-220.

4. Phase diagram, density, refractive index and dielectric permittivity studies of nematogenic compounds and their binary mixtures showing induced smectic Ad phase, Prithwi Dev Roy, Malay Kumar Das, and, Sukla Paul, accepted for presentation at the 20th International Liquid Crystal Conference, Ljubljana, Slovenia, and July 4 – 9, 2004.

5. X-ray diffraction and refractive index measurements of a binary mixture of bicyclohexane compounds, Banani Das, Prithwi Dev Roy, Malay Kumar Das, Sukla Paul and Ranjit Paul, accepted for presentation at the 20th International Liquid Crystal Conference, Ljubljana, Slovenia, July 4 – 9, 2004.

6. Phase transition and physical properties of a binary mixture of bicyclohexane compounds by x-ray diffraction measurements, Malay Kumar Das, Prithwi Dev Roy, Sukla Paul and Ranjit Paul and Banani Das, Conference of Liquid Crystals, Sept. 2005, Stare Jabtonki, Poland.

7. Determination of diamagnetic anisotropy of a binary mixtures showing induced smectic A_d phase. Prithwi Dev Roy and Malay Kumar Das, Conference of Liquid Crystals, Sept. 2005, Stare Jabtonki, Poland.

8. Dielectric permittivity studies of nematogenic compounds and their mixtures showing induced smectic A_d phase. Prithwi Dev Roy, Malay Kumar Das and Sukla Paul, Conference of Liquid Crystals, Sept. 2005, Stare Jabtonki, Poland.